Doctoral Dissertation

博士論文

INVESTIGATION OF TIME DEPENDENT STRESS AT CROWN OF SECOND LINING CONCRETE OF NATM TUNNELS FOR MITIGATING LONGITUDINAL CRACKS

NATM トンネルの二次覆工コンクリート天端部に発生する軸方向ひび割れ抑制のための応力の経時変化の分析

CHAMILA KUMARA RANKOTH

チャミラ クマラ ランコス

Graduate school of Urban Innovation

Yokohama National University

September 2016

INVESTIGATION OF TIME DEPENDENT STRESS AT CROWN OF SECOND LINING CONCRETE OF NATM TUNNELS FOR MITIGATING LONGITUDINAL CRACKS

(NATM トンネルの二次覆工コンクリート天端部に発生する軸方向ひび割れ抑制のための応力の経時変化の分析)

by

Chamila Kumara Rankoth

(チャミラ クマラ ランコス)

A Dissertation submitted to
Yokohama National University

In partial fulfillment of the requirements for the degree of
Doctor of Philosophy

Supervisor

Associate Professor AKIRA HOSODA

Graduate school of Urban Innovation

Yokohama National University

Yokohama, Japan

September 2016

ABSTRACT

In recent past, tunnel constructions in Japan have increased mainly due to the construction of revival road network in Tohoku region in northern part of Honshu Island. Many of the mountainous tunnels constructed in this area utilize New Austrian Tunneling method which has a superior versatility and low initial cost compared to many of other methods. These tunnels are comprised of a double shell lining system. The Inner lining is constructed with shotcrete and the outer lining, which is visible, is made of reinforced or unreinforced concrete. Cracking of the outer, second, lining has become a major concern for tunnel construction specialists as cracking poses a great threat for long term durability.

Three types of cracks were apparent from the tunnel inspection data. The first type of cracks referred to type 1 cracks in this research are the cracks which propagate parallel to the crown line close to the crown region. The second type of cracks type 2 cracks are the vertical cracks starting from the horizontal construction joint between the invert and second lining. The third type of cracks, type 3, are the horizontal cracks starting from vertical construction joint between two lining blocks.

It had been observed that the mechanism of type 1 cracking was not properly understood because the stress of crown of the second lining could vary based on many variables such as self-weight, volume changes of concrete, hydration heat, shrinkage, restraint conditions of joints etc. Regarding type 2 cracks, the cause of the cracking was hypothesized as the restraint from invert for volume change of concrete in the second lining. However, further clarification of behaviour of type 2 cracks was required to investigate the potential crack mitigation techniques.

Three objectives were set for this study. The first objective was to establish appropriate finite element modeling schemes to study stresses generated in the second lining concrete of NATM tunnels mainly caused by short-term thermal movements due to hydration heat and by long-term drying shrinkage. The second objective was to clarify the mechanism of crown stress behaviour as it was crucial to investigate crack mitigation methods at the crown. The third objective was to propose recommendations to mitigate cracking at critical locations. Critical locations considered here included the crown area with high transverse stress and areas of the second lining close to the invert with higher longitudinal stress. The study was carried out for short-term stress behaviour of second lining governed by thermal stress and for long-term stress behaviour of second lining governed by drying shrinkage.

The finite element model of the tunnel was calibrated and sufficiently validated using tunnel field measurement data and proper engineering judgement with observed practical evidence. Validated models were utilized for parametric studies to investigate the stress behaviour at the crown and the bottom of the second lining close to invert. Two finite element modeling tools were utilized considering the different capabilities of software in different aspects. Major finite element package used is known as ASTEA-MACS, which is a well-known software in Japan for thermal stress analysis. This software provides a great flexibility to execute parametric studies. The other software is called LINK3D, that is, an integrated system which is capable of simulating the combined effects of microscopic material behaviour and nonlinear structural behaviour of concrete structures. Because of the integrated multiscale concrete simulation model in the software LINK3D is capable of predicting drying shrinkage with respect to varying environmental conditions, structural geometry and so on.

First, finite element modeling was carried out considering the short term stress behaviour of second lining with respect to field measurements. The joint formed by waterproofing sheet and the vertical construction joint in between second lining blocks were modeled with negligible joint strength in shear and in tension where the normal compressive strength was assumed to be non-negligible. The joint between the second lining and invert was modeled with fixed joint conditions. The form removal mechanism was assumed to be equal to the application of gravity load at the time of form removal. Special attention was given in determining the thermal properties of composite waterproofing sheet. The thermal conductivity of the waterproofing sheet was calculated based on previous studies done on geotextiles assuming steady state conditions. It was observed that the established model could simulate the temperature in the second lining and stresses in an acceptable manner.

Then to analyze the long-term behaviour of the second lining governed by drying shrinkage, a calculation method was proposed by combining LINK3D and ASTEA-MACS software. The free drying shrinkage strain calculated by LINK3D was used as an input to ASTEA-MACS to carry out the stress analysis.

Considering the stress distribution of the stress in the thickness direction at the crown and close to the invert in the calibrated model, it was observed that the crown cracks can be non-penetrating cracks while the cracks close to invert can be penetrating cracks.

From the short term simulation results, the mechanism of crown stress variation was clarified. It could be seen that before the form removal the crown stress was governed only by

temperature rise and capability of the free movement due to the existence of air void. After the form removal up to a short time, stress behaviour of the crown was governed by self-weight, temperature decrease rate difference in the thickness direction and the deformation behaviour of second lining at the crown.

From the parametric study for short term behaviour, it was observed that crown transverse stress was sensitive to prolonged form retention which could cause external restraint. To obtain the advantages of longer form retention, proper care should be taken to make sure that the contraction of the second lining is not inadequately restrained. Among the investigated material properties, the coefficient of thermal expansion and autogenous shrinkage had a considerable influence on the longitudinal stress near invert. It was observed that low temperature concreting might be helpful in reducing the invert longitudinal stress but might not affect the crown transverse stress so much. In the current study expansive additive was observed to be effective in controlling the stresses close to the invert but it might be necessary to be further investigated considering the tensile strength of expansive concrete which was not considered in this study.

It could be observed that the tensile stress near the surface at crown was small compared to the tensile strength without considering drying shrinkage. This depicts that the crown cracking might not be generated only by thermal stress and self-weight. Therefore, proper construction and ensured material quality might be the key for preventing early age cracking near the crown.

In terms of long-term stresses, drying shrinkage governs the stress at the crown. It was observed that shrinkage property of concrete had a considerable effect on crown stress level and should be taken into account carefully. It could be seen that the crown stress was not highly depended on the tunnel section size. Effect of other factors such as concrete creep, air temperature and humidity variation in the long term should be clarified in future to make an accurate conclusion regarding the belief about increased cracking risk in large blocks with evacuation spaces.

ACKNOWLEDGEMENT

First of all, I would like to express my sincere gratitude to my research supervisor, Associate professor Akira HOSODA for the endless support, guidance and motivation throughout the course to successful completion of the study.

I am extremely grateful to Professor Tatsuya TSUBAKI for providing me the essential guidance in the time of need and valuable suggestions throughout the study.

My special thanks goes to Assistant professor Satoshi Komatsu for the continuous support from the starting of the study.

Sincere gratitude is given to Nishimatsu Constructions Co. Ltd. and RCCM Inc. for the great support and collaboration.

I am extremely thankful to the other members of the research committee Professor Kimitoshi HAYANO, Professor Hitoshi YAMADA, and Associate professor Mayuko NISHIO for the guidance and the instructions at essential times.

Special gratitude goes to the Ministry of Education, Culture, Sports, Science and Technology of Japan for providing me with the opportunity to study in Japan by providing me the essential financial support.

I would like to thanks my fellow members of the laboratory for the enormous support given in times of need.

My special gratitude is directed to my parents, family members and my dearest wife for their continuous support and encouragement during this study.

TABLE OF CONTENTS

ABSTRACT……..……I
ACKNOWLEDGEMENT……III
TABLE OF CONTENTS……..V
LIST OF FIGURES…….……IX
LIST OF TABLES ……..……XIII

1 Introduction 1

1.1 Background 1
1.2 Requirement of the research.....6
1.3 Objectives and Scope 7
1.4 Methodology 8
1.5 Dissertation arrangement.....10

2 Literature review.....12

2.1 Introduction 12
2.2 NATM tunnels and the function of concrete second lining 12
2.3 Construction of NATM tunnels.....15
2.4 Previous research regarding cracking of the concrete second lining 19
2.4.1 Previous research related to simulation of tunnels 19
2.4.2 Previous research on construction methods of lining systems of NATM tunnels 20
2.4.3 Previous research related to geotextiles related to tunnel lining.....21
2.5 Short and long term behaviour of concrete structures.....22
2.5.1 Factors affecting the short-term behaviour of second lining of NATM tunnels 22
2.5.2 Long term behaviour of concrete second lining 24
2.6 Simulation schemes.....26
2.6.1 Theoretical background of ASTEA-MACS.....26

2.6.1.1 Element type for general analysis 26
2.6.1.2 Joint Element model 27
2.6.1.3 Compensation plane method 28
2.6.1.4 Time integration and solver options 28
2.6.2 Theoretical background of LINK3D 28
2.6.2.1 Modeling of shrinkage in LINK3D 29
2.7 Summary 30
3 Finite element modeling of second lining 31
3.1 Field measurements related to cracking of concrete second lining of NATM tunnels 32
3.1.1 Structural monitoring and experimental studies by Taisei Corporation 32
3.1.2 Structural monitoring and experimental studies for Kodsuchi tunnel constructed by Nishimatsu Construction Co. Ltd. 35
3.2 Establishing finite element simulation scheme for second lining of NATM tunnels 37
3.2.1 Major assumptions in modeling 37
3.2.2 Finite element modeling with Astea-Macs 39
3.2.2.1 Determining the boundary conditions and material properties related to thermal analysis 39
3.2.2.2 Determining the appropriate rock thickness for the finite element model . 42
3.2.2.3 Setting the properties of waterproofing sheet 44
3.2.2.4 Structural properties of the Joints J1, J3 48
3.2.2.5 Variation of the air temperature 48
3.2.2.6 Mesh sensitivity analysis 50
3.3 Calibration Results with Astea-Macs 60
3.3.1.1 Calibration of temperature variations 60
3.3.1.2 Calibration of stress and strains close to invert at point P 61
3.3.1.3 Calibration of crown stress 64

3.3.1.4 Deformation of the second lining 65

3.4 Modeling for investigation of long term behaviour of second lining governed by drying shrinkage 66

3.4.1 Calibration of model for calculation of long term drying shrinkage 67

3.4.2 Calculation of drying shrinkage based on environmental, material and structural conditions for second lining of NATM tunnels 68

3.5 Summary 70

4 Short-term stress behaviour of second lining governed by thermal stress 72

4.1 Setting a base model for the parametric study 72

4.2 Investigation of the transverse stress generation mechanism at the crown of the second lining of NATM tunnels 74

4.2.1 Clarification of the behaviour of the transverse stress at crown 74

4.2.1.1 Behaviour of isolated lining in imaginary conditions 75

4.2.1.2 Mechanism of crown transverse stress generation of second lining in short term due to thermal movements and gravity 75

4.2.1.3 Effect of the air void 78

4.3 Stress behaviour of second lining governed by early age volume changes 79

4.3.1 Comparison of analysis results 79

4.3.2 Effect of Autogenous shrinkage on stress variations at the crown and close to the invert 80

4.3.3 Effect of the coefficient of thermal expansion of concrete on the crown and the invert stress 81

4.3.4 Effect of concreting temperature 84

4.3.5 Effect of time of formwork removal 85

4.3.6 Crown and close to invert stress behaviour with respect to the existence of the air void between first and second linings at crown 88

4.3.7 Investigation the effect of expansive additive 90

4.4 Summary 91

5 Long-term stress behaviour of second lining governed by drying shrinkage 93

5.1 Calculating crown stress using calculated drying shrinkage strains 93

5.2 Stress variation at the crown with changing tunnel section size 94

5.3 Variation of stress at crown with varying concrete shrinkage 97

5.4 Summary 99

6 Conclusions 100

6.1 Conclusions regarding finite element modeling of second lining of NATM tunnels 100

6.2 Conclusions regarding short term stress behaviour of second lining governed by thermal stress 101

6.3 Conclusions regarding long term stress behaviour of second lining governed by drying shrinkage 102

6.4 Future tasks. 102

REFERENCES……..……106

APPENDIX-1…….i

LIST OF FIGURES

Figure 1.1. Details of under construction tunnels (a) number of tunnels constructed with each method from total 587 tunnels (b) contract sum based on tunnel construction method from total of 1.74 trillion yen....1
Figure 1.2. Cracking of concrete structures....2
Figure 1.3 Cross section of a typical NATM tunnel....3
Figure 1.4. Crack map of a damaged tunnel....4
Figure 1.5 Research methodology for short term stress behaviour analysis governed by thermal stress....9
Figure 1.6 Stress analysis at crown considering long term drying shrinkage....10
Figure 2.1. Surrounding stress conditions of a tunnel excavation....13
Figure 2.2 Relationship between the radial stress radial deformation supports and time for a tunnel opening....14
Figure 2.3 Longitudinal view of an under construction NATM tunnel....15
Figure 2.4 steel ring that is installed as a part of first lining....16
Figure 2.5 Drilling for rock bolts and advancement surface of the tunnel....16
Figure 2.6. Invert close to the tunnel mouth and re-bars....17
Figure 2.7 tunnel section with laid waterproofing sheet....17
Figure 2.8 (a) Cross section of the water proofing layer (b) how waterproofing layer is bonded to the surface of first lining....17
Figure 2.9 Moving formwork (a) form outside (b) from Inside....18
Figure 2.10 Enclosed space used for concreting in some tunnels....18
Figure 2.11 Windows provided for concreting at the top part of the formwork....18
Figure 2.12 Various curing methods for second lining (a),(b) balloon curing with water supply different support system (c),(d) sheet curing without water supply – different type of sheets 19
Figure 2.13 Surface of waterproofing membrane (a) Without using high ETAS (b) with high ETAS method....20
Figure 2.14 Concreting temperature and site temperature during a year....23
Figure 2.15 Isoparametric formulation of finite element (a) In global coordinates (b) In natural coordinates....26
Figure 2.16 Stress deformation behaviour of Joint element....27
Figure 2.17 Computational scheme of DuCOM....28
Figure 3.1 Measurement points and quantities in real tunnels extracted from literature....32

Figure 3.2 Measured quantities by Taisei (a) Temperature variations (b) Relative humidity variation at site (c) Crown stress variation (d) Longitudinal stress variation 33
Figure 3.3 Compressive strength development measured from laboratory tests 34
Figure 3.4 Adiabatic temperature rise calculated from laboratory tests 34
Figure 3.5 Autogenous shrinkage measured by tests 34
Figure 3.6 Measurement locations and tunnel dimensions of Kodsuchi tunnel 35
Figure 3.7 Drying shrinkage values measured by standard JIS tests 36
Figure 3.8 Measurements close to invert in Kodsuchi tunnel (a) concrete temperature (b) longitudinal stress 36
Figure 3.9 Installation of plastic sheet to prevent friction between construction joints between blocks 38
Figure 3.10 Completed model in Astea-macs 39
Figure 3.11 Definition of heat transfer boundaries 40
Figure 3.12 Temperature contours of initial model 43
Figure 3.13 Initial model to determine the appropriate rock thickness for the model 43
Figure 3.14. Temperature variation at location P close to invert with changing rock thickness 44
Figure 3.15 Arrangement and dimensions of the composite waterproofing membrane 45
Figure 3.16 Damaged EVA sheet in the bottom parts of the second lining 46
Figure 3.17 Existence of an Air gap at the crown – composite waterproofing sheet 46
Figure 3.18 width of the air gap 47
Figure 3.19 Variation of peak temperature at crown with void thickness 47
Figure 3.20 Variation of thermal conductivity of WPS with void thickness 47
Figure 3.21 Definition of K(t) for air temperature 49
Figure 3.22. Modeled air temperature variation in vertical direction of the tunnel 50
Figure 3.23 Initial 2D mesh utilized for mesh sensitivity analysis 52
Figure 3.24 Three types of meshes used to analyze various aspects of meshing 53
Figure 3.25 Comparison of time dependent temperature for different mesh sizes and time steps (a) at surface of Location A (b) close to waterproofing sheet at Location A (c) Invert and lining joint 55
Figure 3.26 Location of maximum temperature (a) mesh-1, (b) mesh-2 56
Figure 3.27 Transverse stress at crown comparison for Mesh-1 and Mesh-3 57
Figure 3.28 Meshing to study longitudinal stress behaviour (a) Default mesh form Astea-Macs-M3D1 (b) Uniform mesh - M3D2 (c) Optimized mesh - M3D3 58

Figure 3.29 Variation longitudinal stress close to invert with mesh size 59
Figure 3.30 Simulation and measurement results for temperature variation inside second lining 61
Figure 3.31 Measured and calibrated stresses at Location P 61
Figure 3.32 Measured and simulated strain (a) Structural strain (b) Temperature strain (c) Effective strain 62
Figure 3.33 Simulated and site calculated stress at crown 63
Figure 3.34 Strain variations at crown (a) structural strain (b) Temperature strain (c) effective strain 64
Figure 3.35. Deformation pattern of the second lining (a) Time dependent deformation (b) Deformation at middle section (c) deformation in 3D 65
Figure 3.36 Simulation scheme for drying shrinkage stress analysis 67
Figure 3.37. Model for calibration of drying shrinkage 68
Figure 3.38. Calibrated results for drying shrinkage 68
Figure 3.39 Model used to calculate drying shrinkage of second lining 69
Figure 3.40 Application of unrestrained drying shrinkage to the stress analysis model 69
Figure 4.1 Comparison of simulation results of 2D and 3D base models (a) Temperature variation (b) Crown stress variation 73
Figure 4.2 Temperature variation and stress variation at the crown – Location is shown as a ratio to the lining thickness from surface 75
Figure 4.3 Imaginary, Isolated lining (a) FE model (b) Transverse stress at crown (c) Deformation at crown 76
Figure 4.4 Temperature profile in thickness direction of the actual model at crown 77
Figure 4.5 Deformation pattern of the second lining (a) Just after form removal 1.16 days (b) at 20 days 77
Figure 4.6 Longitudinal stress variation with distance (a) In vertical direction (b) Distance in thickness direction 79
Figure 4.7 Calculated shrinkage strain at the crown according to JCI guideline 80
Figure 4.8 Stress variation with autogenous shrinkage (a) Crown transverse stress (b) Close to invert longitudinal stress 80
Figure 4.9 Effect of autogenous shrinkage, tensile stress/strength ratio (a) At crown (b) close to invert 81
Figure 4.10 Stress variations with respect to coefficient of thermal expansion (a) transverse stress variation at crown (b) Longitudinal stress variation at invert 82

Figure 4.11 Effect of CTE, tensile stress/strength ratio at maximum stress (a) at crown (b) at invert 83
Figure 4.12 stress variations with respect to initial concreting temperature (a) Transverse stress variation at crown (b) Longitudinal stress variation at invert 84
Figure 4.13 Effect of concreting temperature, tensile stress/Strength ratio (a) At crown (b) At invert 85
Figure 4.14 Idealization of the formwork 86
Figure 4.15 Stress variations with respect to form removal time (a) transverse stress variation at crown (b) longitudinal stress variation close to invert 86
Figure 4.16 Crown stress variation in thickness direction 87
Figure 4.17 Effect of formwork removal, tensile stress/ tensile strength (a) at crown (b) at invert 88
Figure 4.18 Stress variations based on crown temperature (a) transverse stress variation at crown (b) longitudinal stress variation at location P 89
Figure 4.19 Temperature variation at crown middle thickness with and without air gap 89
Figure 4.20 Effect of expansive additives on stress (a) Transverse stress variation at Crown (b) longitudinal stress variation at location P 90
Figure 4.21 Effect of expansive additives stress/strength ratio (a) at crown (b) close to invert 91
Figure 5.1 calculated shrinkage strains from Link3D after temperature adjustment relative humidity of 80% 94
Figure 5.2 calculated quantities by integrating with stress analysis tool (a) transverse stress at crown (b) Thermal cracking index at crown 94
Figure 5.3 Normal and service sections in the Kodzuchi tunnel 95
Figure 5.4 LINK3D model to calculate drying shrinkage values for large service sections. ..95
Figure 5.5 Astea-Macs model for stress analysis of large service section 96
Figure 5.6 calculated strain variations for large and normal sections (a) strain variation at surface with varied relative humidity (b) strain variation comparison in thickness direction for 70% relative humidity 96
Figure 5.7 Stress variations at crown of large and small sections at different relative humidity values 97
Figure 5.8 Variation of shrinkage of concrete 98
Figure 5.9 Crown stress variation based on varying shrinkage property 98
Figure 5.10 Calculated shrinkage for tunnel lining based on varying shrinkage property 98

LIST OF TABLES

Table 1.1 Cracking details of few tunnels in Tohoku region 5
Table 1.2 Type 1 crack data in Akabu Tunnel 5
Table 3.1 Concrete mix proportion used for tunnel investigated by Taisei 35
Table 3.2 Mix proportions used in Kodsuchi tunnel 36
Table 3.3. Heat transfer coefficients used for convection boundaries 41
Table 3.4 Material properties for thermal analysis 42
Table 3.5 Properties used for joint elements for considered joint conditions 48
Table 3.6 element layout of the initial model used for mesh sensitivity analysis 52
Table 3.7 Different types of meshes and their purpose 53
Table 3.8 Minimum time step size limited by element dimensions 54
Table 3.9 Maximum temperature value with time integration method and mesh size 56
Table 3.10 Details of the final mesh 59
Table 4.1 parameters set for the standard model 73

1 INTRODUCTION

1.1 Background

Tunneling is widely utilized worldwide in many fields of civil engineering such as transportation, irrigation, hydropower, etc. In Japan, there are enormous numbers of tunnel structures used in the complicated highway network and the demand for new tunnel constructions has increased considerably in recent years. One of the main reasons for this increasing demand is the ongoing constructions in "Revival Road" highway network in Tohoku region in northern Honshu island recovering from the 2011 earthquake and tsunami disaster. The newly proposed ultra-high speed magnetic levitation train network from Tokyo to Osaka is also expected to have a considerable number of tunnel structures.

It is a common practice to utilize New Austrian Tunnel Method (NATM) for mountainous tunnels in Japan because of its versatility and cost effectiveness. Some of the advantages of NATM can be identified as the flexibility to achieve challenging geometries, low initial capital cost compared to some other tunneling methods such as Tunnel Boring Machines (TBM) etc., [1]. Tunnels under construction at the end of the year 2012 is shown in Figure 1.1.

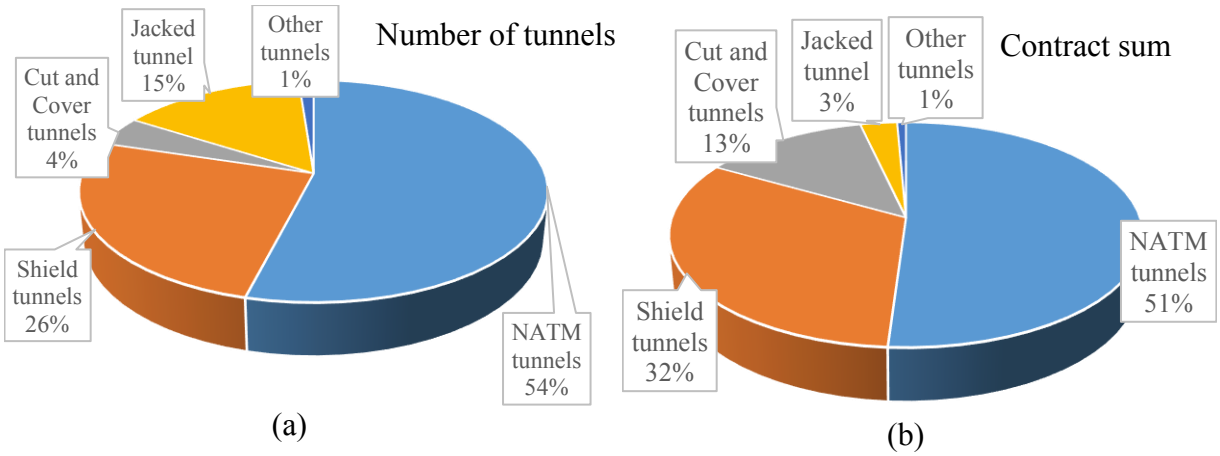

Figure 1.1. Details of under construction tunnels (a) number of tunnels constructed with each method from total 587 tunnels (b) contract sum based on tunnel construction method from total of 1.74 trillion yen

It can be observed that the New Austrian tunnel method had been used for more than 50% of tunnels that were under construction at the end of the year 2012. And the amount spent was also a huge sum of 0.86 trillion yen which is more than 50% of the budget reserved for tunneling.

In recent past, a considerable amount of newly constructed tunnels in Japan has experienced severe cracking in the concrete second lining. Some of the damaged structures are shown in Figure 1.2.

(a) Natusmoto tunnel

(b) Shimogasawa tunnel

(c) Shimogasawa tunnel

(d) Box culvert

Figure 1.2. Cracking of concrete structures

To understand the cracking patterns and the presumed causes, the structural arrangement of typical NATM tunnels should be explained here. A cross section of a NATM

tunnel is presented in Figure 1.3. NATM tunnels consist of two lining systems called first lining and second lining. The second lining is the outer lining in which the cracks can be observed.

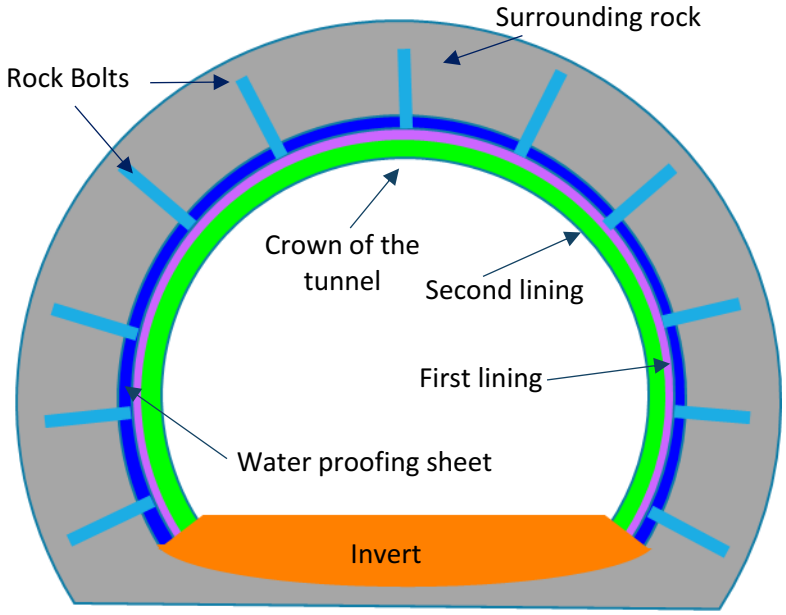

Figure 1.3 Cross section of a typical NATM tunnel

Rock bolts are installed to stabilize the surrounding rock, and the first lining is usually constructed by shotcrete. A waterproofing sheet is installed in between the first lining and the second lining to prevent water intrusion to the second lining. The second lining can be reinforced or unreinforced depending on the design requirements. Invert is a special structural component to increase the arch action of the double shell lining system and installed only in special cases such as soft surrounding soil/rock or close to the tunnel mouth.

A crack map of the second lining of a tunnel is shown in Figure 1.4. Mainly, three types of crack patterns can be recognized from this figure. First, longitudinal cracks can be recognized near to the crown of the tunnel (referred as Type 1 cracks and shown in Figure 1.2(a)). Second, vertical cracks starting from invert and propagating towards the shoulder can be recognized (referred as Type 2 cracks shown in Figure 1.2(c)). Finally, horizontal cracks starting from vertical construction joint between two blocks (referred as Type 3 cracks shown in Figure 1.2(b)). From site investigations, it has been observed that the Type 2 cracks penetrate through the full thickness of the second lining, whereas the Type 1 cracks do not penetrate in many.

According to Figure 1.4, it can be observed that Type 1 cracks are concentrated close to the tunnel mouth. But, it was known that in some tunnels these longitudinal cracks could be seen in inner parts of the tunnels as well. The appearance of crown longitudinal cracking is

frequently reported in the blocks with evacuation space. Tunnel diameter is enlarged in those blocks to provide additional space for evacuation compared to the normal size tunnel sections, and normally the length of those blocks is about 6 m compared to the normal block length of 10.5m. Besides, this type of longitudinal cracking has been observed in other structures besides tunnel lining, such as box culverts as shown in Figure 1.2(d).

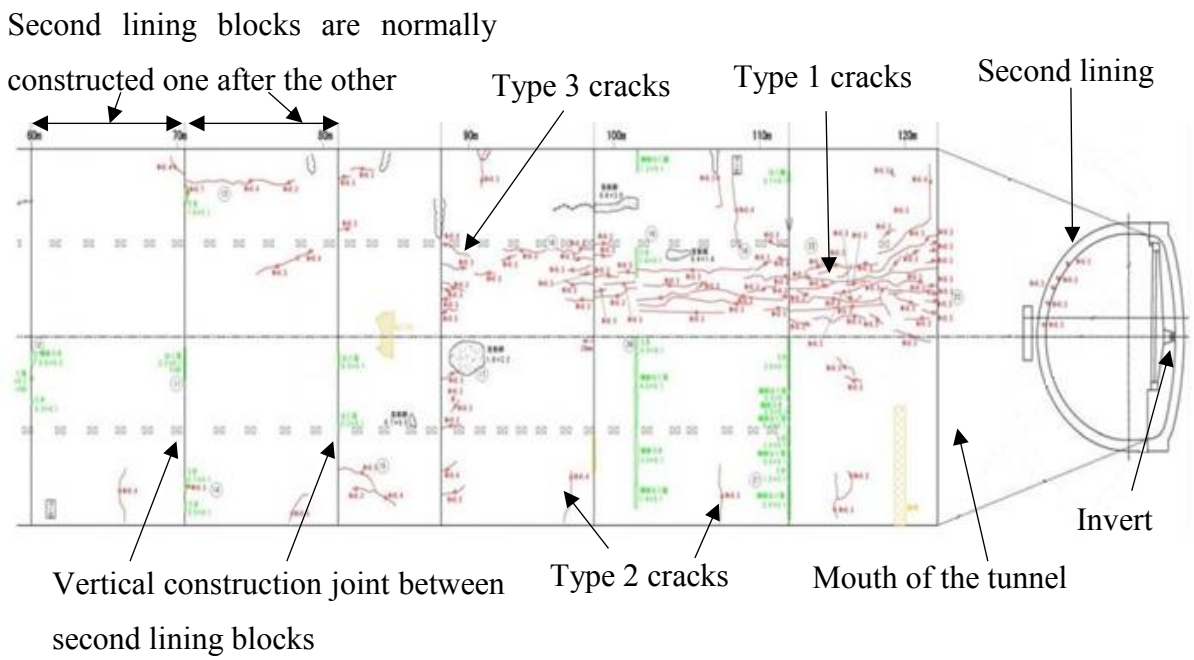

Figure 1.4. Crack map of a damaged tunnel

Analyzed results of tunnel inspection data are shown in Table 1.1 and Table 1.2. Inspections were carried out by the concrete laboratory of Yokohama National University.

When Table 1.1 is considered, it can be seen that the cracking is highly irregular. In some cases, only Type 1, crown cracks, can be observed such as Natsumoto tunnel and Iwaki-mizuishi tunnel. In some cases, only other types of cracks can be seen without Type 1 cracks such as Shimutsu tunnel and Iwaki-miwa tunnel, and in the cases of Akabu tunnel and Mise tunnel, all types of cracks are observed. From these data, it can be seen the crown cracks can appear without the influence of other types of cracks, and it is interesting to note that not every tunnel which shows Type 2 or Type 3 cracks showed Type 1 cracks. And it should be noted that in tunnels with all types of cracks, it is not clear that all the cracks are in the same block. So any relationship between crown Type 1 cracks and other cracks cannot be deduced from the shown few tunnel inspection data.

From Table 1.1, it can be seen that in Akabu tunnel Type 1 cracks has occurred in more blocks compared to the blocks with other types of cracks. Table 1.2 describes the Type 1 cracking in

Akabu tunnel in detail. It can be seen that 50% of blocks with large section has shown Type 1 cracks, while only 5.5% of normal size blocks has damaged due to Type 1 cracks. In other terms, Table 1.2 implies that the risk of Type 1 cracking is increased with the section size increment.

Table 1.1 Cracking details of few tunnels in Tohoku region

Tunnel	**Time of Inspection (Years after completion)**	**Number of spans with Type 1 cracks**	**Number of spans with other cracks**	**Ratio of span with Type 1 Cracks**	**Ration of Spans with cracks**
Natsumoto	10	2	0	18.2%	18.2%
Mise	4	2	3	3.8%	9.6%
Mukaiochiai	3	1	6	1.0%	6.9%
Yuinada	3	0	0	0.0%	0.0%
Shinutsu	11	0	34	0.0%	26.4%
Tenpakusan	8	0	3	0.0%	3.4%
Iwaki-mizuishi	4	6	0	4.6%	4.6%
Iwaki-miwa	0	0	1	0.0%	1.4%
Akabu	3	10	5	9.5%	14.3%

Table 1.2 Type 1 crack data in Akabu Tunnel

Portion	Spans with longitudinal cracks	Total Spans	Type 1 Cracks/ Total Spans ratio
Whole Tunnel	10	105	9.5%
Large section spans	5	10	50.0%
Normal section spans	4	73	5.5%
Spans with fiber-reinforced concrete	1	22	4.5%

Some common explanations for tunnel lining concrete cracking already exist. For Type 1 cracks, a common belief is that long-term drying shrinkage causes cracking although it is not sufficiently proved. For example, the effects of thermal stress and own weight have not been sufficiently discussed. For type 2 cracks, one of the expected causes is the restraint from reinforced concrete invert to early age volume change of concrete due to hydration heat and shrinkage. Regarding Type 3 cracks, it is believed that the restraint from the already constructed block causes external restraint leading to cracking damage close to the vertical construction joint. But besides these, in practical aspects, there can be many driving forces for cracking of

second lining such as non-uniformity of second lining due to non-uniform excavations, restraint due to the wavy shape of the surface of first lining due to the installation of steel rings etc.

To understand the importance of crack prevention in the concrete second lining of NATM tunnels, it is important to clearly understand the function of second lining in double shell tunnel lining systems. The details regarding this matter are presented in section 2.2. However, briefly, it can be stated that the durability aspects of second lining can be more important regarding passenger safety than the structural importance because major load bearing function is primarily accomplished by the first lining in many cases although it depends on the design and service time. With more cracks, the second lining will tend to spall faster compromising the passenger safety and incurring high maintenance cost and disturbance to operation in extreme cases.

1.2 Requirement of the research

As explained in previous section a considerably high budget is utilized for NATM tunnel constructions in Japan. Cracking of second lining of NATM tunnels make the second lining vulnerable to faster deterioration and increased maintenance costs. Therefore many organizations which are responsible for durable infrastructure has paid attention to crack prevention and has taken necessary steps to establish proper guidelines to ensure the quality of tunnel lining. For example, under the requirements of the road construction section of Tohoku regional bureau of MoLIT , the liability period of tunnels for contractors is five years and within this period the crack width should be less than 0.3mm. Therefore the contractors also have a great interest in the crack prevention of tunnel lining to reduce the unnecessary maintenance costs. Considering these facts investigation of crack mitigation was a timely requirement at the starting point of this study.

Many design firms use finite element method to determine the potential of thermal cracking and to design the requirement of reinforcement to prevent early time thermal cracks. But it is extremely important to follow accurate modeling techniques to obtain reliable and economical results. It was observed that the modeling of the second lining of tunnels requires special analysis techniques such as proper joint element molding to ensure accurate stress distribution. Therefore establishing proper modeling for tunnel lining concrete was necessary.

When type 2 and type 3 cracks mentioned in the previous section are considered, the cracking mechanism is explained to some extent as the external restraint for early age volume changes.

But sufficient explanation of the causes of type 1, crown longitudinal cracking, was not available. Therefore proper understanding of the stress variation mechanism of the crown stress was necessary to be clarified to grasp the real reason for longitudinal cracking and to study possible solutions for crack mitigation.

Even though some theories were available about Type 2 cracking, further explanation of longitudinal stress which causes Type 2 cracks was necessary to investigate the possibility of crack reduction.

1.3 Objectives and Scope

Since the cracking of concrete second lining of tunnels possess a greater threat for long-term durability of the structure, the final goal of the project was to identify the effects of various variables such as material properties, construction practices etc. on stress variations in critical locations such as crown and close to invert to propose recommendations to mitigate cracking risk. The study is broadly divided into three objectives.

1. Establishing proper finite element modeling schemes to understand the behaviour of second lining due to early thermal stress and long-term drying shrinkage
2. Clarifications of stress behaviour patterns on critical locations with varying influential parameters
3. Investigations / recommendations to prevent or reduce cracking of second lining in critical locations.

First, appropriate finite element modeling method will be established with the help of field measurement data obtained from past studies or experimental studies executed by research laboratories of tunnel contractors. Early age stress behaviour is considered to be governed by thermal stresses due to the heat of hydration and long-term behaviour was thought to be governed by drying shrinkage stresses. Proper modeling techniques will be established with sufficient verifications to investigate behaviour governed by both thermal effects and drying shrinkage.

Under the objective two, as the first step, the short-term behaviour of second lining until 20 days from casting is studied to understand the stress generation mechanism at the crown of the second lining because the cracking mechanisms at other locations are understood in a substantial manner. Crown transverse stress can be the main cause of longitudinal cracking at the crown. Therefore, an attempt is made to clarify the stress generation mechanism for short-

term behaviour with the help of the calibrated finite element model. Major driving forces of cracking considered for short-term analysis include volume change due to hydration heat and autogenous shrinkage, temperature variation inside the tunnel, and self-weight of the second lining, whereas the load exerted by surrounding soil was assumed to be negligible for short-term behaviour. In this section, the effects of parameters such as concreting temperature, different concrete properties, different environmental parameters etc.., are studied to understand the stress variation at the crown and close to the invert.

As the second step of objective two, long-term behaviour of the tunnel lining considering the stress generation due to drying shrinkage is executed. The effects of concrete shrinkage property and tunnel dimensions with estimated drying shrinkage are investigated to obtain the stress variations at the crown.

The final objective will be mainly achieved based on the results of the objective two. Construction solutions or material modifications are proposed based on the results of the parametric study.

1.4 Methodology

Research methodology is summarized in this section briefly. The whole study was carried out using finite element simulation tools and utilizing reliable site measurement data and experiments carried out by industrial research laboratories. The methodology is presented in two sections Figure 1.5 presents the strategy for short-term stress analysis governed by thermal stress caused by hydration heat. First, model calibration and verification was done. Next, using the verified model, stress generation mechanism at crown was explained. Then parametric studies were carried out to investigate the stress behaviour with respect to a selected set of variables. Results of the parametric study were explained using the clarified stress generation mechanism. Recommendations were made based on the sensitivity analysis.

Figure 1.6 describes the analysis scheme for long-term analysis governed by drying shrinkage. The model which was verified for short-term analysis was utilized in combination with estimated long-term drying shrinkage strain. Two simulation tools were combined to carry out

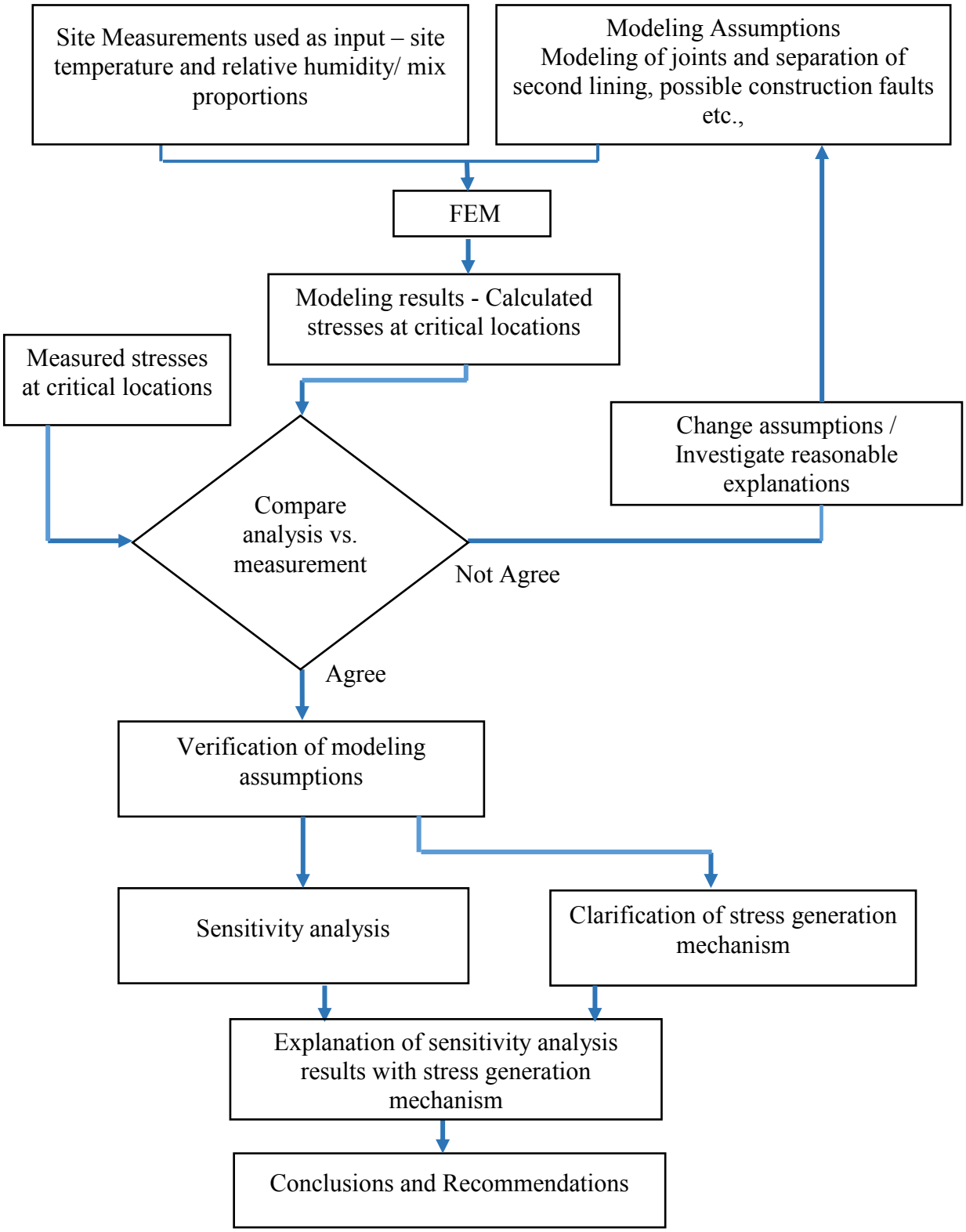

Figure 1.5 Research methodology for short term stress behaviour analysis governed by thermal stress

the total simulation where thermal and structural analysis was carried out in Astea-Macs and the long-term material simulations were carried out in Link-3D. Further explanations are

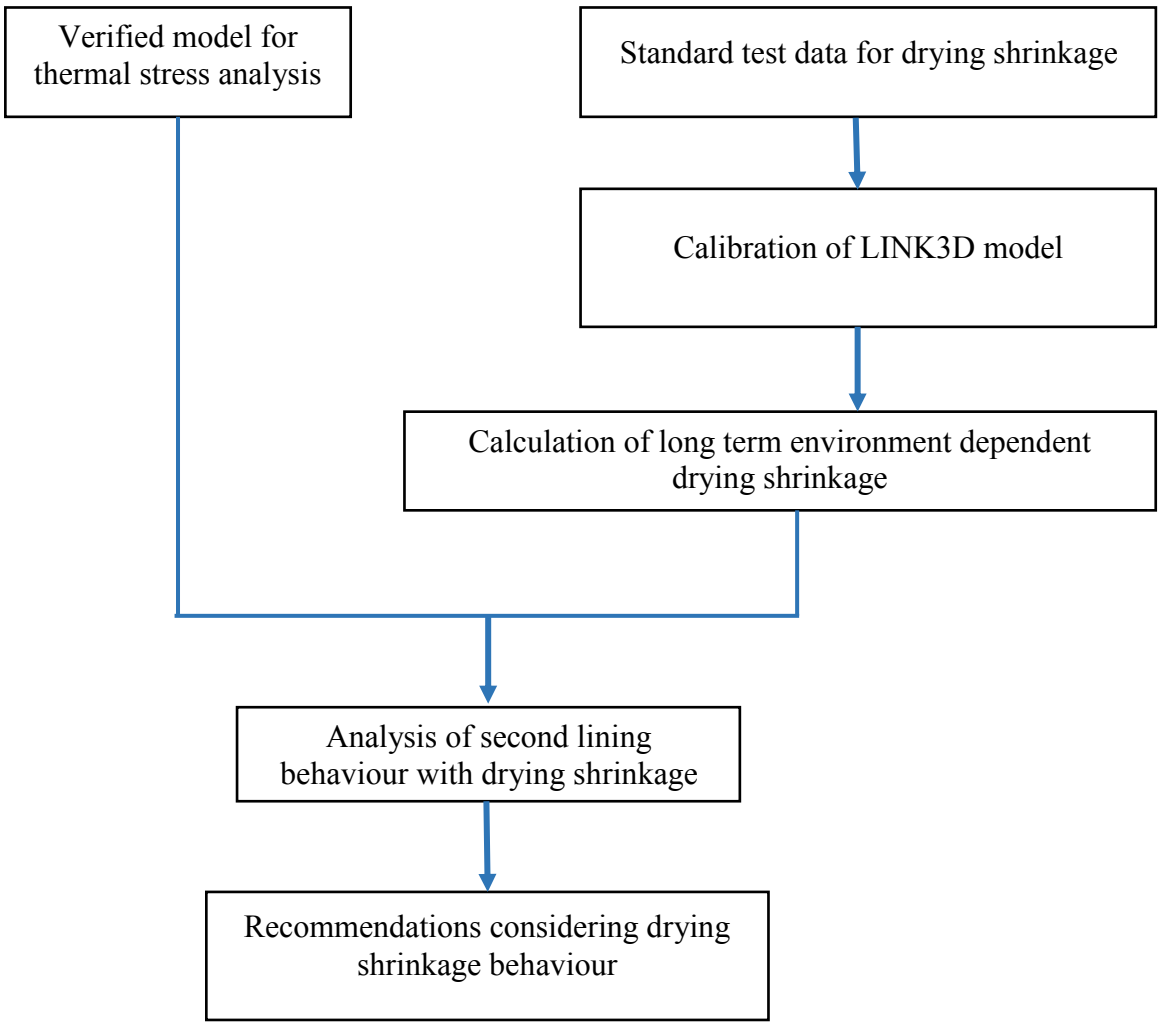

Figure 1.6 Stress analysis at crown considering long term drying shrinkage

presented in chapter 3.

1.5 Dissertation arrangement

The complete research study is presented in 6 chapters.

As the starting point, chapter 1 provides some general details about tunnel construction and the problem facing with cracking of second lining. The overall idea of the research project is provided with the explanation to the problem, solution approach, and the outcome.

The second chapter mainly provides the important information about the theoretical background of the NATM tunneling and the simulation schemes. The construction process of

NATM tunnels is also explained as the understanding of construction process and theoretical background of NATM tunneling is essential to clarify the assumptions made in the simulations.

Chapter 3 describes in detail, the finite element modeling approach including relevant data for model calibration and verification.

Explanation of stress generation mechanism at the crown of the second lining and the parametric studies are presented in chapter 4 considering the short-term stress behaviour of lining concrete governed by thermal stress. Thermal movements are governed by hydration heat, environmental temperature and temperature of the ground.

Chapter 5 describes the parametric study considering the crown stress with respect to long-term drying shrinkage utilizing the established finite element model in chapter 3. Two main parameters were considered. The shrinkage property of concrete and the tunnel diameter as the increase of both these causes can increase the stress generated in the second lining.

Finally, conclusions and recommendations that could be drawn from the research study are presented in chapter 6.

2 LITERATURE REVIEW

2.1 Introduction

For conducting an innovative and useful study, a clear understanding of the current level of knowledge and research carried out about the problem is essential. An extensive literature survey was done regarding the cracking of concrete second lining of NATM tunnels and about required research techniques to obtain a good foundation for the study.

The basic knowledge about the NATM tunneling and function of the second lining is essential for simulations and for proper engineering judgements and presented in section 2.2. The general construction process of NATM tunnels is explained in section 2.3. Some details about previous research are summarized in section 2.4. Some details about previous research are also provided in relevant locations such as in section 3.1 also. Some key factors that affect the behaviour of concrete structures are generally described in section 2.5. Two modeling tools were utilized for the study and some basic theory and details about simulation tools are presented in section 2.4

2.2 NATM tunnels and the function of concrete second lining

NATM or New Austrian Tunneling Method is a very popular tunneling technique developed in Austria and gained popularity in the early 1960s. But actually, the concept has raised with Ladislaus Von Rabcewicz's application for the patent in 1948 for a tunneling system which utilizes the ground strength surrounding the tunnel as an integral part of the load-bearing mechanism. NATM's principle is based on the respond of the ground due to an artificially excavated hole. The ground movement around the hole mobilizes the inherent shear strength of the soil or rock mass to obtain a stable support for the hole if the dimensions are appropriate. Based on this behaviour in a typical NATM tunnel, the excavation is made with curvilinear surfaces to avoid stress concentrations and to reduce bending and shear forces. The tunnel lining usually consists of two lining systems. First one is a flexible lining which is made by shotcrete in many cases and the second one is a cast in-situ concrete lining. A waterproofing membrane will be installed in between two lining systems for water tightness[1].

Although the name of the tunneling method is based on the location of origin, the same tunneling method is addressed by many names all over the world. In the USA in modern days it is known as the SEM or Sequential Excavation Method because in many cases the tunnel section is excavated sequentially allowing controlled ground motion around the excavation. In 70's and early 80's in Germany same tunneling method was addressed as "The Shotcrete Method" while in early 90's in the UK it was known as "Sprayed Concrete Lining" or SCL. Other names include "Conventional Tunneling Method" mainly in used in Austria and Germany as opposed to new TBM driven methods, "Observational Method" because the tunneling techniques might need extensive ground monitoring, and in some cases as "Cyclic Method" because same process is repeated over several sections to complete a tunnel[1].

The basic structural concepts of the system can be explained with the ground response to a created hole through the soil. Figure 2.1[1] shows the stress conditions in ground surrounding an artificially created hole

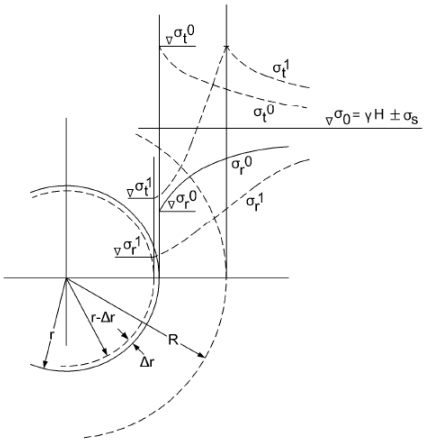

Figure 2.1. Surrounding stress conditions of a tunnel excavation

The stress conditions before any excavation depend on the overburden and shown as σ_0. σ_s Represents the tectonic stresses. When the excavation is made this stress will increase to σ_t^0. If the tangential stress σ_t^0 and the radial stress $\sigma_r^0$is greater than the soil shear strength yielding will occur in the surrounding soil and yielded area is shown as a dashed line in distance R. this yielding will progress with the radial deformation Δr as shown in the figure. The concept is to control the deformation of the soil so that no loosening will occur to provide as an intrinsic support for the tunnel excavation

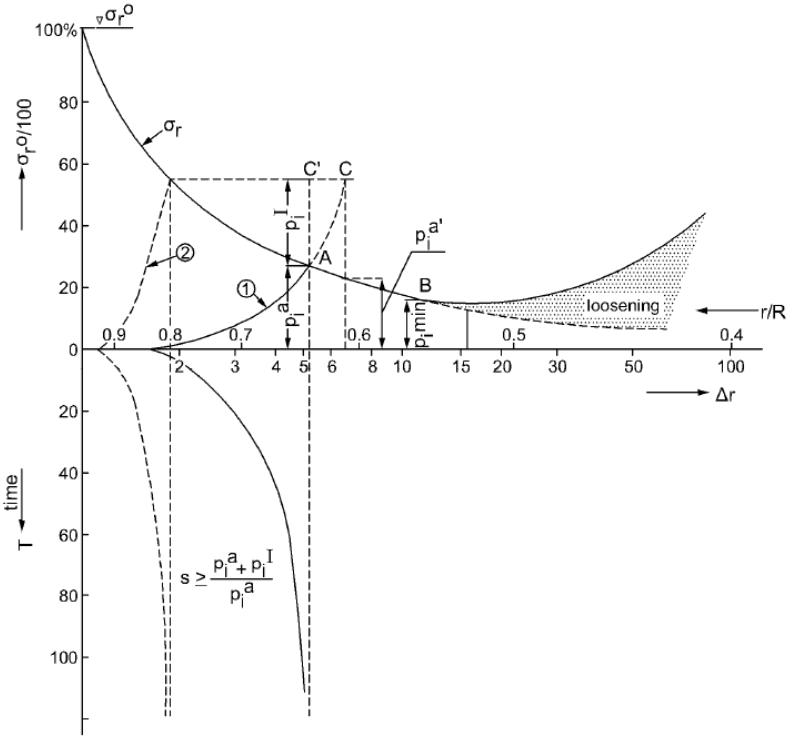

Figure 2.2 Relationship between the radial stress radial deformation supports and time for a tunnel opening

Figure 2.2 [1] shows the relationship between radial stress σ_r, radial deformation Δr , supports p_i and time t and known as a ground response curve. According to the figure it can be seen that the radial stress drops with radial deformation up to some point and then increases. The increasing point represents the point where ground starts to lose the strength and starting of loosening. Therefore principle of NATM follows installing of ground supports before this point. After the loosening point thicker lining will be required to bare the overburden pressure.

Curve 1 and curve 2 represents the installation of ground support. p_i^a Represents the support provided by strengthened ground by itself. Ground strengthening is normally carried out by rock bolts, steel plates and shotcrete. According to curve 1 support p_i^a has provided before Δr exceeds 2 and equilibrium has occurred at dashed line C' when Δr just exceeded 5 points. This theoretically stabilizes the opening and no other support is necessary if provided supports can withstand without any deterioration and overburden does not increase. But in practical scenario another secondary lining will be installed to obtain a higher factor of safety. The secondary support is shown as p_i^I. When the support given by the first support deteriorate

with time second support will be activated and the loaded and unloaded conditions of second support is shown in cases C and C' respectively. $p_i^{a'}$ Represents the support given by the deteriorated first support when second support is loaded. Curve 1 represents the installation of a more stiffer support much earlier which will support the same level of support as represented by curve 1 and provides less deformation but might be uneconomical due to the requirement to utilize stronger materials or thicker section size. p_{imin} Represents the minimum support required to prevent the soil loosening.

It should be noted that in this study for many cases a major assumption was made such that the support provided by first lining is effective enough to bear the overburden pressure and the cracks in the second lining is mainly due to intrinsic behaviour of concrete and only due to self-weight of the second lining. In other words, it was assumed that concrete second lining does not have a structural function of load bearing at the time of crack appearing. This can be dependent upon the design conditions but might be highly reasonable especially to explain the short-term behaviour.

2.3 Construction of NATM tunnels

The typical construction process of NATM tunnels used by Japanese contractors is described briefly in this section as it can help understanding some modeling assumptions made in the

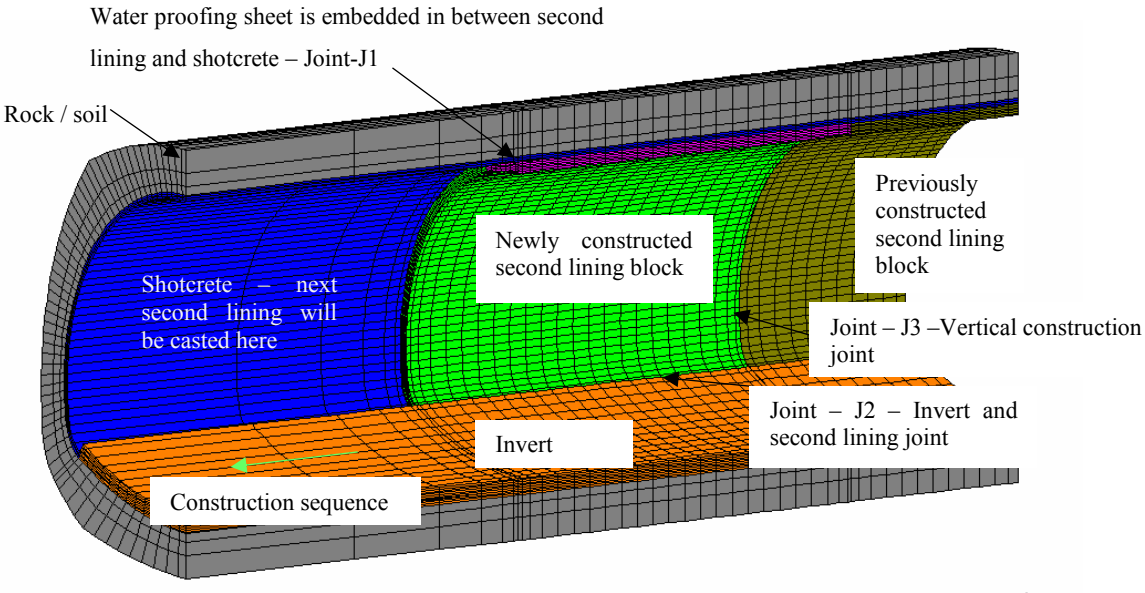

Figure 2.3 Longitudinal view of an under construction NATM tunnel

current study. The observed construction method by the author is explained rather than explaining the general construction process of NATM tunnels. The observations were mainly made in rock tunnel construction and some steps are applied only to rock tunnel construction.

A schematic view of a longitudinal section of an under construction tunnel is shown in Figure 2.3.

1. Tunnel excavation – by blasting

Tunnel advancement is mainly done by placing explosives in the excavation face and blasting the rock. A single advancement is normally about 1.5m.

2. Apply Shotcrete

Blasted surface is shotcreted to prevent any failures due to the weak ground or due to unexpected loosening caused by the blasting.

3. Adding steel rings and shotcrete layer

A steel ring which follows the tunnel shape is installed very close to the blasted surface and the lateral surface is also shotcreted to strengthen the surface. Unmounted steel ring portions are shown in Figure 2.4. This shotcrete layer and the steel ring will serve as an integral part to control the rock movement before installation of rock bolts.

Figure 2.4 steel ring that is installed as a part of first lining

Figure 2.5 Drilling for rock bolts and advancement surface of the tunnel

Next step is to drill the lateral surfaces to install rock bolts. Rock bolts will be added and the outer ends of the rock bolts will be covered by a Styrofoam material to reduce the damage from sharp metal edges to the waterproofing layer and second lining. Figure 2.5 shows a rock bolting machine. The ends of rock bolts can be seen in Figure 2.4 as dots.

5. Construction of the invert

Invert is a reinforced concrete component of NATM tunnels which is installed to stabilize the lining arch in weak soils and rocks and also installed close to the tunnel mouth. In many cases,

it can be observed that short reinforcing bars are provided from invert to the second lining to provide a rigid connection. A reinforced concrete invert is shown in Figure 2.6.

6. Placing the waterproofing layer

A waterproofing membrane which consists of a geotextile and a vinyl sheet is laid on top of the first lining. The sheet is attached to the wall of the fist lining with nails and with some special material strip. The joints are properly connected through thermal fastening to make sure the joints are water tight.

Figure 2.6. Invert close to the tunnel mouth and re-bars

Figure 2.7 tunnel section with laid waterproofing sheet

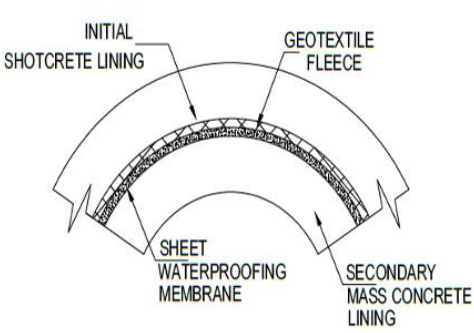

Figure 2.8 (a) Cross section of the water proofing layer (b) how waterproofing layer is bonded to the surface of first lining

7. Placing the moving formwork

Next, the moving steel formwork, which operates on rails, will be set and concreting pipelines will be fixed for the concreting. The form is properly placed with steel supports. Moving formworks does not include the lateral face and the lateral face is constructed with plywood sheets. In some cases, the formwork and the concreting area are covered with a plastic sheet to retain an appropriate environment for concreting without a high level of wind or dust.

8. Concreting of the second lining

Concreting the second lining is a laborious task. Concrete should be placed using small windows provided in the formwork. Concreting will be sequentially carried out to balance the

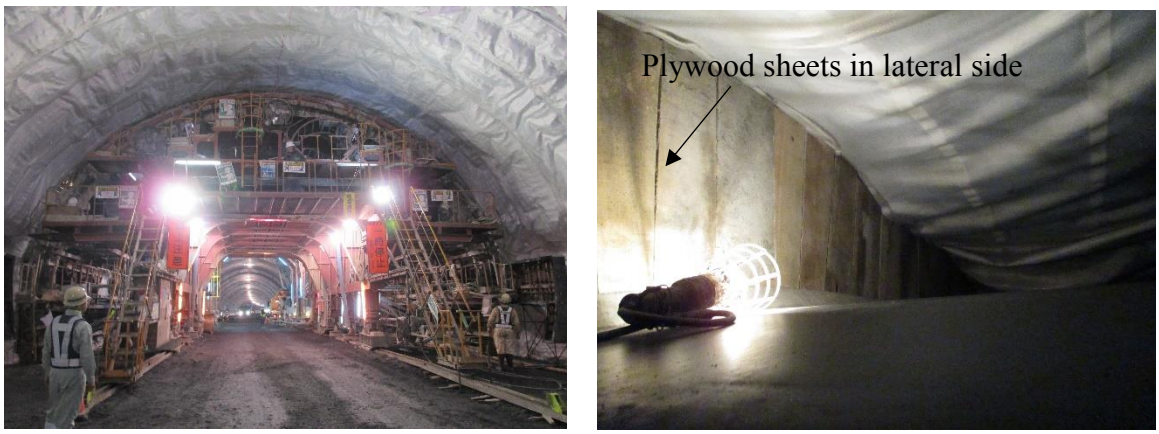

(a) (b)

Figure 2.9 Moving formwork (a) form outside (b) from Inside

Figure 2.10 Enclosed space used for concreting in some tunnels

Figure 2.11 Windows provided for concreting at the top part of the formwork

level of concrete in the both wall sides and the concrete pumping window will change with rising concrete level. When the concreting level is reached to the top, concreting will be carried out from the top row of windows from one side to the other sequentially in the longitudinal direction.

9. Formwork removal and curing

Formwork is removed after keeping for the recommended period. In some extreme cases, the form removal time can be as low as 16 hours from construction. And then curing will be conducted using water or covering sheets. There are many techniques utilized in tunnel lining curing and some are shown in Figure 2.12.

(a) (b)

(c) (d)

Figure 2.12 Various curing methods for second lining (a),(b) balloon curing with water supply different support system (c),(d) sheet curing without water supply – different type of sheets

2.4 Previous research regarding cracking of the concrete second lining

It can be seen from available literature that cracking of second lining of NATM tunnels was a concern for more than a decade in Japan. Some studies carried out with the objective of crack mitigation of NATM tunnel lining can be found and important research data were extracted from reliable sources. Some of the important previous research data are presented in section 3.1 since those were directly utilized for finite element modeling.

2.4.1 Previous research related to simulation of tunnels

Lots of past studies can be found on simulation of tunnel structures [2-6], but very few important studies are summarized in this section.

In a study carried out by Nakamura et. Al. [7], appropriate modeling parameters for thermal analysis have been investigated utilizing a back-calculation process with a particle swarm optimization technique. The values suggested in the study for some thermal properties of some components are higher than standard properties suggested in JCI guideline for mass concrete structures [8]. In addition, the air temperature profile in the vertical direction of the tunnel was

assumed utilizing site measurement data. This idealized air temperature distribution will be utilized in this study and details are mentioned in section 3.2.

Another important study was carried out regarding simulation of concrete structures for thermal behaviour by Ohno and Hosoda [9]. Main observations were the heat transfer coefficient of the surface of the formwork (before formwork removal) can be considerably lower than the values suggested by standard specifications[8].

2.4.2 Previous research on construction methods of lining systems of NATM tunnels

In Japan, tunnel lining construction companies pay utmost attention to improving second lining concrete quality by improved construction methods. Some important researches are summarized in this section.

High ETAS (Endurance Tunnel Arch Structure) is a tunneling method used in NATM tunnels used to improve the waterproofing action and increase the durability of tunnel lining. In this method, the shotcrete surface is made smooth by a filler material to reduce the surface unevenness and to make sure the proper attachment of waterproofing sheet to the surface of the second lining. Shirane et al. [10-11] carried out a study to investigate the stress reduction effect of tunnel lining with high ETAS method. From the measurement results, an apparent reduction of concrete temperature at the crown was observed and the reason was stated as the reduction of concrete volume due to uniform shotcrete surface. Regarding the transverse stress at the crown, stress was mentioned in two tunnel sections constructed with and without High ETAS method. In both blocks crown transverse stress was in tension at the middle of the section and the block using high ETAS method has shown a reduction of tensile stress at the middle. Related to the study by Shirane et al., it should be noted that the idealized analysis executed in

Figure 2.13 Surface of waterproofing membrane (a) Without using high ETAS (b) with high ETAS method

this study assumed a uniform thickness of second lining. Hence, there is a possibility of underestimating the stress results in the analysis due to this assumption. Two tunnel sections constructed with and without High ETAS method are shown in Figure 2.13 [11].

Another important study was carried out by Nishioka et al.[12-14] regarding advantages of prolonged formwork retention in NATM construction using telescopic (Twin Arch Form – TAF) . The study has claimed that quality improvement of second lining can be achieved by moisture retention and extended mechanical support. Further details are available in Kajima Construction Corporation website [14] which claims the denseness of concrete and the strength development are improved with TAF construction and prolonged form retention with laboratory experiments.

A new concreting methodology to ensure proper concreting of shoulder and crown part of NATM tunnels called Meistercrete [15][16] (マイスタークリート in Japanese) is utilized by Nishimatsu construction Co Ltd. This construction method utilizes special strategies such as pressure and contact sensors at the crown to ensure proper concrete filling, special horizontal vibration method to compact concrete at crown part etc. A detailed study regarding Meistercrete was done by Sato and Ito [17]. They found that the concrete quality close to the crown could be improved with Meistercrete method from a series of laboratory experiments where measured the concrete quality at the crown was measured with SWAT [18] (surface water absorption test)

Other two construction systems are utilized by Maeda Corporation to ensure proper concreting of second lining called the multi-lining system and HDL system[19]. Both systems are comprised of improved strategies to pour concrete in second lining construction [20-21].

2.4.3 Previous research related to geotextiles related to tunnel lining

A few important literature related to thermal properties of geotextiles are mentioned in this section.

Singh and Bouzza [22] carried out an experimental study related to determining the thermal conductivity of geosynthetics including non-woven polyester geotextiles widely utilized in tunnel waterproofing membrane. It was discovered that the thermal conductivity could highly depend on the water content of wet geotextiles and also depend on the characteristics of geotextile such as hydrophobic or hydrophilic. The thermal conductivity of waterproofing sheet used in the current study was decided based on outcomes of Singh and Bouzza.

The effect of calendaring process for thermal properties of geotextiles was studied by Kopitar et al[23]. while the thermal properties of non-woven geotextiles with reclaimed materials were investigated by Saktivel and Ramachandran[24]

2.5 Short and long term behaviour of concrete structures

This study can be roughly divided into two phases considering the time dependency of concrete structures as short-term behaviour and long term behaviour. The dominating loads for each case will be different based on the structural conditions and the material behaviour. The major parameters and variables considered for each phase are introduced in this section.

2.5.1 Factors affecting the short-term behaviour of second lining of NATM tunnels

The phrase "Short-term" can be defined based on many aspects such as design life, liability period of the contractor etc. For the current study short-term was considered as around 20 days from construction where the major cause for cracking include heat of hydration, the effect of self-weight upon form removal, restraint due to formwork or form removal time, initial concreting temperature, the strength of the joints and curing conditions.

1. Heat of hydration

Volume change of early age concrete due to heat of hydration is known as a cause for early age cracking in mass concrete [8] [25] . Even though volume change due to hydration might not have any effect on unrestrained concrete, restrained concrete can generate cracks due to high stress concentrations close to the restrained edges[26]. In second lining concrete, the restraint caused by invert is commonly considered as the reason for vertical cracks starting from the bottom of the lining. In very thick structures such as dams or footings the temperature gradient inside the concrete can induce internal restraints leading to early age cracking. But for second lining, cracking due to internal restraint will be hardly generated because the thickness is not very large (about 400mm – 500 mm)

2. Effect of self-weight due to formwork removal

As shown in figure 1.1 second lining is separated from the first lining by a waterproofing sheet which has a very smooth surface. Therefore, the bond between the first and second lining can be ignored [27]. Due to the self-weight, there is a possibility of tensile stress generation due to bending moment generation close to the crown which can help the longitudinal crack development.

3. Formwork removal time

Formwork removal time can affect the stresses in the second lining in two ways. First one is the bending stress caused by self-weight as mentioned above. Especially in second lining construction, form removal time can be as small as 16 hours in some cases. The other one is the stress caused by the restraint of formwork itself. If the formwork is kept for a prolonged time, formwork itself can act as a restraint to the volume changes of concrete leading to increased stress conditions and ultimately cracking. This effect will also be studied in this study. But it should also be noted that some improvement of concrete properties might be achieved with prolonged formwork retention[12].

4. Initial concreting temperature

The initial concreting temperature refers to the temperature of fresh concrete at the time of placing as well as the temperature of the location where concrete is placed. This is primarily important because the ultimate temperature due to the heat of hydration can increase with the increase of initial concreting temperature leading to higher volume change which will ultimately increase the stress due to external restraints. Initial concreting temperature can vary with the season of the year due to the change of environmental temperature. Some measured data regarding the seasonal variation of fresh concrete before placing is shown in Figure 2.14 extracted by measurements done by Taisei Corporation.

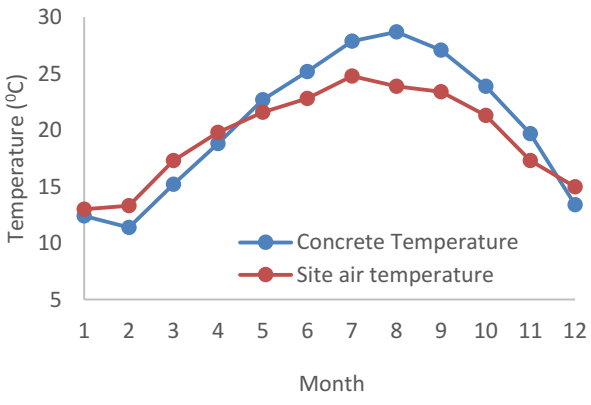

Figure 2.14 Concreting temperature and site temperature during a year

5. Curing conditions

It is well known that the method and the duration of curing have a considerable effect on concrete quality. Appropriate curing aids proper strength gain and low porosity which help

concrete to be resistant to cracking. In terms of the short-term behaviour of lining concrete, moisture or sealed curing can reduce the temperature effects because the form removal is done at a quite early age. But the important fact is that tunnel lining can be one of the difficult and expensive structures for water curing. Some curing methods are shown in Figure 2.12.

6. Joint strength

Three type of joints can be identified for the second lining concrete. First one is the joint formed due to waterproofing sheet at the back of the surface, the second one is the horizontal joint between invert and the second lining and the third one is the vertical joint formed due to construction joint between two blocks. The strength of these joints mainly defines the restraint conditions for deformations both due to the volume change of concrete and due to self-weight. The importance of the joint conditions is described in the modeling assumptions mentioned in chapter 3.

7. Autogenous shrinkage

Autogenous shrinkage of concrete occurs due to contraction of concrete due to water loss from the utilization for the hydration reaction [28]. Same as the hydration heat, autogenous shrinkage is also started at an early age of concrete and progress with the hydration. A considerable degree of autogenous shrinkage can be generated during first 30 days and some design codes [8] assume almost all the autogenous shrinkage is developed in this period.

8. Creep of early age concrete

Creep of concrete occurs due to the expulsion of water from the microstructure of concrete due to applied load. There are two types of creep called basic creep which occurs without any drying due to the applied load and drying creep which occurs due to moisture loss to the environment under applied load. Creep strain can be high in early age concrete.

2.5.2 Long term behaviour of concrete second lining

In the current study, "Long-term" is defined as around several years (at most around five years) from construction. The major reason for this definition is the fact that the liability period for contractors (in Tohoku region) is five years, in which contractors have to perform the crack repair by own expenses. Driving forces for the long-term cracking include drying shrinkage, load sharing between the first and second lining and seasonal environmental variations.

1. Drying shrinkage

Drying shrinkage occurs due to water expulsion from concrete to the outside air due to the lower humidity in the dry air. Unlike autogenous shrinkage which can have an almost uniform strain distribution throughout the structure, drying shrinkage will vary from drying surface to the inner of the element which can cause internal restraint. As tunnels are not directly exposed to the environment the drying shrinkage strain variations in the inner parts of long tunnels can be significantly different from the behaviour close the mouths of the tunnel. Another aspect is the possibility of dew formation on the concrete surface in cold conditions or in humid conditions which will greatly reduce the drying shrinkage. Especially relative humidity measurements done in some studies [29] suggest the relative humidity inside the tunnel before putting into operation can be as high as 85-90%. But when under operation these values might decrease considerably because of the wind accelerated by the movement of vehicles.

In summary, the effects that should be considered with respect to drying shrinkage include the location - inside or close to the tunnel mouth and the operational conditions to determine a realistic humidity value in considered portions of the tunnel.

2. Load sharing between second lining and first lining

According to the design concepts of NATM tunnel lining systems explained in section 2.2, it should be noted that the level of loading on the second lining depends on the design requirement itself. But with time, the stiffness of the first lining can be reduced due to several factors such as deterioration of rock bolts, fault movements etc. In such cases, the second lining will start to act as a structural element which supports part of the structural loading due to soil/rock overburden. The amount of load sharing will depend on many factors such as bond stiffness between two lining systems, rock mass stiffness, the level of deterioration of the first lining etc. In this study the load sharing between lining systems was not considered as a major cause of cracking as the level of deterioration within five years can be assumed as very low and the load sharing inherently makes much of a limit state condition which should be addressed during the design stage.

3. Seasonal changes in environment conditions

Air temperature and relative humidity will change in the environment depending on the season and can affect the volume change due to drying and thermal expansion. These changes in environmental conditions might cause stress variations in the second lining.

2.6 Simulation schemes

Two simulation tools were used for finite element modeling of the second lining of tunnels due to specific advantages and disadvantages of two different tools.

The primary simulation tool is known as ASTEA-MACS by Research Center Computational Mechanics (RCCM).Inc [30]. This FEM package is specially designed for concrete structural analysis and mainly for thermal stress analysis of mass concrete. It is a design oriented analysis tool and provides very flexible options to execute rich parametric studies. Constitutive laws of materials can be defined by code equations or based on experimental data.

Link3D is a software developed by the concrete laboratory of The University of Tokyo and consists of advanced multiscale constitutive models for concrete, steel, and interaction between concrete and steel. For this study, LINK3D will be utilized to estimate the drying shrinkage of concrete.

A basic introduction to the underlying theory of each simulation tool related to the current study is summarized in this section.

2.6.1 Theoretical background of ASTEA-MACS

Astea-Macs is based on general finite element formulations and special features of the software are described in the software manual [31]. Some of the important theories that are utilized in the study are explained in this section.

2.6.1.1 Element type for general analysis

The primary element type available for thermal and concrete stress simulation is a linear hexahedral isoparametric element with nine integration points. Schematic figure of such an element is shown in Figure 2.15 [32]. Constitutive models can be defined based on

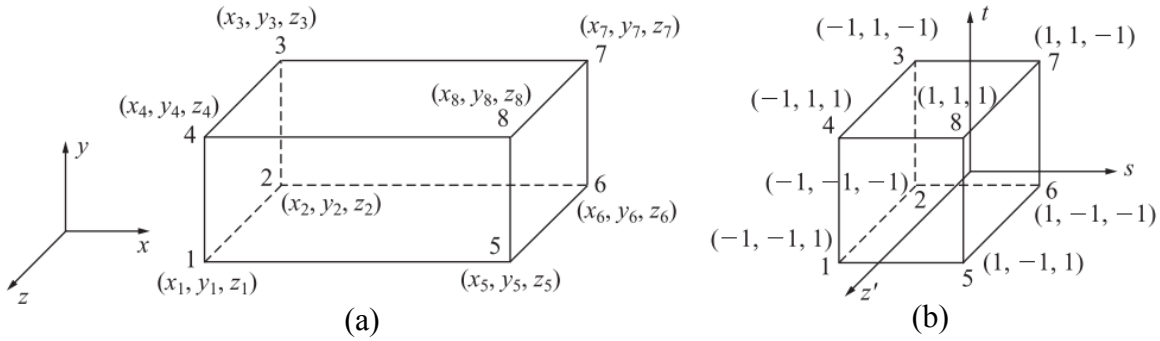

Figure 2.15 Isoparametric formulation of finite element (a) In global coordinates (b) In natural coordinates

experimental data or based on code equations [8] [33]. Cracking of concrete cannot be simulated using normal elements in this software. However, cracking risk can be obtained as Thermal cracking index as defined in JCI guideline [8].

2.6.1.2 Joint Element model

Joint elements in Astea-Macs are utilized to model the joint formed by waterproofing sheet and the vertical construction joints in between two lining blocks. The joint elements are capable of modeling the normal and shear behavior of the joints while thermal properties can also be defined. The definition of stress-deformation relationship of the joint elements for normal and shear directions are shown in Figure 2.16

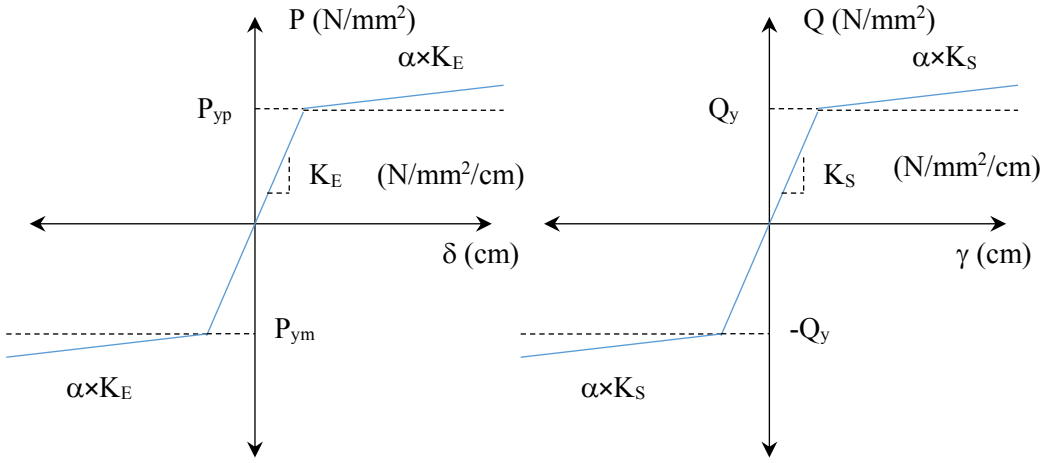

Figure 2.16 Stress deformation behaviour of Joint element

Values of K_E and K_S should be calculated from Equation 2.1 and 2.2 where E is the young's modulus of the actual joint material, υ is the poisons ratio and h is the shortest dimension of the joint element. P_{ym} P_{yp} and Q_Y defines the failure load for normal compression loads, normal tensile loads and shear loads respectively and should be defined as failure stress in N/mm^2 Further information about the joint element model such as local coordinate system definition can be fiound in the software manual[31].

$$K_E = E(1-\upsilon)/(\upsilon+1)(1-2\upsilon)/h \qquad \text{Equation 2.1}$$

$$K_S = \upsilon K_E/(1-\upsilon) \qquad \text{Equation 2.2}$$

An important point to be noticed is that in the default joint model the coefficient $\propto$ which defining the slope of the stress-displacement curve after yielding was set to 0.01. But it was observed that this value was not sufficient to model the displacement behaviour of second

lining after the separation hence the inbuilt model was modified to use appropriate values with the collaboration of RCCM inc.

2.6.1.3 Compensation plane method

Compensation plane method is an analysis method used to determine the restraining stresses due to volume changes caused by temperature effects. This method is utilized in the simulation system and basic theory can be found in [33-36].

2.6.1.4 Time integration and solver options

Time integration options of the software can be set to explicit Forward Euler method or implicit Crank-Nicolson method and Backward Euler method [32]. The most accurate method is known as Crank-Nicolson method with smaller time steps but can generate fake oscillations in simulation results if temperature gradients are considerably large and time step size is also large [32]. Backward Euler method is suitable for larger time steps and accurate as well [37].

Two solver options are available in the used software version direct integration solver is the Skyline solver and iterative solver Conjugate gradient solver (CG)[38-39]. CG solver is faster for the current purpose.

2.6.2 Theoretical background of LINK3D

Link 3D is a software developed based on decades of research carried out by the concrete laboratory of the University of Tokyo. The theoretical background is well explained in textbooks published by the developer [40-43]. For the sake of completeness, their simulation concepts are shown in figures extracted from reference [42].

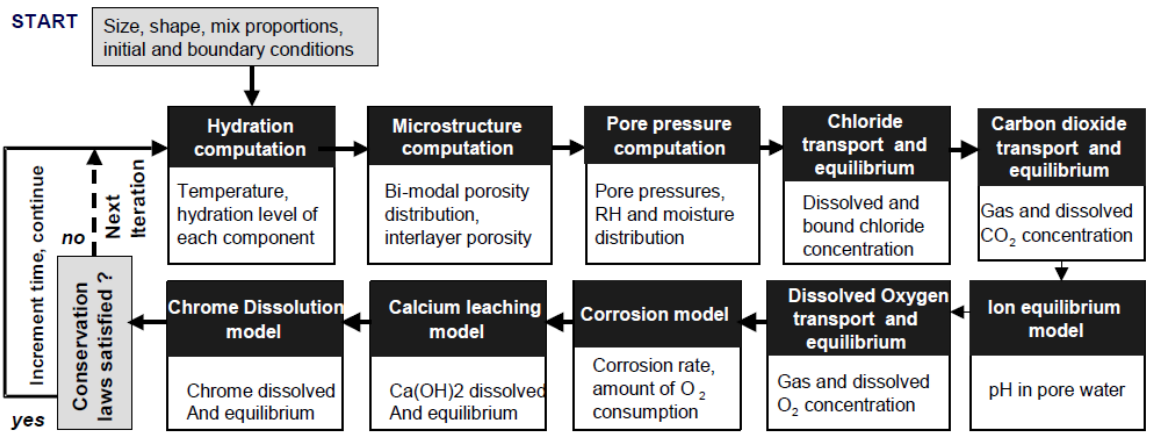

Figure 2.17 Computational scheme of DuCOM

The software comprises of two modules namely DuCOM and COM3. The first module, DuCOM, is the material simulation module and the computational scheme is shown in Figure 2.17. Although simulation scheme is capable of modeling many aspects of concrete, for this study only hydration, microstructure computation, and pore pressure computations were utilized. Macro structural properties of concrete are calculated by DuCOM module and are used in the COM3 module for stress analysis. Multiscale constitutive models in DuCOM extracted from Yoneda et al. [44] are shown in **Error! Reference source not found.**.

2.6.2.1 Modeling of shrinkage in LINK3D

As LINK3D is used to calculate the drying shrinkage strain of second lining concrete, the modeling concepts of shrinkage is briefly described in this section.

Modeling of shrinkage strain in LINK3D is done considering five main aspects [40] and can be divided into two groups that are factors related to cement paste and factors related to aggregate properties.

The first mechanism is related to the condensed water in capillary pores of cement paste structure and the stress incorporated is modeled using equation 2.3. The driving force for shrinkage stress is explained as the surface tension of condensed water acting of gel microspore structure of cement paste.

$$\sigma_{sc} = \beta . P \qquad \text{Equation 2.3}$$

In Equation 2.3, σ_{sc} is the shrinkage stress related to the decrase of pressure of condensed water, P is the capillary tension of the condensed water in the pore structure. β is an effective coefficient for the volume acted upon by the capillary tension and can be calculated with the multiscale model.

The second mechanism is related to the adsorbed water in micropore structure. The mechanism is explained as the increased surface energy of solid gel particles due to the removal of adsorbed water around the solid particles. Shrinkage strain due to increased solid surface energy is modeled with the Equation 2.4 in DuCOM. In the equation, σ_{sd} is the shrinkage stress related to adsorbed water, S_{sd} is the distribution density function for surface tension (1/m) and calculated with combination of micro pore structure model. γ is the surface tension of gel particles.

$$\sigma_{sd} = S_{sd} . \gamma \qquad \text{Equation 2.4}$$

Factors related to aggregate properties include three aspects. First the Young's modulus of the aggregates which can restrict the shrinkage strain of cement paste. The second one is the aggregate porosity which can affect the shrinkage by releasing absorbed water or vice versa. Both these concepts are included in the complicated DuCOM constitutive law and is not explained here as a lengthy explanation is necessary to explain the calculation of composite structural properties and moisture interaction model with aggregates.

The fifth factor is the intrinsic shrinkage of aggregates. Which is molded by adding the intrinsic shrinkage of aggregates to the calculated volumetric strain as shown in Equation 2.5.

$$\varepsilon_{ag} = \frac{1}{3K_{ag}}\sigma_{ag} + \varepsilon_{ag}^{sh} \qquad \text{Equation 2.5}$$

In the equation ε_{ag} is the total volumetric strain of aggregate, σ_{ag} is the volumetric stress of aggregate, K_{ag} is the volumetric stiffness of aggregate (bulk modulus) and ε_{ag}^{sh} is the intrinsic shrinkage strain of aggregate.

2.7 Summary

Essential construction details of NATM tunnels, past research about the second lining of NATM tunnels and the details of simulation schemes were described in this section.

Major conclusions that can be drawn from the section can be summarized as follows.

1. Many individual contractors have tried to achieve good quality concrete second lining and mitigate the stress in second lining concrete by developing new construction techniques.
2. Investigations related to stress generation of second lining utilizing finite element method (or other analytical techniques) are relatively small in number.
3. Considering some investigations done by field measurements, the idealized simulation results might underestimate the crown stresses compared to field measured values due to the neglecting of uneven shotcrete surface which might increase the second lining concrete volume.

3 FINITE ELEMENT MODELING OF SECOND LINING

Finite element method is widely utilized to solve engineering problems with complex behaviour patterns. For this study finite element method was utilized to understand the stresses generated in second lining concrete of NATM tunnels. The modeling was divided into two sections. First, modeling to investigate the stresses conditions within a short period of time after casting was carried out. The stress in this period was expected to be governed by thermal effects. Second, the modeling was extended to include the effect of drying shrinkage.

Short term stress behaviour of second lining was carried out utilizing a commercial finite element modeling software called "Astea-Macs". Finite Element modeling package is specially designed to utilize for analysis of concrete structures and widely used by design companies for thermal stress analysis. Model calibration to study short term behaviour was carried out with the reference to actual tunnel measurement data obtained from a past research[29]. Modeling parameters were carefully selected based on past research or considering actual site conditions. Site measurement and experimental data utilized for model verification are described with sufficient details in the first section of this chapter.

The long term stress patterns of the second lining depend on both structural loading and environmentally induced loading in varying environmental conditions. Mainly the stress due to long term drying shrinkage will change with respect to exposed environment. The integrated concrete material model in the software, Link3D, is capable of assessing the macro structural components such as long term drying shrinkage, concrete creep etc..., with respect to components such as microstructure development and moisture movement in microspores in concrete. Therefore Link3D could be effectively used with proper engineering judgment to assess driving for cracking induced due to environmental changes in combination with inherent concrete material behaviour.

The structural behaviour of the second lining mainly depends on the self-weight and joint conditions except the load induced due to environmental effects. The restraint due to various joints was observed to be playing a major role in stress variations. Therefore a logical way of

simulating the second lining of NATM tunnels considering environmentally induced loading and nonlinear structural behaviour is presented in this chapter.

3.1 Field measurements related to cracking of concrete second lining of NATM tunnels

Field measurement data extracted from a study carried out by Taisei Corporation[29], played a vital role in this study as those information were utilized for verification of the finite element model used to study short term stress behaviour governed by thermal movements. The material behaviour to assess long-term drying shrinkage was mainly verified utilizing the results of an experimental study carried out by Nishimatsu Construction Corporation. These measurement and experimental data are presented in this section with sufficient details.

3.1.1 Structural monitoring and experimental studies by Taisei Corporation

The main objective of the study was to confirm the effectiveness of expansive additive to control stress generation of the second lining. The measurement plan included measurements in blocks constructed with normal concrete and blocks with expansive. For the current study, measurements done in blocks constructed only using normal concrete were utilized. The measurement points and the structural dimensions are shown in Figure 3.1.

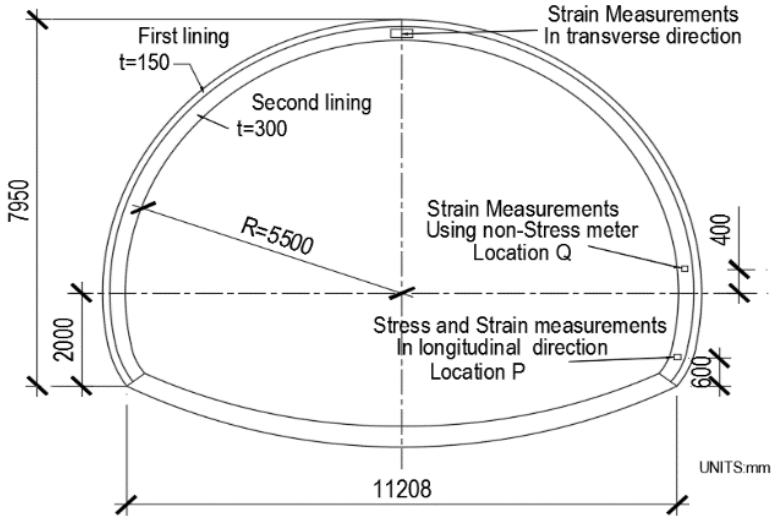

Figure 3.1 Measurement points and quantities in real tunnels extracted from literature

The measurement results included the environmental quantities such as relative humidity variation and temperature variation inside the tunnel, and the quantities related to structural behaviour included the temperature variation of concrete at location P and crown, longitudinal stress and strain measurements close to the invert at location P as well as strain measurements

with non-stress meter close to the invert at location Q, and only the transverse strain was measured at the crown. All measurements were conducted at the middle thickness of the second lining.

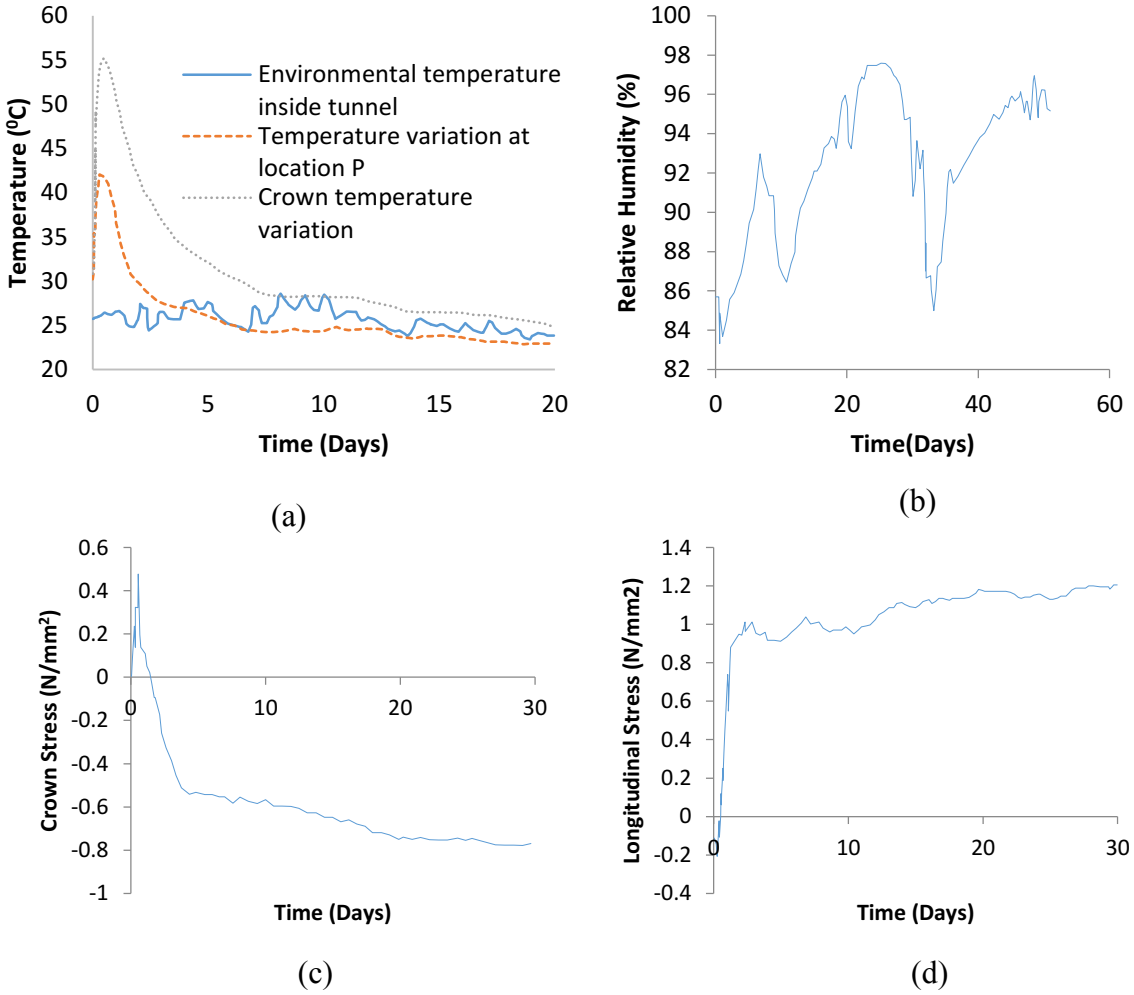

Figure 3.2 Measured quantities by Taisei (a) Temperature variations (b) Relative humidity variation at site (c) Crown stress variation (d) Longitudinal stress variation

As only the crown strain was measured, a calculation process of the crown stress was included in the paper. First, by comparing the structural strain measurements and the isolated concrete strain measurements done with a non-stress meter, the effective strain was calculated for location P. By multiplying this effective strain with appropriate young's modulus, longitudinal stress was calculated for the same location. This calculation process was verified by comparing measured and calculated stresses. Then the same calculation process was applied to crown strain measurements to calculate the crown transverse stress assuming the isolated concrete strain measured at location Q remained constant in the whole structure. The difference

of temperature between the crown and location P was appropriately considered in calculating the crown stress. This computed stress at the crown was also included and utilized for this study as it represented the major cause for longitudinal Type A cracks close to the crown. Site measured temperature and humidity, calculated crown stress and measured longitudinal stresses are shown in Figure 3.2. Furthermore, lab experiments were carried out to obtain concrete properties and are summarized in Figure 3.3, Figure 3.4 and Figure 3.5.

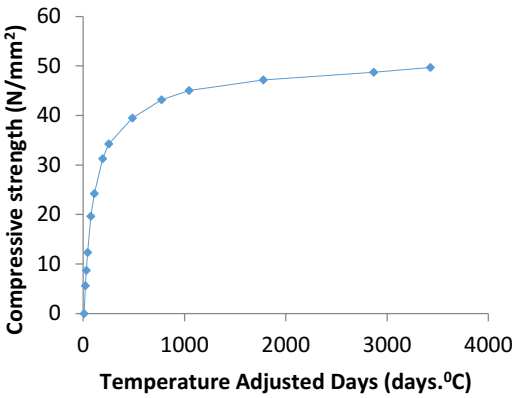

Figure 3.3 Compressive strength development measured from laboratory tests

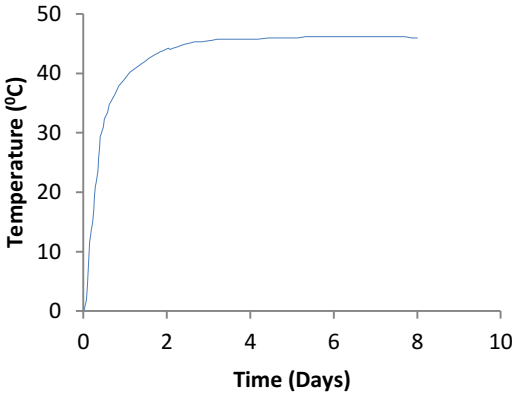

Figure 3.4 Adiabatic temperature rise calculated from laboratory tests

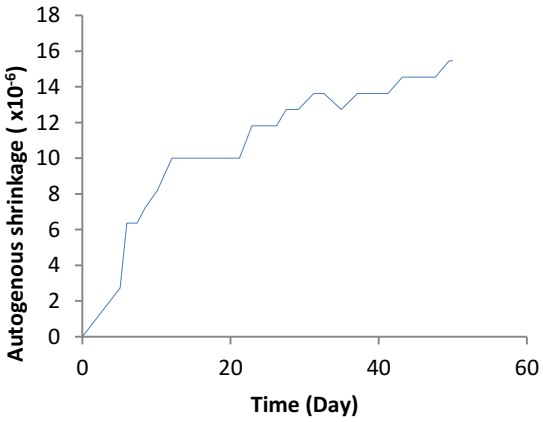

Figure 3.5 Autogenous shrinkage measured by tests

Young's modulus and tensile strength of concrete are also investigated and presented in the form of equations

$$f_t = 0.176 f_c'^{0.8} \qquad \text{Equation 3.1}$$

$$E_c = 10370 f_c'^{0.326} \qquad \text{Equation 3.2}$$

Where f_t the tensile strength of concrete is, E_c is the Young's modulus of concrete and f_c' is the unconfined compressive strength of concrete.

Concrete mix proportions used for the second lining are shown in Table 3.1. The temperature of concrete at casting was measured as 30.9 ^{0}C at location P and 29.8 ^{0}C at the crown.

Table 3.1 Concrete mix proportion used for tunnel investigated by Taisei

Max aggregate size -20mm, Slump – 15, Air entrant – 4.5%						
W/B	S/A	Kg/m^3				
%	%	water	cement	sand	gravel	admixtures
52.9	44.2	169	319	788	1031	3.19
Cement is normal Portland cement						

3.1.2 Structural monitoring and experimental studies for Kodsuchi tunnel constructed by Nishimatsu Construction Co. Ltd.

More recent study of tunnel second lining behaviour was carried out by Nishimatsu Construction Co. Ltc. in the construction of Kodsuchi tunnel in Tohoku region. Main measurements included the temperature and longitudinal stress measurements close to the invert and temperature measurements close to the crown. Standard laboratory experiments according to JIS1192-3 were carried out to find the drying shrinkage of concrete utilized for

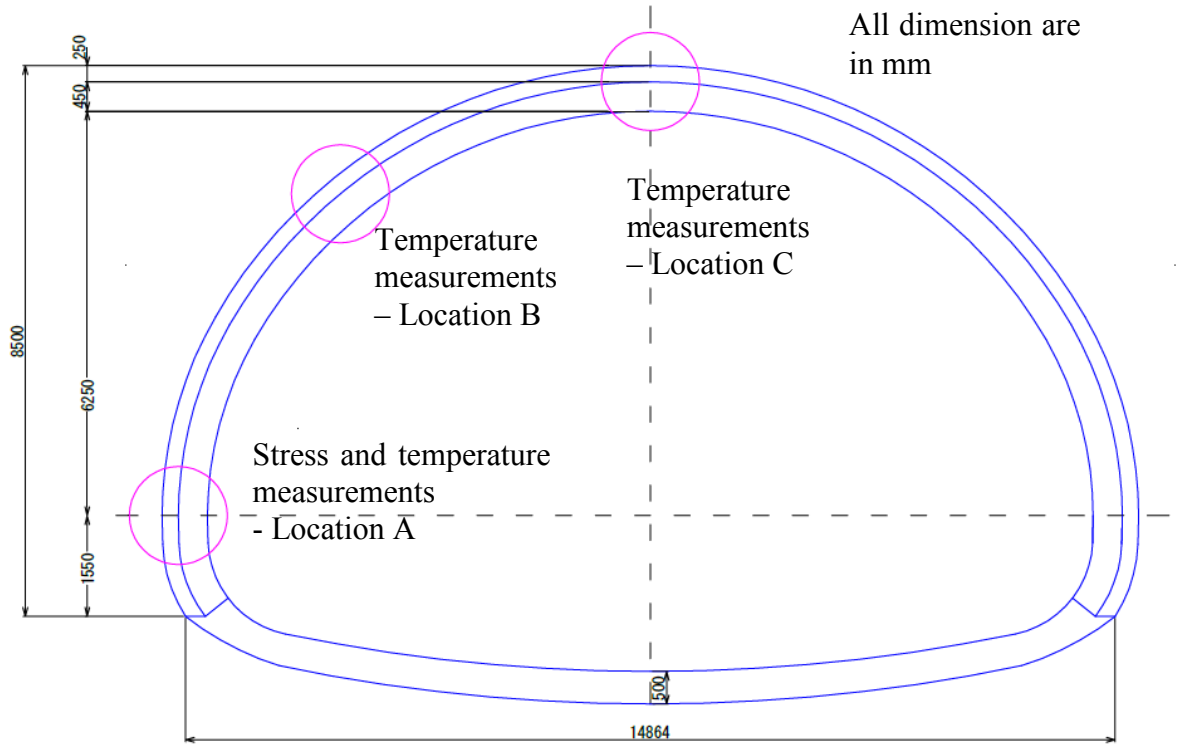

Figure 3.6 Measurement locations and tunnel dimensions of Kodsuchi tunnel

the construction of several blocks of tunnel including the monitored ones. Tunnel dimensions and measurement locations are shown in Figure 3.6.

Temperature measurements and longitudinal stress measurements close to the invert at location A are shown in Figure 3.8. These measurements were utilized for model verification used for long term stress behaviour considering drying shrinkage

Table 3.3.2 Mix proportions used in Kodsuchi tunnel

Max aggregate size -20mm, Slump – 15, Air entrant – 4.5%						
W/B	S/A	Kg/m^3				
%	%	water	cement	sand	gravel	admixtures
51.0	52.4	155	304	978	901	4.26
Cement – Blended cement – Blast furnace slag cement class B						

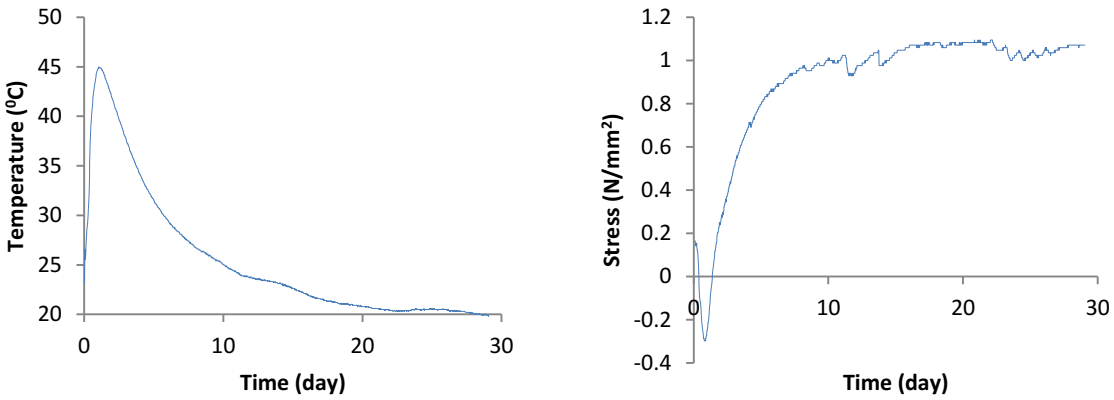

Figure 3.8 Measurements close to invert in Kodsuchi tunnel (a) concrete temperature (b) longitudinal stress

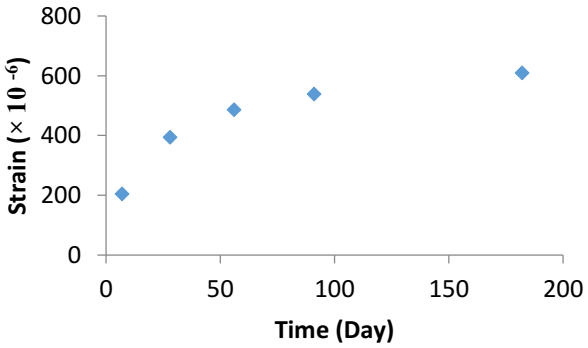

Figure 3.7 Drying shrinkage values measured by standard JIS tests

.

Laboratory experimental results using standard drying shrinkage test is shown in Figure 3.7.

3.2 Establishing finite element simulation scheme for second lining of NATM tunnels

Even though finite element method is widely used for engineering analysis, proper modeling techniques are essential with reasonable evidence and with engineering judgement. As the behaviour of second lining depends on a large number of parameters including material and environmental conditions, an attempt was made to establish a dependable simulation scheme to understand the stress patterns of second lining concrete with reasonable assumptions.

3.2.1 Major assumptions in modeling

Some major assumptions in the modeling will be explained here based on the site observations and site measurement data obtained from the literature explained in section 3.1.

1. Load sharing between first and second lining

The load transferred from first lining to second lining was assumed to be negligible in terms of normal tensile stress and shear stresses while the normal compressive stresses were considered to be effective. Although this assumption might be true for short term behaviour within about 30 days, it may not be very accurate for long term analysis as deterioration of first lining can transfer some loads to the second lining. The background details of this assumption are described in detail in section 2.2 and section 2.5.2.

2. Modeling the joints

Three main joints exist for a second lining block as shown in Figure 2.3. These joints define the level of external restraint to the movements of the second lining due to self-weight and due to volume changes in concrete and played an important role in the modeling process.

a) Joint 1(J1) - the joint formed in between second lining and first lining due to installation of the waterproofing layer

It is known that, in double shell lining systems, structural behaviour of the first and the second linings can be assumed as independent from each other [27]. Therefore, this joint was assumed to have no strength in terms of normal tensile or shear terms while normal compressive strength was assumed to be equal to the concrete compressive strength. The surface of the waterproofing sheet which faces the second lining is made of smooth EVA sheet which can be assumed to have no bonding capability with the concrete.

b) Joint 2 (J2) - The horizontal joint between the second lining and the invert

In some cases, the reinforcing bars embedded in the invert continues through this construction joint as shown in Figure 2.6. Therefore this joint was assumed to be a fixed joint which can transfer both shear and normal stresses.

c) Joint 3 (J3) - The vertical construction joint between the blocks

Negligible joint strength was assumed for this construction joint based on two factors. First one is the idea that the joint formed during construction will be weakened by the movements due to the volume change of concrete and the weakening will continue until the ability to stress transfer of the joint is lost. This assumption is done based on the observation that in many blocks a vertical crack appears and separation occurs along this vertical joint and in some cases lot of localized damage can be observed in close vicinity of the joint in the form of spalling. The second reason was that some contractors were already installing a plastic sheet in between the new and the old second lining blocks to reduce unnecessary friction leading to localized damage near the joint area as shown in Figure 3.9.

Figure 3.9 Installation of plastic sheet to prevent friction between construction joints between blocks

d) The formwork removal mechanism

In this research, formwork removal mechanism in the actual construction was assumed to be equal to the application of gravity load in the numerical simulation at the time of the formwork removal. The important factor to notice is that with this assumption any probable restrictions to volume changes of concrete that can be imposed because of the existence of actual form is not modeled in the simulation scheme.

3.2.2 Finite element modeling with Astea-Macs

A three-dimensional model was created to observe the stress behaviour at the crown and at Location P. All the assumptions mentioned in Section 3.2.1 were applied to the model and the completed model is shown in Figure 3.10 and components of the model are introduced. The step by step process to establish the finite element model is described in detail in this section.

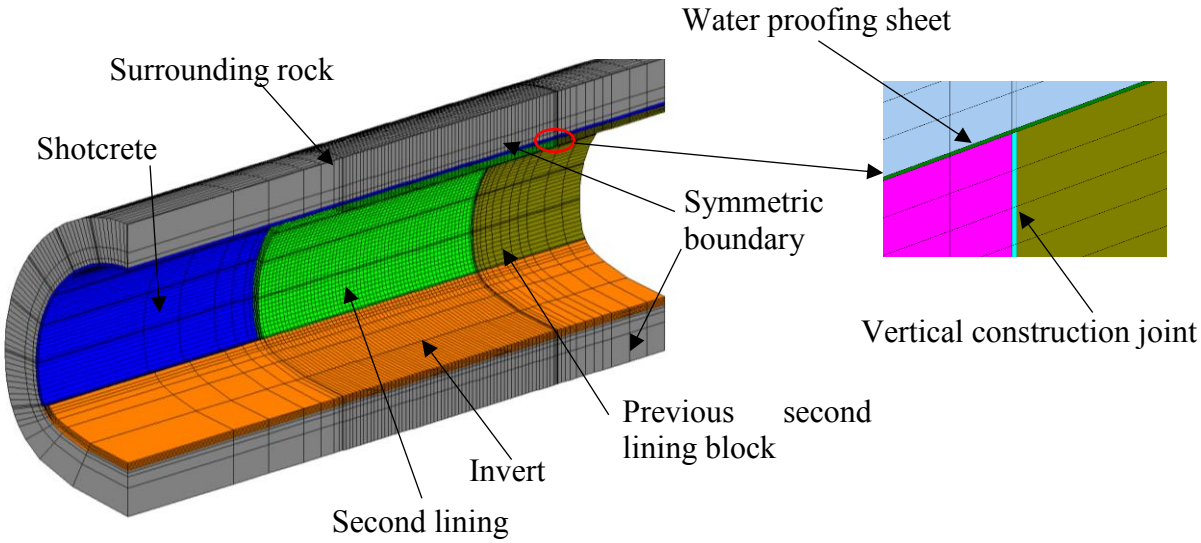

Figure 3.10 Completed model in Astea-macs

3.2.2.1 Determining the boundary conditions and material properties related to thermal analysis

To establish the finite element model the thermal and structural properties were initially decided in a logical manner based on previous studies and the experience. Then the mesh sensitivity and parametric studies were carried out to determine some properties which are not well established in previous studies such as thermal properties of waterproofing sheet.

1. Available material properties from laboratory experiments

Quantities related to concrete material properties which were available in the reference [29] are summarized in Section 3.1.1. Measured quantities include estimated adiabatic temperature rise, time dependent development of compressive strength, tensile strength and Young's modulus, and autogenous shrinkage. Those data were directly input to the software as time dependent material properties. In the case of compressive strength development, the temperature dependency of the compressive strength was also included as the compressive strength development was defined based on accumulated temperature. Tensile strength and Young's

modulus were modeled as functions of compressive strength as shown in Equation 3.1 and Equation 3.2.

Adiabatic temperature rise model is shown in Equation 3.3

$$T = K\left(1 - e^{(-\alpha(t-t_0)^{\beta})}\right) \qquad \text{Equation 3.3}$$

Values of K, α, β, and t_0 were calibrated to fit the model to the measured adiabatic temperature rise shown in Figure 3.4. The calibrated values are respectively 46.26, 1.85 , 0.8 and 0.

In JCI guideline [8], a simple equation is provided to simulate the creep of concrete by reducing the young's modulus as shown in Equation 3.4.

$$E_e(t_e) = \emptyset(t_e).E_c(t_e) \qquad \text{Equation 3.4}$$

$E_e(t_e)$is the effective young's modulus at age of t_e (Temperature adjusted age), $\emptyset(t_e)$ is the reduction coefficient and $E_c(t_e)$ is the actual Young's modulus of concrete at the age of t_e. the reduction coefficient should be specified in temperature increasing period and in decreasing period in early age concrete. These values were available in the paper by Usui et al[29] calculated from the site measurements. The coefficient was specified as 0.8 in temperature rising period and 0.64 in temperature decreasing period. (the default values included in JCI guideline is 0.42 and 0.65 respectively)

2. Determining the appropriate heat transfer coefficient values for convection boundaries.

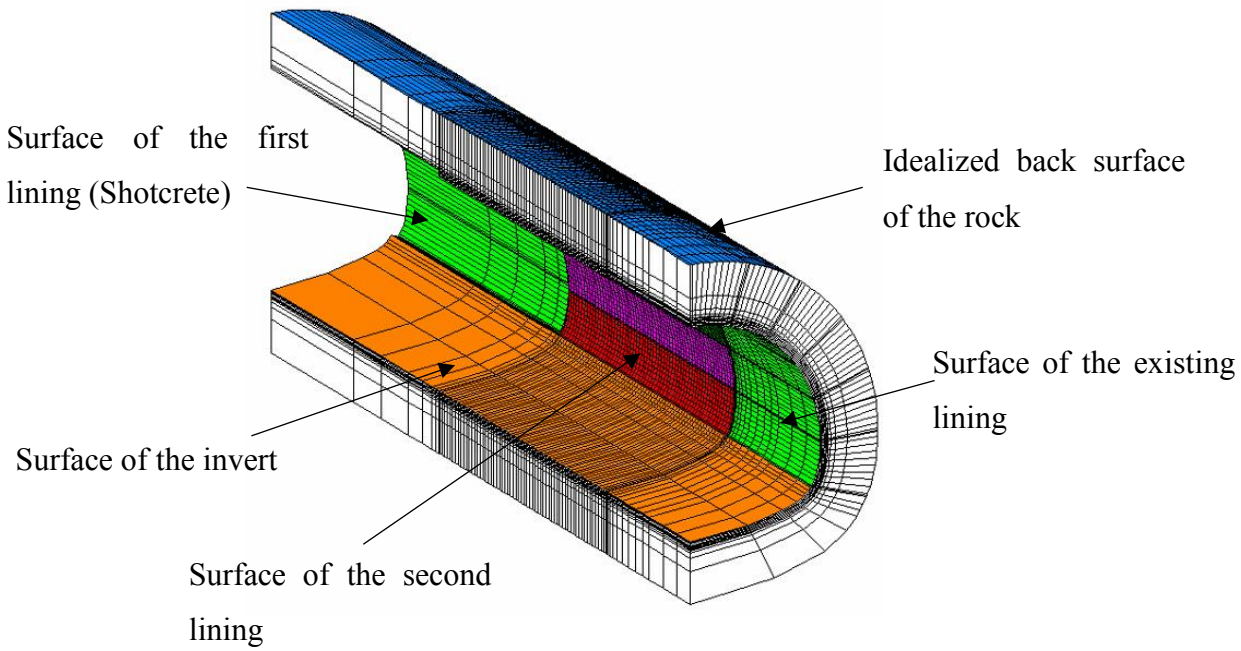

Figure 3.11 Definition of heat transfer boundaries

Heat transfer coefficients of the convection boundaries were set based on JCI standard values or based on the results of previous, similar studies. Main convection boundaries are shown in Figure 3.11.

The values of the heat transfer coefficients Table 3.3. Heat transfer coefficients used for convection boundaries are summarized in Table 3.3. In the case of second lining surface, the JCI [8] recommended value for both steel formwork surface and concrete surface is 14 W/m^2k^{-1}. But based on previous studies [7] [9], it was observed that the heat transfer coefficient of the concrete surface with formwork can be lower than the recommended value in the practical scenario for many cases. Therefore, it was set to 6 W/m^2k^{-1} before formwork removal based on the findings of [9]. Especially in tunnels, the heat transfer coefficient of the formwork surface can be reduced in some tunnels because concreting is done in a covered environment (Figure 2.10). Heat transfer coefficient of the invert surface was also set to a lower value considering the fact that this surface is covered by soil all the time. The thermal boundary condition for the back surface of rock was determined from 3.2.2.2. For other places, JCI recommended values were used.

Table 3.3. Heat transfer coefficients used for convection boundaries

Component	Heat Transfer Coefficient (W/m^2k^{-1})		Reference/ Reason
	Before formwork removal	After formwork removal	
Second lining surface	6	14	[9]/JCI[8]
Invert surface	6	6	Covered in soil
Existing lining surface	14	14	JCI [8]
Surface of the first lining	14	14	JCI [8]
Idealized surface of the rock	3.5	3.5	Section 3.2.2.2

3. Determining the thermal properties of materials

The established thermal properties for all the components are shown in Table 3.4. Thermal conductivity, specific heat, and density of second lining, shotcrete, invert and existing lining were set based on the recommended values by JCI [8] to be equal to properties of concrete. The thermal conductivity of waterproofing sheet was set based on a parametric study and the process is separately described in section 3.2.2.3. Specific heat and the density of waterproofing sheet were set based on a previous study [7].

Table 3.4 Material properties for thermal analysis

Component	Thermal conductivity W/(m ^{o}C)	Initial temperature ^{o}C	Specific heat kJ/(kg ^{o}C)	Density kg/m^3
Second lining	2.7	30	1.15	2400
Waterproofing sheet - top 1/3	0.246	20	2.3	1000
Water proofing sheet bottom - 2/3	0.0064	20	2.3	1000
Shotcrete	2.7	20	1.15	2400
Rock	3.5	15	0.8	2650
Invert	2.7	15	1.15	2400
Existing lining	2.7	20	1.15	2400

The initial temperature of each component was decided based on actual site conditions or with reasonable assumptions. In the case of rock, the temperature was set to a constant value of 15^0C based on the site observations and the experience by tunnel contractors. The Same temperature was set for the invert considering the fact that invert is also covered by soil. The initial temperature of second lining concrete was set as 30^0C based on the available data [29] . According to site measured environmental temperature shown in Figure 3.2 (a), it can be observed that the environmental temperature was varied around 25^0C. Therefore, simply considering steady state heat transfer between air and rock the initial temperature of other components were set to 20^0C

3.2.2.2 Determining the appropriate rock thickness for the finite element model

Appropriate rock thickness of the model should be determined to establish an accurate thermal analysis system by ensuring the appropriate heat propagation that can simulate the large soil mass in real structures. This was necessary to reduce the inclusion of undesirable deformations of soil layer due to self-weight. This task was accomplished by a simple parametric study by changing the rock thickness from a very large value to a small value. For this parametric study thermal conductivity of waterproofing sheet was assumed to equal throughout the section to a value of 0.3 W/ (m^0C).

The initial model is shown in Figure 3.13 and the heat flux of the back surface was assumed to be 0 for the initial part of the analysis. For this model during the analysis period temperature at the boundary of the rock was checked and made sure to be unchanged. Then based on the results of this model rock thickness was reduced to 2m and 1m to observe the temperature variations with respect to measured values at location P (Figure 3.1 and Figure 3.2 (a)).

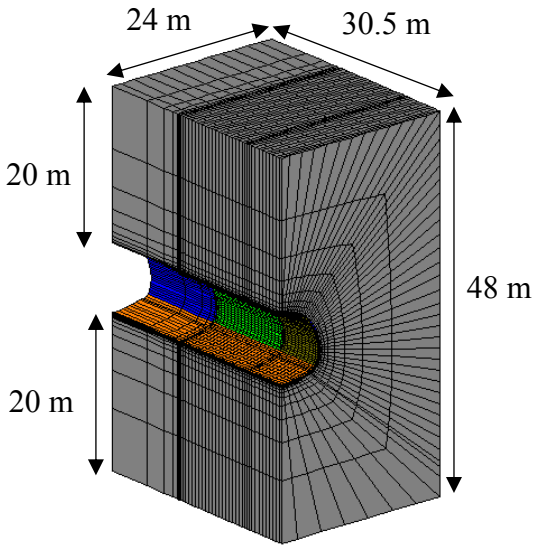

Figure 3.13 Initial model to determine the appropriate rock thickness for the model

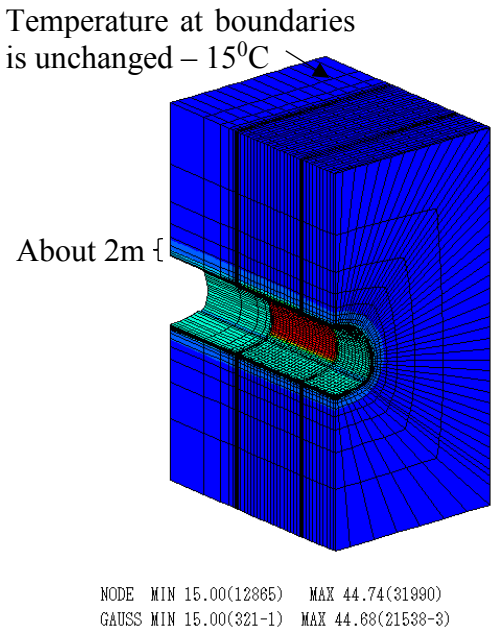

Figure 3.12 Temperature contours of initial model

Temperature variations at location P when rock thickness is changed are shown in Figure 3.14. It was observed that temperature variation was affected when rock thickness was reduced to 1m (with zero heat flux at the back surface of the rock). Therefore, the minimum appropriate rock thickness was determined as 2m without any assumed flux at the back surface of the rock. But finally, to reduce heat accumulation in the rock, heat transfer coefficient of the back surface of the rock was set to 3.5W/mK^{-1} and the temperature was set to 15^{0}C making sure the temperature variation of second lining was not affected by this setting.

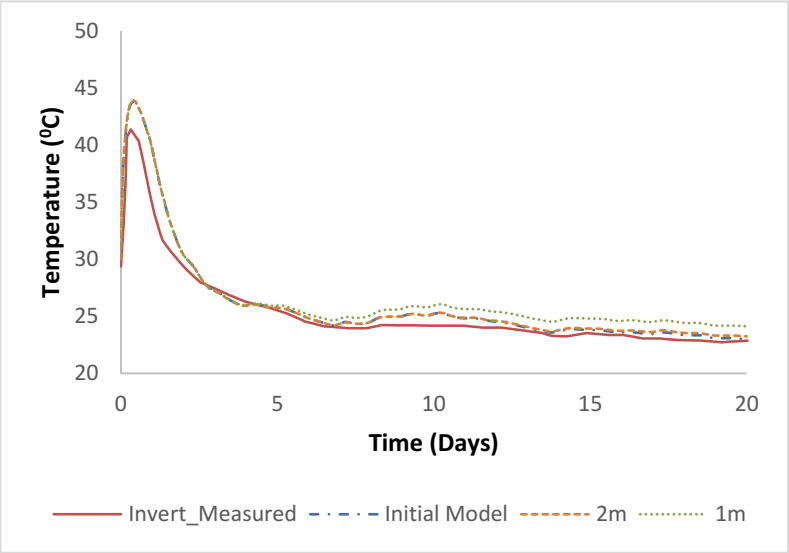

Figure 3.14. Temperature variation at location P close to invert with changing rock thickness

3.2.2.3 Setting the properties of waterproofing sheet

As described in section 3.2.1, in the mechanical point of view, waterproofing sheet was assumed to behave as a joint which does not have any strength in normal or shear behaviour. In the same time, the thermal properties were also given a considerable attention as none of the past studies that came across have taken the composite nature of the waterproofing sheet into account when defining the thermal properties.

1. Thermal properties

Waterproofing sheets used in NATM tunnels in Japan consist of two components namely EVA (Ethylene Vinyl Acetate) [45] waterproofing sheet and a polyester geotextile [46] as shown in Figure 2.8. Actual components and a schematic figure with measured dimensions are shown in Figure 3.15. It could be observed that the thermal properties of the composite material are not well established and in some previous studies, the thermal properties of the composite material have been assumed to be equal to the properties of EVA sheet[7]. But in this study, an attempt was made to estimate the thermal properties of the composite material in a more rational way considering the properties of individual components.

When the thermal properties of individual components are considered, density, thermal conductivity and the specific heat capacity of EVA sheet were obtained from reliable sources and known to be 1000 kg/m^3, 0.3 W/m^{0}C, and 2.75 kJ/kg^{0}C respectively. Important studies about thermal properties of nonwoven geotextiles could be found in [22-24]. From these the

thermal conductivity of polyester geotextiles under dry condition was obtained based on a investigated by Singh and Boussa [22] and the mean value was found to be 0.085 W/m^{0}C .

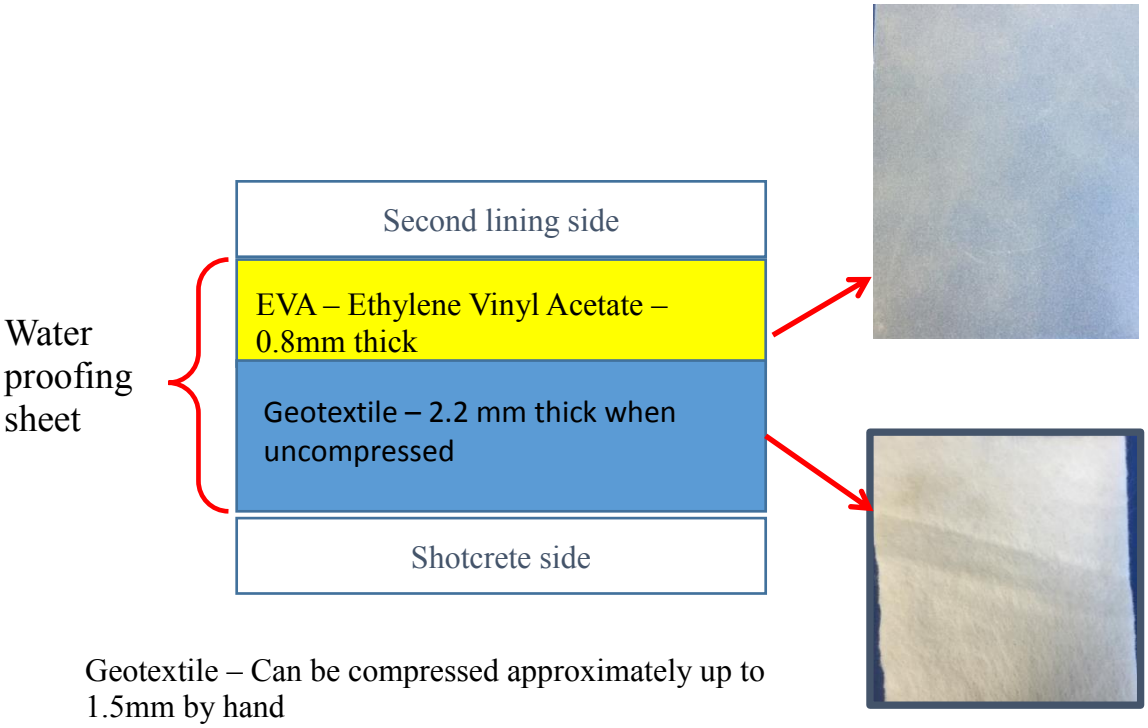

Figure 3.15 Arrangement and dimensions of the composite waterproofing membrane

In a previous study carried out by Nakamura et. Al [7], specific heat and density of waterproofing sheet were set to 2.3 kJ/kg^{0}C and 1000 kg/m^3. In the current analysis, these two properties were assumed to be the same the study by Nakamura et. Al. But the thermal conductivity of composite material was calculated assuming steady state thermal conduction based on thermal resistance. If the thermal conductivities of EVA sheet, Geotextile, and Composite waterproofing sheet are K_e, K_G, and K_{com} , for steady state heat transfer K_{com} can be calculated [47] as shown in Equation 3.5.

$$\frac{t}{k_{composite}} = \frac{t_e}{K_e} + \frac{t_G}{K_G} \qquad \text{Equation 3.5}$$

Where t, t_e, t_G are the thicknesses of composite material, EVA sheet, and the Geotextile respectively. Values of thermal conductivity for uncompressed and compressed thicknesses of the geotextile were obtained as 0.175 W/m^{0}C and 0.246 W/m^{0}C respectively considering the modeling thickness of the waterproofing sheet as 5mm.

2. Determination of composite thermal conductivity of waterproofing sheet assuming the existence of an air gap close to the crown

The concreting process of the second lining is described in Section 2.3. it should be noted that with this tedious labor dependent concreting work and the inherent slope of normal NATM

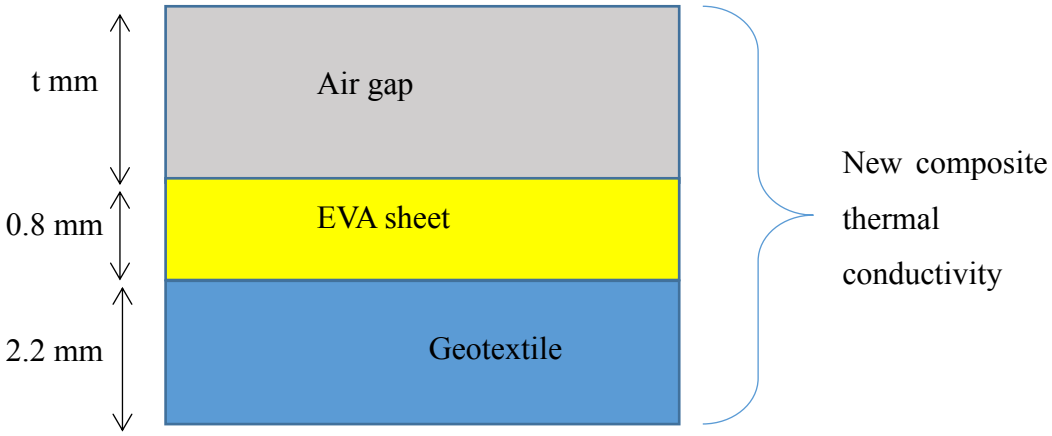

Figure 3.17 Existence of an Air gap at the crown – composite waterproofing sheet

tunnels [48], it was thought that there might be a possibility of existing a thin gap between the second lining and waterproofing sheet/first lining close to the crown. Therefore the thermal conductivity of waterproofing sheet was calculated incorporating the effect of air gap by calculating the composite thermal conductivity considering EVA, geotextile and the air gap under steady-state heat transfer. A schematic representation is shown in Figure 3.17.

Figure 3.16 Damaged EVA sheet in the bottom parts of the second lining

The width of the air gap in the circumferential direction of the lining was set to be 1/3 of the angle of the second lining from the crown based on an indirect site observation. During a tunnel second lining demolition, the condition of waterproofing sheet was observed for the bottom

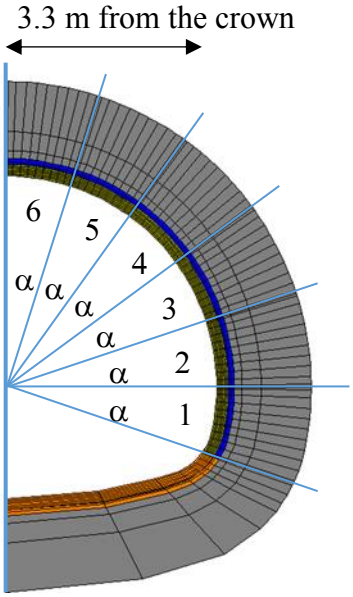

Figure 3.18 width of the air gap

two-thirds in shown in Figure 3.16. It had been observed that in the bottom two-thirds of the lining in the circumferential direction, the waterproofing sheet was highly damaged (Figure 3.16) while in the top one-third portion the damage was minimal. Depending on this actual site observation the width of the air gap was set to top one-third of the second lining as shown in Figure 3.18.

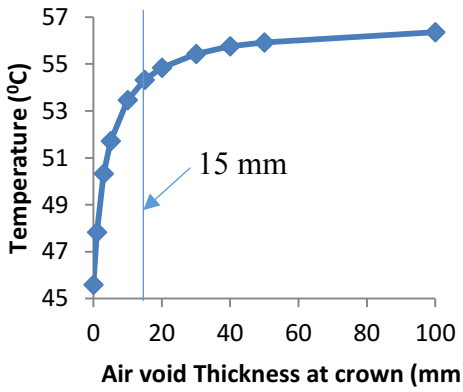

Figure 3.19 Variation of peak temperature at crown with void thickness

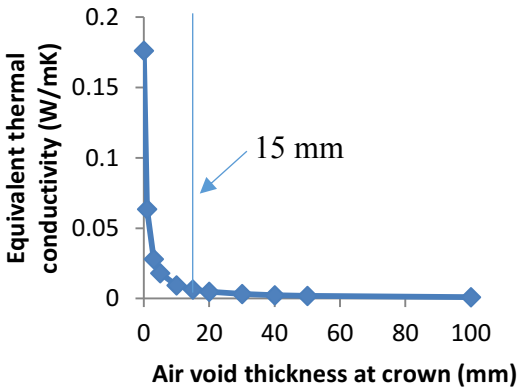

Figure 3.20 Variation of thermal conductivity of WPS with void thickness

Then, to determine the effect of the air gap, a parametric study was carried out by changing the air gap thickness. The variation of the peak temperature at the crown was observed with varying

air gap thickness. Variation of peak crown temperature at the middle of the lining and composite thermal conductivity is shown in Figure 3.19 and Figure 3.20 respectively.

From Figure 3.19 and Figure 3.20, it could be observed that 15mm air void thickness can be treated as a marginal value considering the peak temperature variation at the crown. Therefore, this value was used for the model calibration.

3.2.2.4 Structural properties of the Joints J1, J3

The theory behind the joint element model used for the modeling was briefly described in Chpater2. Properties defined for three joints are shown in Table 3.5. Properties shown in the table are described in

Table 3.5 Properties used for joint elements for considered joint conditions

Property	Description	Joint (J1) With Air gap	Joint (J2) Without air gap	Joint(J3)
P1	Joint Type (for shear)	1	1	1
P2	Shear stiffness (N/mm^2/cm)	0.01	0.01	0.01
P3	Normal stiffness (N/mm^2/cm)	0.00001	30000	30000
P4	Cohesion (N/mm^2)	0.01	0.01	0.01
P5	Yielding - Normal tension (N/mm^2)	0.01	0.01	0.01
P6	Yielding - Normal compression (N/mm^2)	-100	-100	-100
P7	Yielding - Shear	0.01	0.01	0.01
P8	Reduction factor after yield	0.01	1×10^{-7}	1×10^{-7}

3.2.2.5 Variation of the air temperature.

From the experience of the author as well as from some previous studies, it was known that the air temperature inside the tunnel during construction is not constant in vertical direction. It is the case especially when the concreting is done in a covered space. One reason for this temperature gradient might be the accumulation of heat generated from hydration in the confined environment. It was observed that this temperature difference in vertical direction is normally reduced after the formwork removal. It should be noted that this temperature gradient can be one of the reasons for the temperature difference in concrete close to invert and at the crown.

Vertical air temperature distribution is idealized in the study done by Nakamura et. Al. [7] based on environmental temperature measurements along the circumference of the tunnel. This Idealized model was thought to reasonable enough to be used in the current study. Temporal

temperature difference distribution function idealized by Nakamura et. Al. is shown in Equation 3.6 . $\Delta T\ (t, y)$ is the temperature difference at y height ratio from invert compared to the measured temperature close to the invert. K(t) is the time dependent components of the temperature distribution shown in Figure 3.21 and Equation 3.7. y is the height to the considered point divided by the total height of the tunnel from invert to crown.

$$\Delta T\ (t, y) = K(t).e^{-\propto(1-y)} \quad \text{Equation 3.6}$$

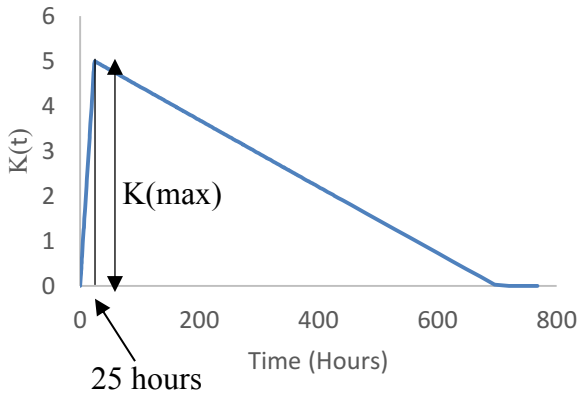

Figure 3.21 Definition of K(t) for air temperature

Definition of K(t)

$$K(t) = \begin{cases} \dfrac{K_{max}}{25} \times t & \text{0-25 hours} \\ \dfrac{K_{max}}{675} \times (700 - t) & \text{25-700 hours} \\ 0 & \text{After 700 hours} \end{cases} \quad \text{Equation 3.7}$$

Defined air temperature distribution according to above mentioned behaviour is shown in Figure 3.22. Where α was set to 1 and K(max) was set to 5^0C based on the recommendations by Nakamura et. Al. [7]. t-con-1-6 imply the temperature of construction stages defined in Figure 3.18.

3.2.2.6 Mesh sensitivity analysis

As an integral part of the finite element analysis process mesh sensitivity analysis was carried out to make sure the mesh dependency of results is within acceptable limits. The target was to obtain an appropriate time step size and a mesh size which can produce dependable results.

Even though the final finite element model should be in 3D to investigate both crown transverse stress and the longitudinal stress close to the invert, in the first stage of the mesh sensitivity analysis, investigations were carried out considering a two-dimensional mesh with a single element in the longitudinal direction to verify the mesh sensitivity in cross sectional directions and to save the analysis time.

An initial 2D mesh was set on general conditions which will minimize the number of elements and increase the time step size. Major factors to define initial mesh are listed below

1. The maximum element size should be small enough to model the shape of the tunnel without distorting the shape.

   It was observed that the element size in the circumferential direction can be as large as 300 mm without distorting the tunnel profile but 225mm element size was used

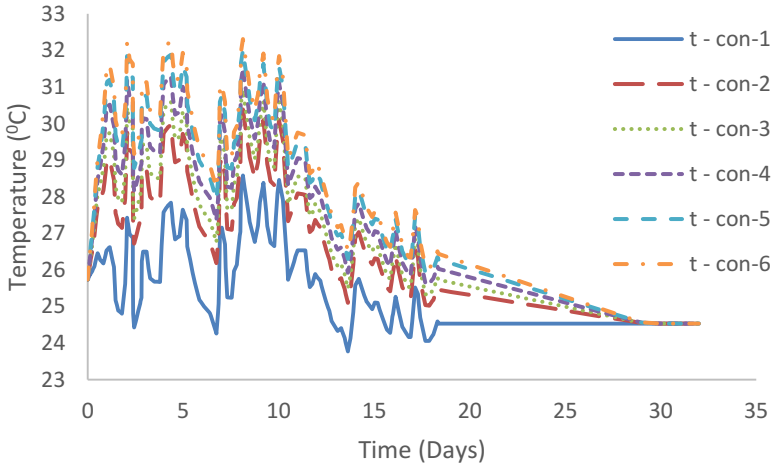

Figure 3.22. Modeled air temperature variation in vertical direction of the tunnel

   in the circumferential direction with some margin.

2. The number of elements should be sufficient in directions with considerable thermal or stress gradients.

   Considering this condition the number of elements in the thickness direction of the second lining was set to 6 elements with 50mm thickness.

3. The largest time step size should be selected in such a way that it can represent the changing environmental temperature functions in an acceptable manner.

   It was observed that the minimum number of steps which can acceptably simulate the air temperature behaviour was about 125 (not uniform time intervals) steps which were set strategically to obtain proper environmental temperature distribution.

4. Time integration scheme was selected as backward Euler because time step in this initial model is the largest possible.

Then the objective was to show that this largest possible mesh with largest possible time stepping can generate temperature and stress results without large mesh dependency compared to smaller meshes with small time step and more accurate time integration method (Crank-Nicolson)

The established initial model and the results comparison points are shown in Figure 3.23. Number of elements used for each region is shown in Table 3.6

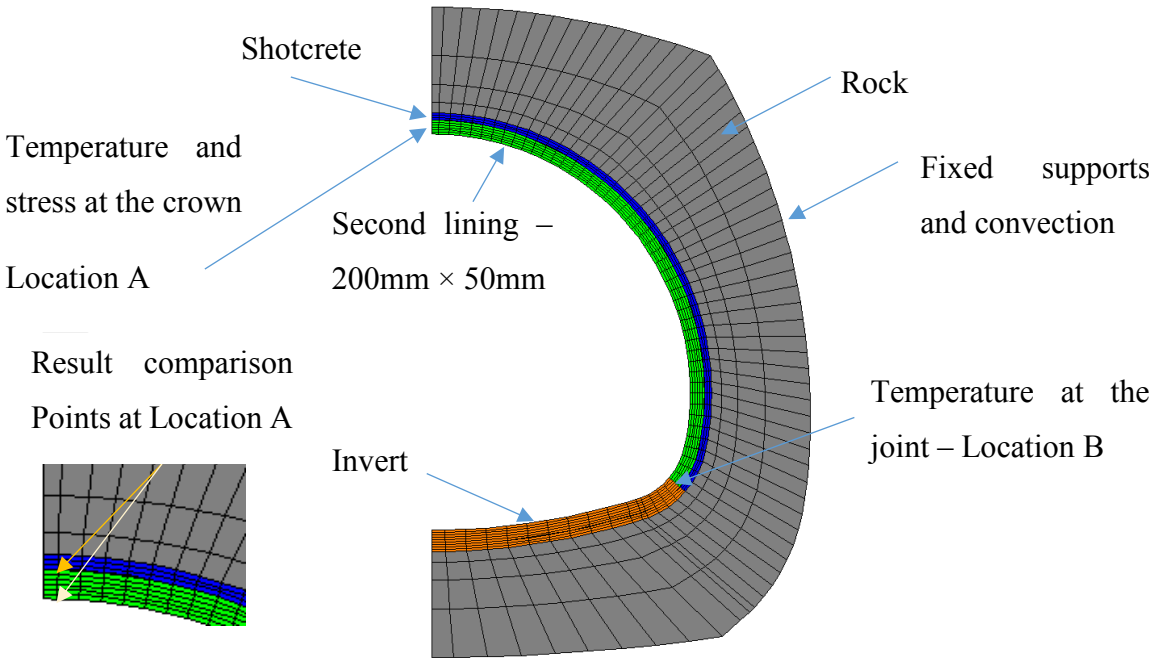

Figure 3.23 Initial 2D mesh utilized for mesh sensitivity analysis

Table 3.6 element layout of the initial model used for mesh sensitivity analysis

Component	**Number of Elements**
Second lining	288 – 6 in radial direction, 48 in circumferential direction
Waterproofing sheet	48– 1 in radial direction, 48 in circumferential direction
Shotcrete	144 – 3in radial direction, 48 in circumferential direction
Invert	160 – 10 in radial direction, 16 in circumferential direction
Rock	288 – 4 in radial direction, 64 in circumferential direction
Total number of elements	928

To check the mesh sensitivity the temperature and stress variation at the crown and the temperature variation at invert-second lining joint was compared with some other meshes which were expected to be more accurate.

The default meshing tool in Astea-Macs does not facilitate the changing of mesh in each component. Only the ratio of element size can be specified in global terms but not for individual components. Therefore, a subroutine was created to export the mesh from LINK3D which has

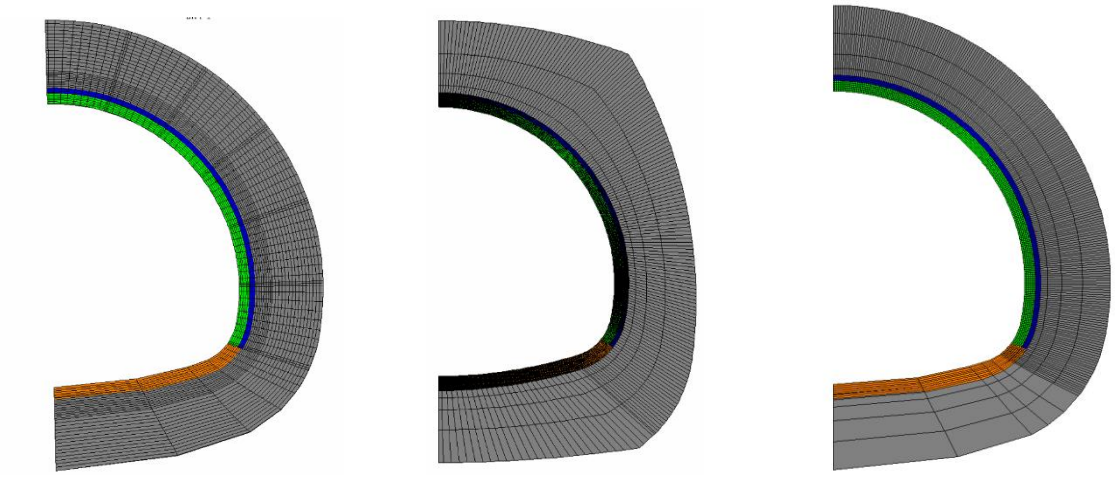

Mesh -1 (a) Mesh -2 (b) Mesh -3 (c)

Figure 3.24 Three types of meshes used to analyze various aspects of meshing

a more flexible meshing tool. Some complicated meshes were generated using this customized subroutines while the simple meshes were generated with default meshing tool in Astea-Macs. The mesh export program is explained in Appendix-1.

Three meshes were created to investigate different types of aspects in 2D. Mesh types are shown in Figure 3.24 and the features and purposes are described in Table 3.7.

Table 3.7 Different types of meshes and their purpose

Mesh	**Purpose**	**Features**
Mesh - 1	Investigate the effect of the mesh density in rock region	Rock with finer elements. Maximum thickness in radial direction was 100mm
Mesh - 2	Effect of mesh size of the second lining	Second lining element size was reduced to 16mm × 80 mm from the initial model
Mesh - 3	Effect of aspect ratio in 2D	Second lining element size 50 mm x 50 mm

The analysis step size should be smaller for smaller mesh considering the heat diffusion. Required step size was determined according to the equations given in the Astea-Macs Manual[31] with respect to the smallest elements in each mesh based on the concept of thermal diffusivity. The minimum time step size was determined from Equation 3.8

$$\Delta t = \frac{(\Delta l)^2 \rho C}{4\lambda}$$ Equation 3.8

Δt is the minimum time step size in hours , Δl is the element smallest dimension in governing direction in meters , ρ is the density in kg/m^3 , C is the specific heat capacity in kcal/kg^{0}C, and λ is the thermal conductivity in kcal/mh^{0}C. Minimum step size calculated from above equation for above meshes considering the governing elements are shown in Table 3.8

Table 3.8 Minimum time step size limited by element dimensions

Mesh Name	Material	**Δl** (m)	**ρ** (kg/m^3)	**C** (Kcal/kg^{0}C)	**λ** (Kcal/mh^{0}C)	**Δt** (Hours)
Mesh 1,3	Concrete	0.050	2400	0.275	2.323	0.177
Mesh 2	Concrete	0.016	2400	0.275	2.323	0.018
Mesh 1,2,3	WPS (Bottom)	0.005	1000	0.550	0.212	0.016
Mesh 1,2,3	WPS (top)	0.005	1000	0.550	0.006	0.624
Mesh 1	Rock	0.050	2650	0.191	3.011	0.105

It was observed that the minimum time step size is governed by the element properties of waterproofing sheet in the bottom portions. The time stepping was set to the required value to observe the dependency of thermal analysis results in mesh 1 and mesh 2. Time dependent temperature and maximum temperature was compared for two meshes. Time dependent temperature behaviour is compared in two locations as shown in Figure 3.23 where the temperature gradient was thought to be significant. In Location A, the temperature was compared in the closest gauss point to the surface and closest gauss point to the waterproofing sheet in the second lining and in Location B, at the common node to the invert and second lining in the middle in the thickness direction. The naming of the temperature curves (for example CN-32000-mesh-1) follows the time integration method, number of time steps and the corresponding mesh shown in Figure 3.25. CN stands for Crank-Nicolson method and BE stands for Backward Euler method. Time step size of mesh-3 was set to a larger value based on the results of the mesh-1 and mesh-2. However, it was set in a way that time step size shown in Table 3.8 for concrete elements are not violated. Time step size was set to 0.16 hours.

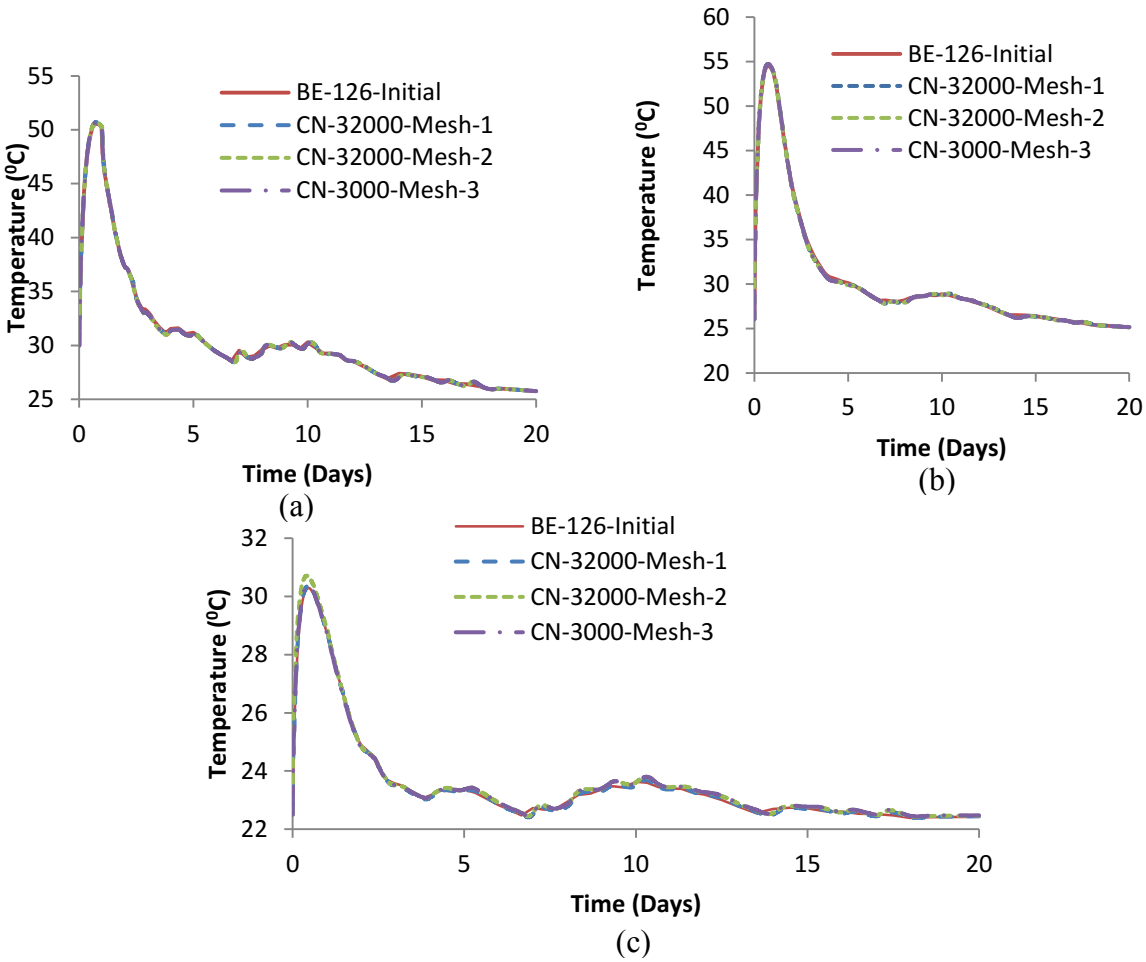

Figure 3.25 Comparison of time dependent temperature for different mesh sizes and time steps (a) at surface of Location A (b) close to waterproofing sheet at Location A (c) Invert and lining joint

Location of maximum temperature was observed to be unchanged with the combinations of the time steps and the meshes. Location and the maximum temperature values are shown in Figure 3.26 and Table 3.9 respectively. It was noted that the mesh dependency of temperature results was not considerable and the mesh-1 with larger time stepping is reasonable enough to be used.

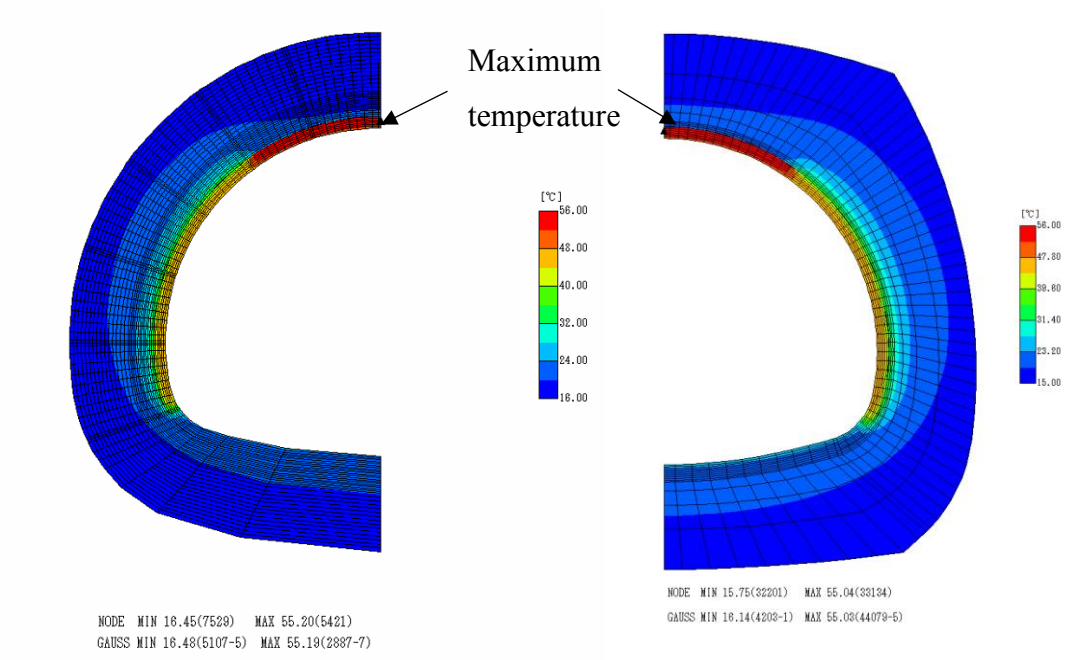

(a) (b)

Figure 3.26 Location of maximum temperature (a) mesh-1, (b) mesh-2

Table 3.9 Maximum temperature value with time integration method and mesh size

Mesh	Time Integration	Maximum Temperature (^{0}C)	Error
Mesh-1	BE	55.04	-0.29%
Mesh-1	CN	55.22	0.04%
Mesh-2	CN	55.2	_
Mesh-3	CN	55.22	0.04%

The objective of the mesh-3 was mainly to investigate the effect of aspect ratio of the elements of second lining on the stress analysis. Comparisons of the results of mesh-1 and mesh-3 for the transverse crown stress are shown in Figure 3.27. It was observed that the finer mesh and finer time stepping could not improve the simulated stress results in a considerable manner. The low mesh dependency of the results might be due to the slow nature of the thermal propagation with the materials properties that are engaged in this type of simulation in general.

Even though the mesh dependency seems to be negligible, an optimized mesh was created by using smaller elements in the places where temperature gradients are expected such as the

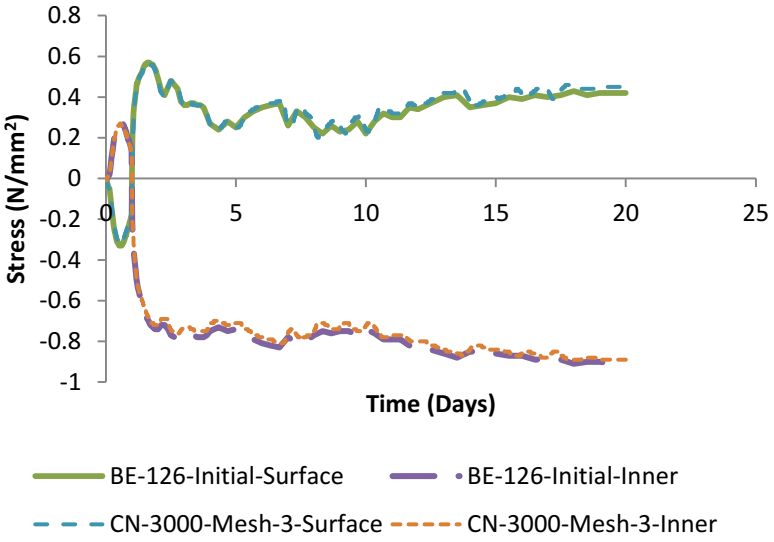

Figure 3.27 Transverse stress at crown comparison for Mesh-1 and Mesh-3

starting and end points of the construction stages shown in Figure 3.18 to obtain smooth temperature contours. The optimized model was used to study longitudinal mesh sensitivity.

Longitudinal mesh sensitivity was studied considering a uniform mesh size in the longitudinal direction mainly to investigate the effect of aspect ratio of elements in the longitudinal direction. The control over the longitudinal mesh generation in the default meshing tool is limited. Therefore, a uniform mesh was generated using the program shown in Appendix-1.

Three meshes were compared to study the mesh sensitivity in the longitudinal direction and shown in Figure 3.28. In the default mesh, M3D1, the largest element size in the longitudinal direction is about 600mm while in other two it was limited to 200mm. The largest circumferential length was limited to about 200mm in all three meshes. In the optimized mesh, M3D3, the element density of the invert region was reduced while smaller elements were created in locations where air temperature is changed

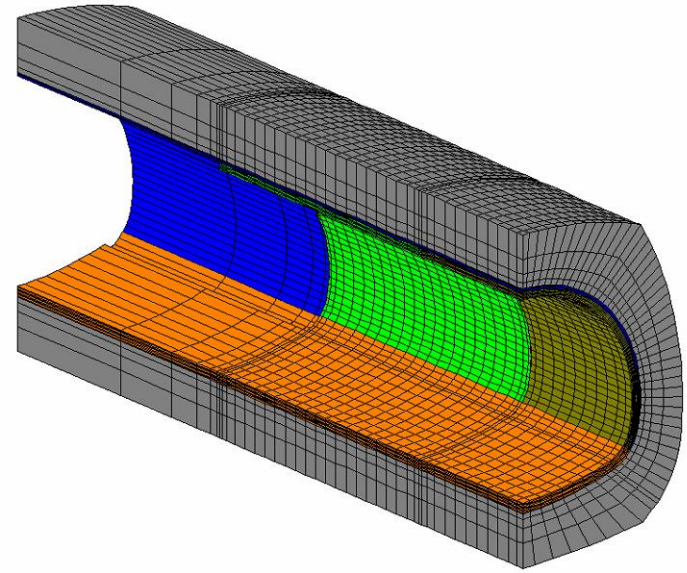

(a)

Mesh (a) maximum element size in longitudinal direction 611 mm default mesh.

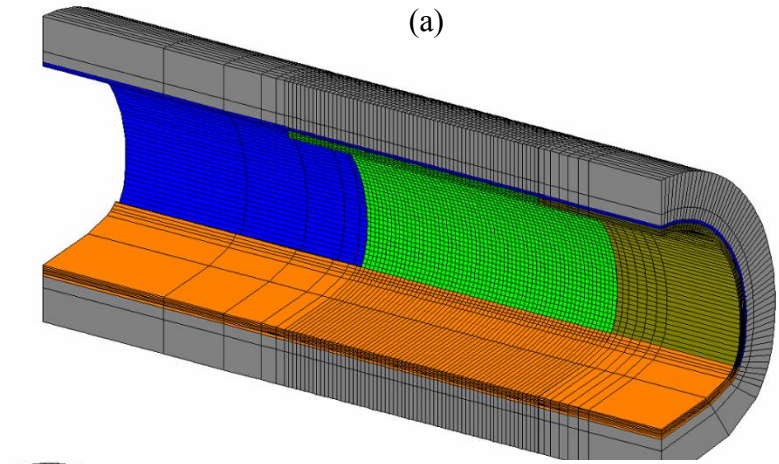

(b)

Mesh (b) maximum element size in longitudinal direction 200 mm .

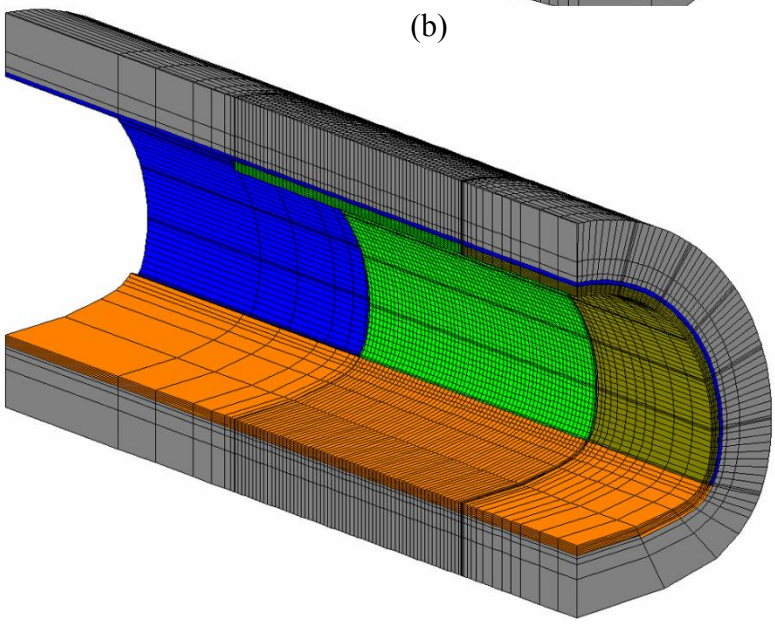

(c)

Mesh (c) maximum element size in longitudinal direction 200 mm. Small elements of 50mm are used in places with temperature gradients

Figure 3.28 Meshing to study longitudinal stress behaviour (a) Default mesh form Astea-Macs- M3D1 (b) Uniform mesh - M3D2 (c) Optimized mesh - M3D3

The analysis was carried out with a larger time step size as the analysis time was observed to be extremely time consuming if very fine time steps were utilized as in the 2D analysis. Only

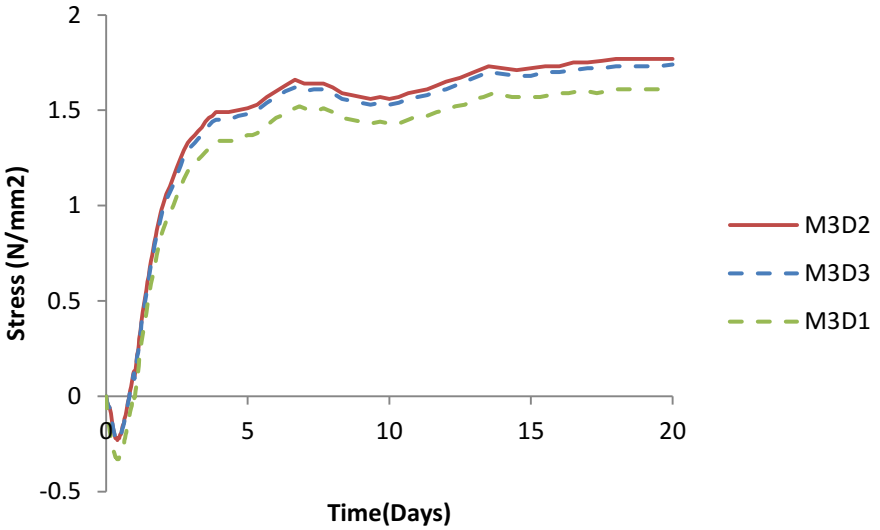

Figure 3.29 Variation longitudinal stress close to invert with mesh size

the comparison of stresses in the longitudinal direction for three meshes are shown in Figure 3.29 for the sake of completeness. It was noted that the final longitudinal stress value was varied in about 8% from uniform 20cm mesh to the default mesh. The optimized mesh which was finally used showed close results to the uniform 20cm mesh. Mesh data of the final mesh are shown in Table 3.10.

Table 3.10 Details of the final mesh

Component	Circumferential divisions (Cir)	Radial divisions (Rad)	Longitudinal (Lng)	Element size roughly (mm) (Cir × Rad × Lng)
Full model	**77**	**12**	**85**	
Second lining	70	6	65	200 × 50 × 200
Waterproofing sheet	70	1	77	200 × 5× 200
Shotcrete	70	2	85	200 × 100 × 200
Existing lining	70	6	12	200 × 50 × 200
Invert	7	9	85	Varying
Rock	77	3	85	Varying
Vertical Joint	70	6	1	200 × 50 ×5

3.3 Calibration Results with Astea-Macs

The finite element modeling process to investigate the behaviour of second lining was described in detail in section 3.2. It should be noted that the process was logically developed considering a large number of variables such as the joint behaviours, load transfer from surrounding rock/ground to the second lining, properties of waterproofing sheet and much more. Some simplifications done for the purpose of simulation such as the uniform thickness of second lining, the dimension of air gap might not be hundred percent true. Considering these conditions any attempt to obtain full calibration to get perfect matching between analysis and measurement results was not attempted. Instead, it was attempted to understand the stress behaviour at the crown and at location P close to invert with sufficient model calibration and understanding the causes for the discrepancy of measured and analysis results.

Results were compared mainly with temperature variations, crown transverse stress variation which is responsible for crown longitudinal cracking and longitudinal stress close to invert (location P in Figure 3.1) which is responsible for vertical cracking close to the invert.

Appropriate care should be taken with respect to the setting of zero time when measurement and simulation results are compared. Even though measurement was started after casting, meaningful stress and strain can be obtained only after proper strength development of concrete. The initial setting time of concrete was selected as the zero time in measurement in the study by Usui et al [29]. Therefore, the simulation results were shifted to set appropriate zero time complying with the field measurements. The initial setting time of second lining concrete had been determined as 0.16 days. However, temperature increment can be measured from the beginning in reality and the simulation results were also compared with simulation zero time.

3.3.1.1 Calibration of temperature variations

Temperature results are shown in Figure 3.30. It was observed that a reasonable agreement of temperature results at critical locations could be obtained with the established modeling process. However, the peak temperature at location p showed an overestimation about 3.5 ^{0}C. There are several reasons which can cause this overestimation where one reason can be the estimation of heat transfer coefficient of the second lining surface and another can be the thermal properties of waterproofing sheet. It should also be noted that the heat of hydration model used in the simulation was not a temperature dependent model where in the actual scenario the temperature rise of second lining might depend on external temperature conditions because second lining

thickness is relatively low compared to mass concrete structures such as footings, pile caps etc. However, one important fact to be noted is that the temperature results discrepancy might have a slight effect on the stress variation at location P.

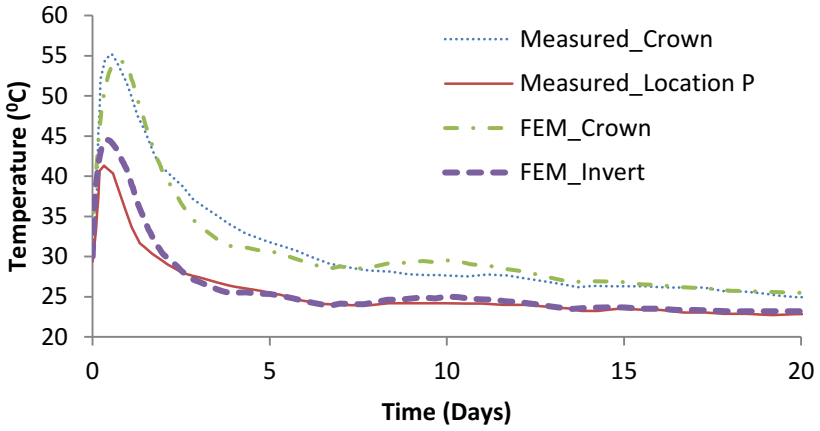

Figure 3.30 Simulation and measurement results for temperature variation inside second lining

3.3.1.2 Calibration of stress and strains close to invert at point P

The measured and the simulated stress variations at Location P at the middle thickness of the seconding is shown in Figure 3.31. Initial stress variation was well simulated. But in the later stages, after the increment of tensile stress, simulated stress values showed a higher tensile stress value by a factor of about 1.5.

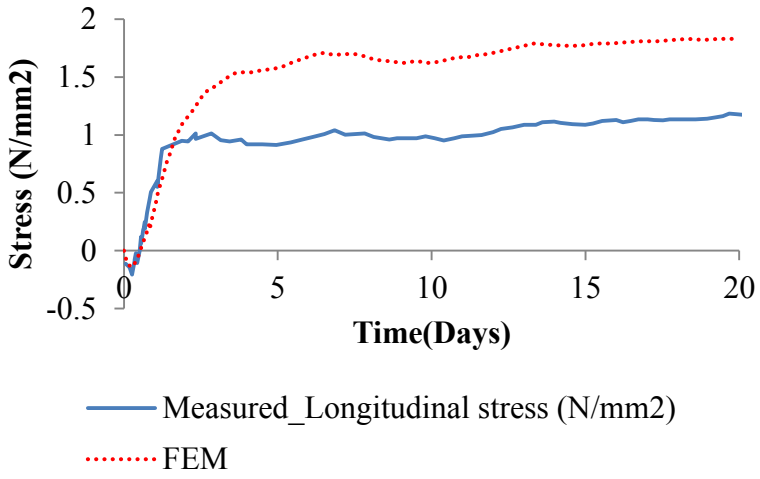

Figure 3.31 Measured and calibrated stresses at Location P

It should be noted that the behaviour pattern of the simulation followed the measurement. The difference might have been caused partially due the discrepancy of temperature results. However, the major portion of the stress overestimation occurred during the temperature decreasing period. The discrepancy of stress results might be caused by the discrepancy of calculated strain values or the Young's modulus.

Measured and simulated strain results are shown in Figure 3.32.

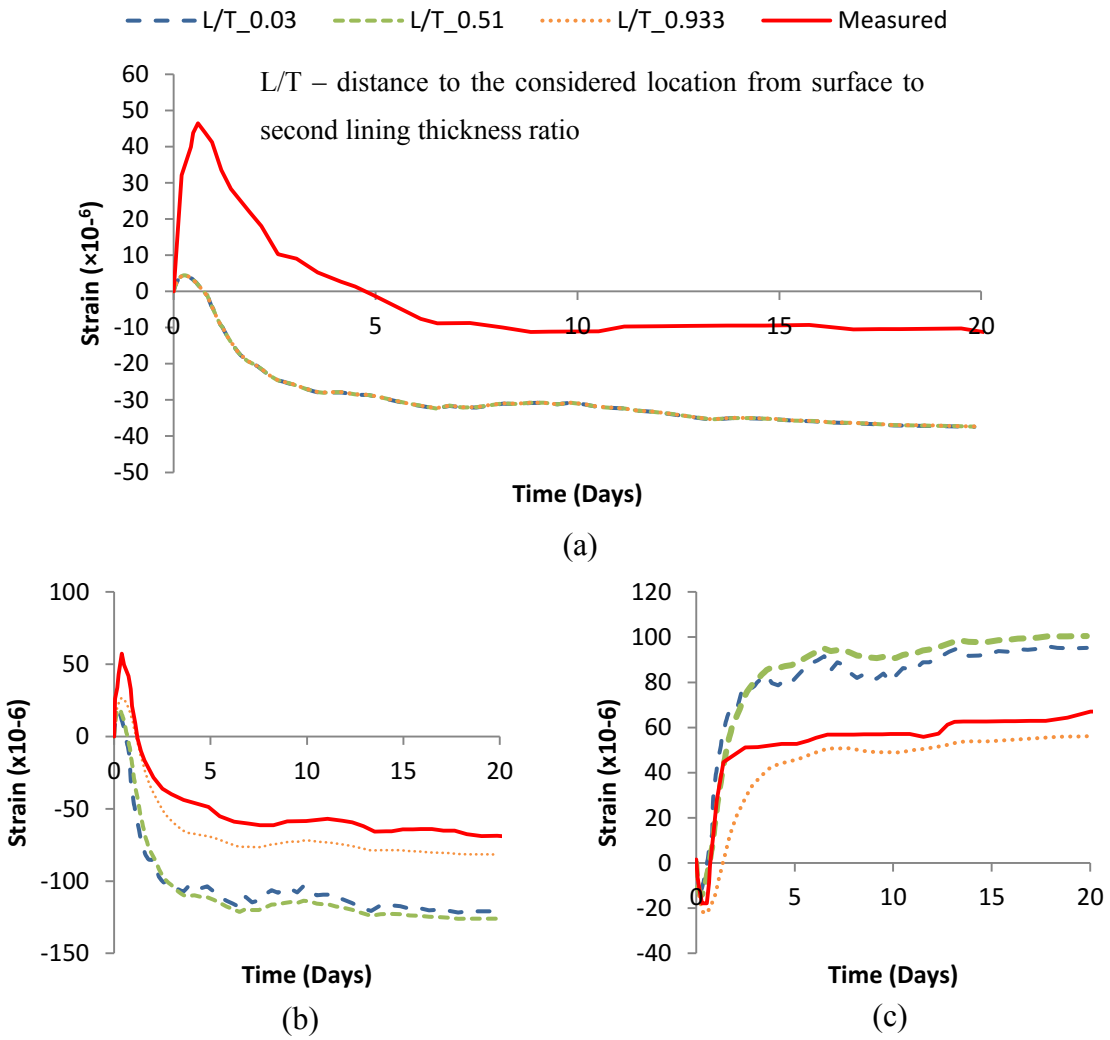

Figure 3.32 Measured and simulated strain (a) Structural strain (b) Temperature strain (c) Effective strain

In Figure 3.32, shown measurement was conducted at the middle thickness of the second lining but simulation results of few more points are shown in the figure to understand the strain distribution in the thickness direction. The location of considered point is shown as the ratio of the distance to the point from second lining surface divided by second lining thickness (L/T). The main quantity that should be compared in measurement with simulation is the structural

strain as it can be directly measured. It was observed that the measured and simulated values of structural strain values did not agree well. One of the reasons for the discrepancy of strain results was considered as the setting of zero time for measurements.

It was known that the starting point for the measurement was set as the initial setting time of the second lining concrete. But according to the studies carried out by YNU concrete laboratory, this time setting was not appropriate to obtain real structural measurements as the hardening of concrete might not be started from initial setting time. The more accurate starting point is said to be the hardening point which might come after a significant time from initial setting time. During this time gap between initial setting time and hardening time the CTE of concrete might be larger than the laboratory measured value (6.8 $\mu/^0C$) and the Young's modulus can be significantly smaller. Therefore, the measurement results were expected to be inclusive of larger structural strains compared to the simulated strains.

Effective stress in measurement is estimated by the difference of measured structural strain and the measured strain from the non-stress meter where the temperature strain should be calculated based on temperature difference and the measured coefficient of thermal expansion. Therefore the simulated and calculated temperature strains should be at lease show a close relation if the starting point is set correctly

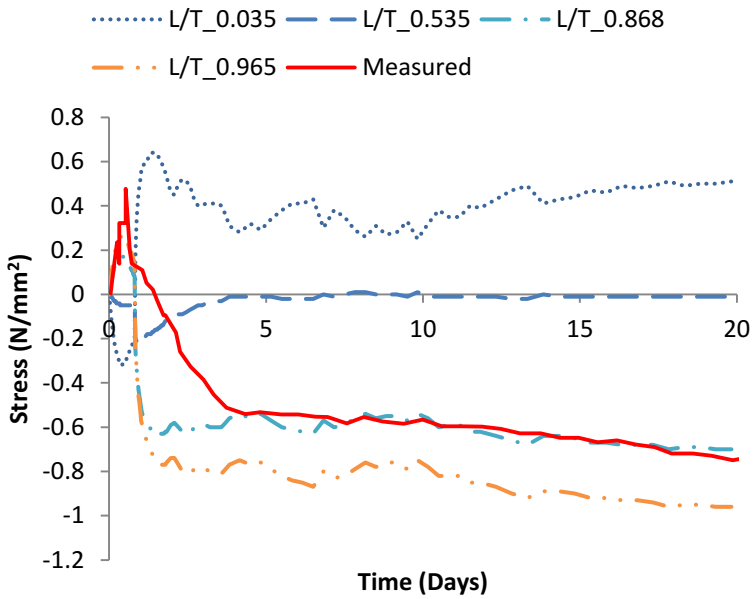

Figure 3.33 Simulated and site calculated stress at crown

3.3.1.3 Calibration of crown stress

Measured and simulated crown stress is shown in the Figure 3.33. Simulation results are shown in a few locations to obtain an idea about the stress variation in the thickness direction as investigated in the case of longitudinal stress at Location P.

It was observed that the simulation and measurement results showed a similar behaviour pattern but simulation results at middle thickness and measurement values did not agree. However, simulated stress behaviour at 0.85 thickness shows some level of agreement with the measured values. Any special attempt was not made to obtain perfect matching of results because of the possibility of the existence of many non-uniformities or imperfections.

According to Figure 3.33, the stress at the surface of the lining is in tension while the inner elements are in compression. Even though any cracking risk was not observed with the

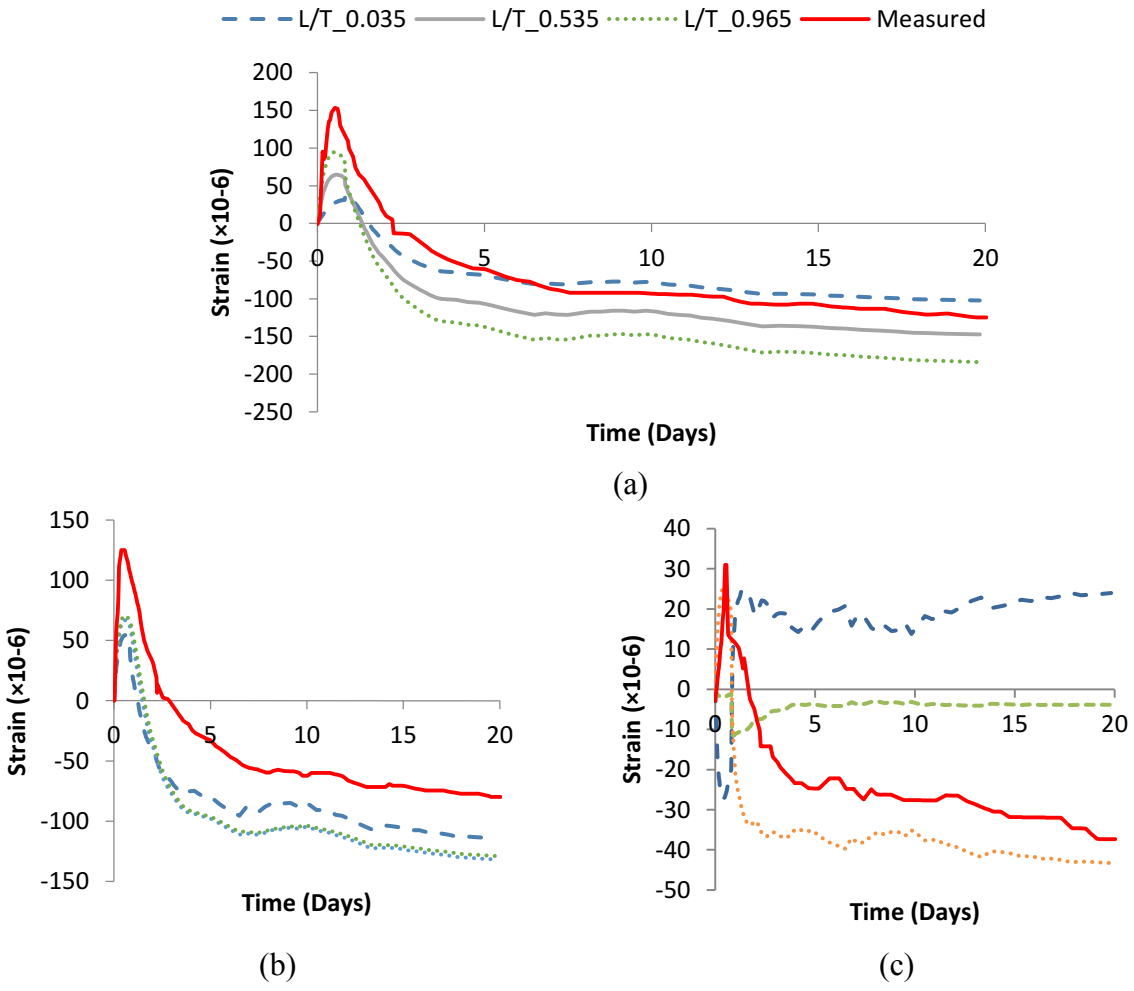

Figure 3.34 Strain variations at crown (a) structural strain (b) Temperature strain (c) effective strain

measurement results, from simulation it can be seen that a crack can occur if the tensile stress at the surface exceeds the tensile strength. However, this crack cannot penetrate the full thickness as the inner portion of the second lining in the thickness direction is in compression.

Measured and simulated strains are shown in Figure 3.34. Similar to the measurements close to the invert the stress discrepancy at crown also could be observed in strains.

One possible reason for the discrepancy of strain results might be the calculation process adopted in the study of Usui et al. In this study the quantities measured by non-stress meter was assumed to be constant for the whole structure but in reality this assumption cannot be considered fully valid and can generate significant amount of error considering the high temperature difference of concrete observed inside concrete lining.

3.3.1.4 Deformation of the second lining

Deformation pattern of the second lining is shown in Figure 3.35 and it can be observed that the

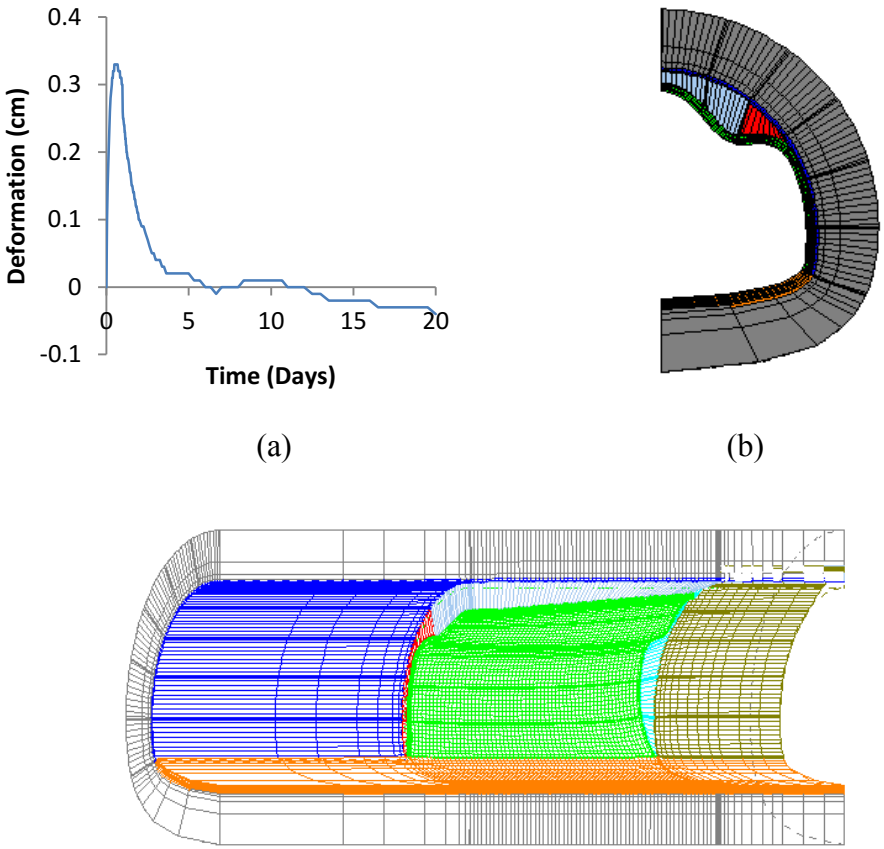

Figure 3.35. Deformation pattern of the second lining (a) Time dependent deformation (b) Deformation at middle section (c) deformation in 3D

independent behaviour of second lining was well simulated with used analysis conditions. Due

to the assumption of the air gap close to the crown part, the top portion of the lining moved vertical upward direction in temperature increasing period and then moved in the vertically downward direction with temperature decrease and with the gravity load. Time dependent deformation of the second lining is shown in Figure 3.35 (a) and it was observed that the maximum upward movement at the middle is about 3.5 mm and downward deformation was about 0.5mm.

3.4 Modeling for investigation of long term behaviour of second lining governed by drying shrinkage

Dry shrinkage of concrete structures is a long term phenomenon which highly depends on environment temperature and relative humidity. As it is a governing factor for long term cracking and deterioration of concrete structures, it is important to investigate the effect of drying shrinkage on cracking risk of concrete tunnel lining.

As drying shrinkage is dependent on temperature variations, drying shrinkage amount should be estimated with respect to varying environmental conditions. Link3D is a proven tool to obtain dependable drying shrinkage values considering both environmental and material parameters and utilized in this study to quantify the drying shrinkage amount with varying environmental conditions. Furthermore, because of the ability of Astea-Macs for superior sensitivity analysis, the quantified drying shrinkage was used as an input to Astea-Macs for stress calculations. The analysis scheme is shown in Figure 3.36.

Although extensive verification was carried out for short term thermal stress behaviour of second lining using measurement data extracted from Taisei measurements presented in 3.1.1, drying shrinkage calculation verification was not possible from those data as no investigation was carried out regarding drying shrinkage behaviour of used materials. Therefore drying shrinkage analysis was carried out based on measurements done for Kodsuchi tunnel shown in section 3.1.2.

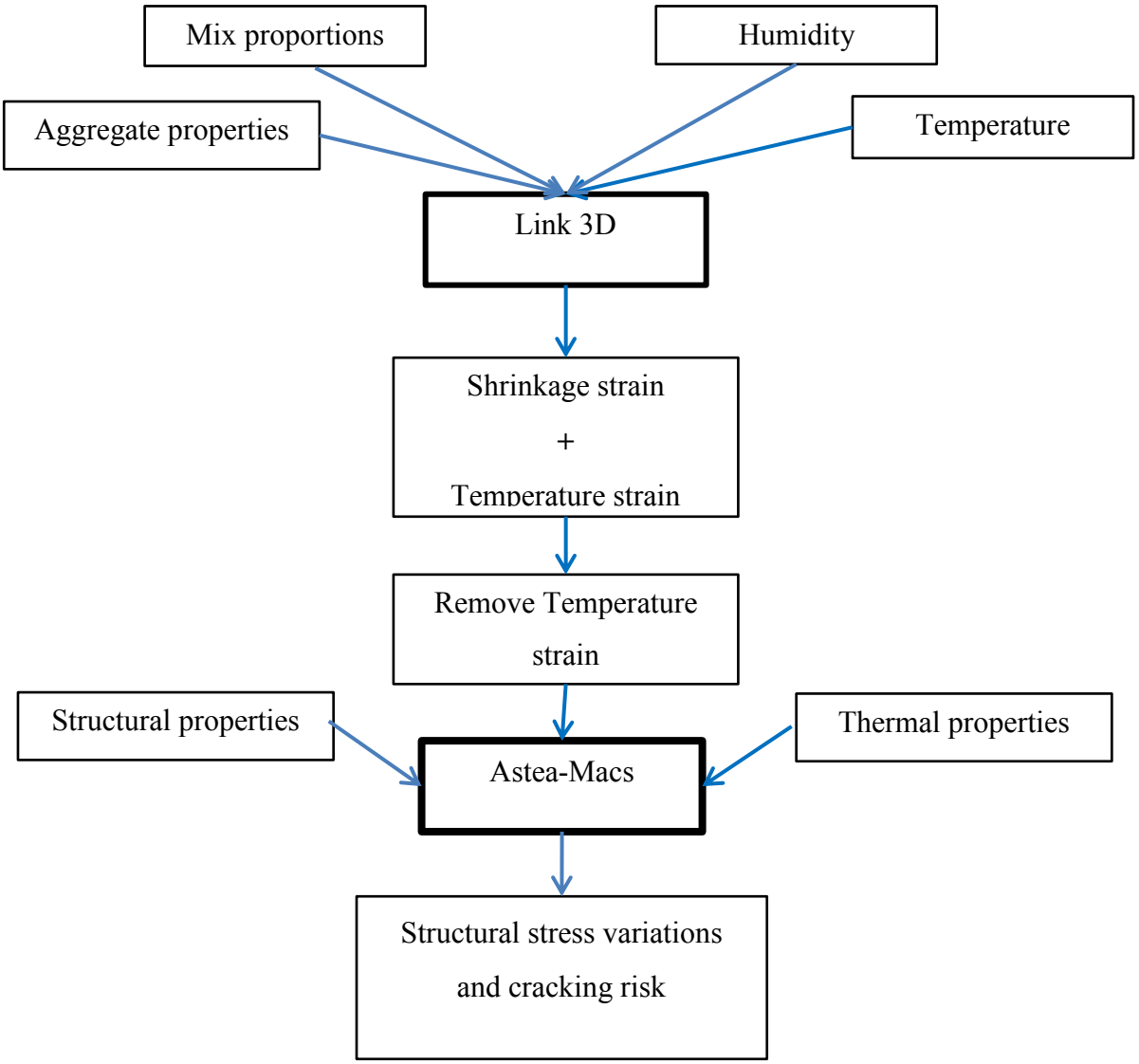

Figure 3.36 Simulation scheme for drying shrinkage stress analysis

3.4.1 Calibration of model for calculation of long term drying shrinkage

Model calibration for long term drying shrinkage was carried out based on the standard experimental studies carried out for Kodsuchi tunnel. One-eighth of the standard model was created in Link3D considering the symmetry. The model utilized for verification boundary conditions are shown in Figure 3.37. Model calibration was done by adjusting shrinkage value of limestone aggregate which was set to 80 [49] microns and Blaine value for blast furnace slag which was set to 4200 cm^2/g [50]. Calibrated drying shrinkage results are shown in Figure 3.38.

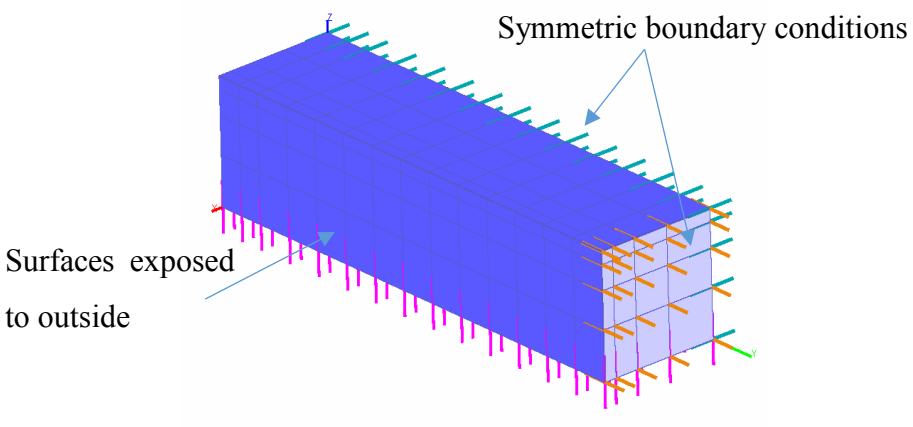

Figure 3.37. Model for calibration of drying shrinkage

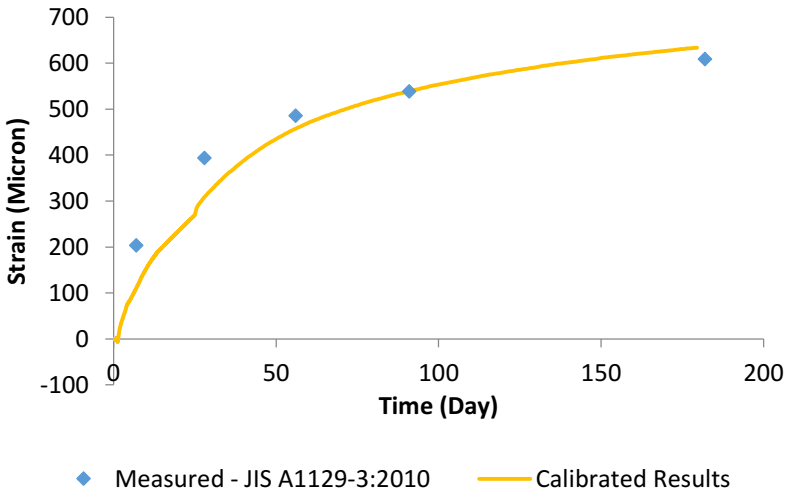

Figure 3.38. Calibrated results for drying shrinkage

3.4.2 Calculation of drying shrinkage based on environmental, material and structural conditions for second lining of NATM tunnels

The exposure conditions for drying shrinkage behaviour of the second lining is a little different from the standard test which was verified in the previous section. In actual lining concrete, only one surface is exposed to the environment, though in the standard test for drying shrinkage all the faces of the specimen are exposed to the environment. Therefore, to calculate drying shrinkage strain to be used for stress analysis, a separate model should be created which can represent the actual condition of the tunnel lining. The model used to calculate shrinkage strain for tunnel lining is shown in Figure 3.39. Cross-sectional dimensions were selected as 100mm

x 100mm to be equal to the standard specimen. The section in the thickness direction was modeled with other actual components which are the shotcrete layer and the rock.

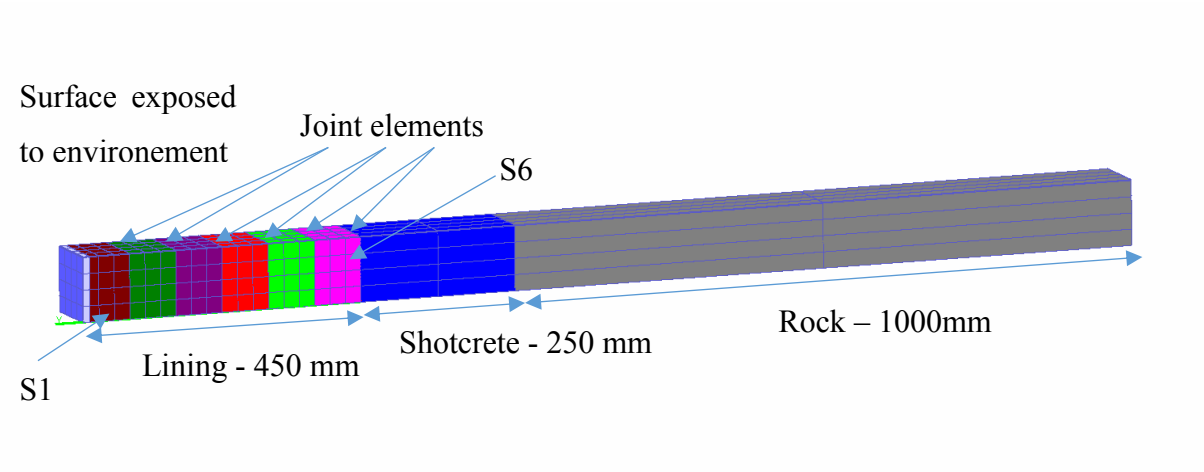

Figure 3.39 Model used to calculate drying shrinkage of second lining

The model was created with 25mm elements and the second lining was divided into 6 sections as shown in Figure 3.39. The average strain of all the elements in three dimensions was input to the stress analysis software per section. Application of drying shrinkage to the stress analysis model is shown in Figure 3.40

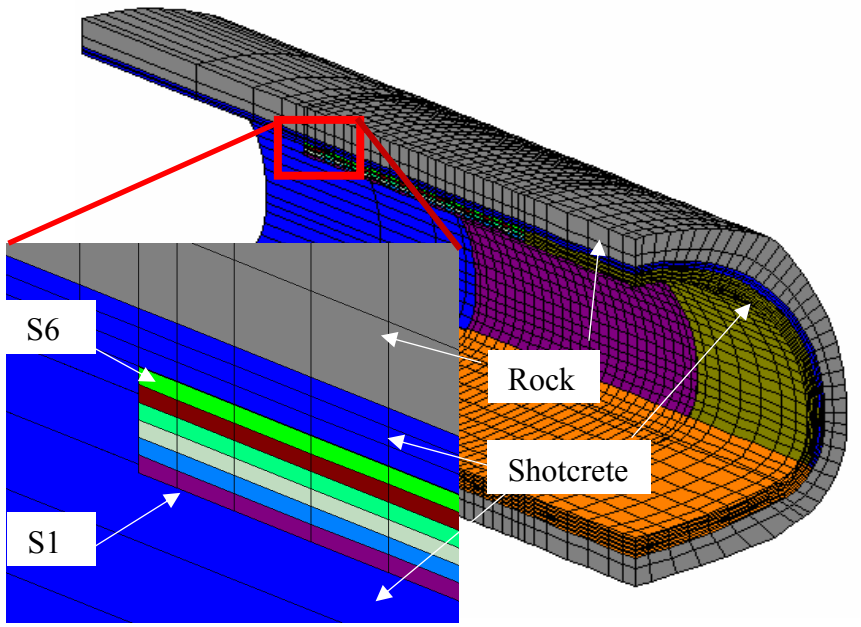

Figure 3.40 Application of unrestrained drying shrinkage to the stress analysis model

It should be noted that the drying shrinkage strain calculated by Link3D software should be free shrinkage strain without any effective external restraint. Therefore each section of shown in Figure 3.39 was separated by frictionless joint elements which used the settings similar to the joint properties used to model the waterproofing sheet in Section 3.2. It should be noted that this calculated drying shrinkage should be free from temperature strain and autogenous shrinkage as these values are set separately in stress analysis software. Temperature strain was removed considering the thermal expansion coefficient of the software as 10 microns/^{0}C. As the crown stress does not depend on autogenous shrinkage that much, in the cases where special attention was not given on invert stress both drying shrinkage and autogenous shrinkage was entered directly into the software.

3.5 Summary

Finite element modeling of second lining concrete of NATM tunnels was established to understand the transverse stress behaviour at the crown and the longitudinal stress variation close to the invert.

The analysis was proved to be not mesh dependent in the 2D investigation which did not take the longitudinal behaviour into account. But in 3D model the longitudinal mesh size seems to have an effect as the maximum stress was underestimated by about 8% with the larger mesh. Therefore, an optimized mesh was used which provided 1:1 aspect ratio in longitudinal and circumferential directions.

Special attention was paid on determining the thermal properties of waterproofing sheet considering the composite nature and the possibility of the existence of an air void between first and second linings at the crown part. Heat transfer coefficient of the second lining surface was decided with experience and with the knowledge of the previous studies. The measured difference of temperature peak at the crown and close to the invert location could be reasonably simulated with the assumed conditions.

In the case of modeling assumptions, special attention was given to the modeling the mechanical behaviour of joints formed by waterproofing sheet (J1) , the horizontal joint between lining and invert (J2) and the vertical construction joint (J3). It was observed that the modeling of joints combined with other parameters could be acceptable considering the stress behaviour patterns instead of exact values.

From simulation results, the vertical penetrating crack pattern close to the invert and the non-penetrating crack at the crown could be understood by referring to the stress variation pattern in the thickness direction.

Some difference in simulation results and the measurement results should be accepted considering the assumptions made in the calculation process of the measurement data and considering the idolized conditions of the second lining in the simulation.

4 SHORT-TERM STRESS BEHAVIOUR OF SECOND LINING GOVERNED BY THERMAL STRESS

To understand the cracking of second lining of NATM tunnels, as the first step, it is essential to understand the sensitivity of the stress variations at the locations which have the highest cracking risk. Highest cracking risk locations were previously identified as crown and the region close to the invert in the bottom part of the tunnel lining based on the crack patterns.

In the first part of this Chapter, an attempt was made to explain the stress generation mechanism at the crown of the second lining of NATM tunnels based on the established simulation method in Chapter 3. Then the sensitivity of stress variations at the crown and close to invert was investigated in a form of a parametric study with a set of selected variables to understand the importance of those variables in terms of cracking. The explained crown stress generation mechanism was used to understand the stress variations obtained in the sensitivity analysis.

4.1 Setting a base model for the parametric study

In Chapter 3, the finite element model was calibrated with some material properties obtained from laboratory tests or by field measurements. Mainly, the adiabatic temperature rise of concrete, time dependent developments of compressive strength, tensile strength, and Young's modulus, creep coefficients according to JCI guideline [8] and autogenous shrinkage calculated from field measurements, and site measured air temperature variation was used for the model calibration.

It was noted that using some field measured or laboratory test based quantities are not always very meaningful to be used in a parametric study. Therefore, some parameters of the models were changed to more rational values or calculation schemes to establish a base model for the parametric study. The changed quantities and the reasons are shown in Table 4.1. This 3D base model was used as the starting point of the parametric study.

A 2D model similar to the models used for mesh sensitivity analysis in section 3.2.2.6 was also created with the same conditions as the base model to check the dependency of crown stress

on longitudinal structural behaviour. Comparison of temperature and crown stresses are shown in Figure 4.1.

Table 4.1 parameters set for the standard model

Component	Changed from	Changed to	Reason
Air temperature variation	Site measured	A constant value of 25.75 ^{0}C	To eliminate the effects of varying temperature on temperature dependent properties such as compressive strength - Easy to understand the stress mechanism
Autogenous shrinkage	Laboratory measured	JCI standard equation	Laboratory measured shrinkage is not temperature dependent. Temperature dependency should be considered in the parametric study.
Creep coefficient	Calculated – T.rise 0.8 T.decrease 0.64	T. rise 0.42 JCI Standard T.decrease 0.5	Creep coefficient value at temperature decreasing period was set because the standard value seemed to be too large for considered Young's modulus development.

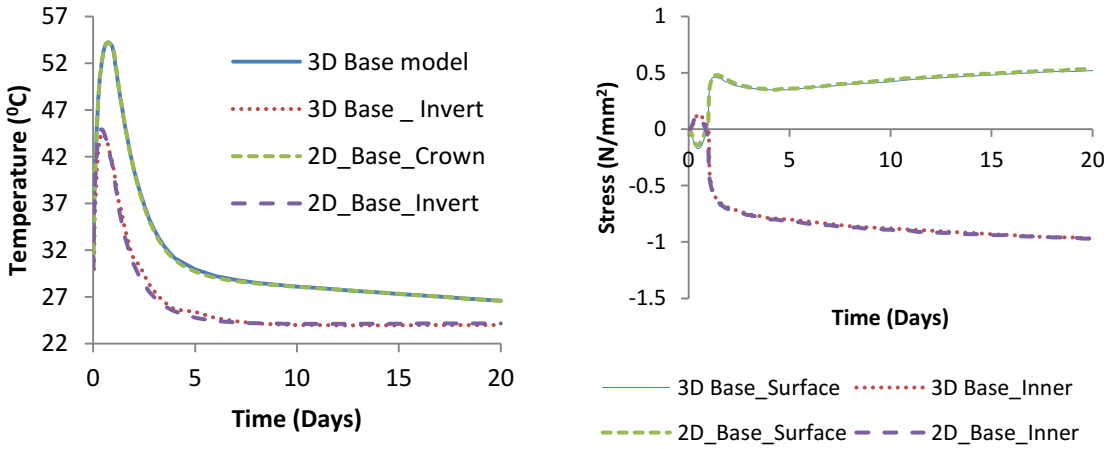

(a) (b)

Figure 4.1 Comparison of simulation results of 2D and 3D base models (a) Temperature variation (b) Crown stress variation

It can be observed that the time dependent temperature and stresses are almost independent of the longitudinal direction. Therefore, to understand the crown stress generation mechanism 2D version of the model was utilized.

4.2 Investigation of the transverse stress generation mechanism at the crown of the second lining of NATM tunnels.

As explained in chapter 1, in the case of Type 2 and Type 3 cracking, the mechanism is understood in a substantial manner. But in the case of crown stress generation mechanism, straight forward assumption was challenging because the crown stress can depend on a large number of variables. The objective of this study was to clarify the short term stress generation mechanism at the crown which can lead to longitudinal cracking.

A simplified model was established from the base model by making another two modifications to understand the crown stress mechanism. First, the thermal properties of the waterproofing sheet were assumed to be uniform without an air gap close to the crown. This was done because the existence of air void makes the mechanism complex. Second, the autogenous shrinkage was removed from the model to understand the behaviour generated only from thermal stresses. After understanding the stress behaviour in a simple manner, the possible effect of the existence of air void is explained in section 4.2.1.3.

4.2.1 Clarification of the behaviour of the transverse stress at crown

To understand the stress generation mechanism at the crown part, transverse stress at three gauss points in the second lining at the crown and the crown concrete temperature variation at middle thickness are plotted for 5 days period in. Figure 4.2.

Transverse stress behaviour was analyzed in three zones based on the temperature variation and the stress variation pattern. Zone 1 includes the temperature rising period from the initial concreting to the peak temperature due to the heat of hydration. This period covers from 0 to 0.4 days in the simulation. Zone 2 is from the temperature peak to the time of the form removal which covers from 0.4 days to 1 day. Zone 3 is from the point of the form removal up to about 5 days (Until thermal effects deplete). The location is again shown as a ratio to the lining thickness from the surface

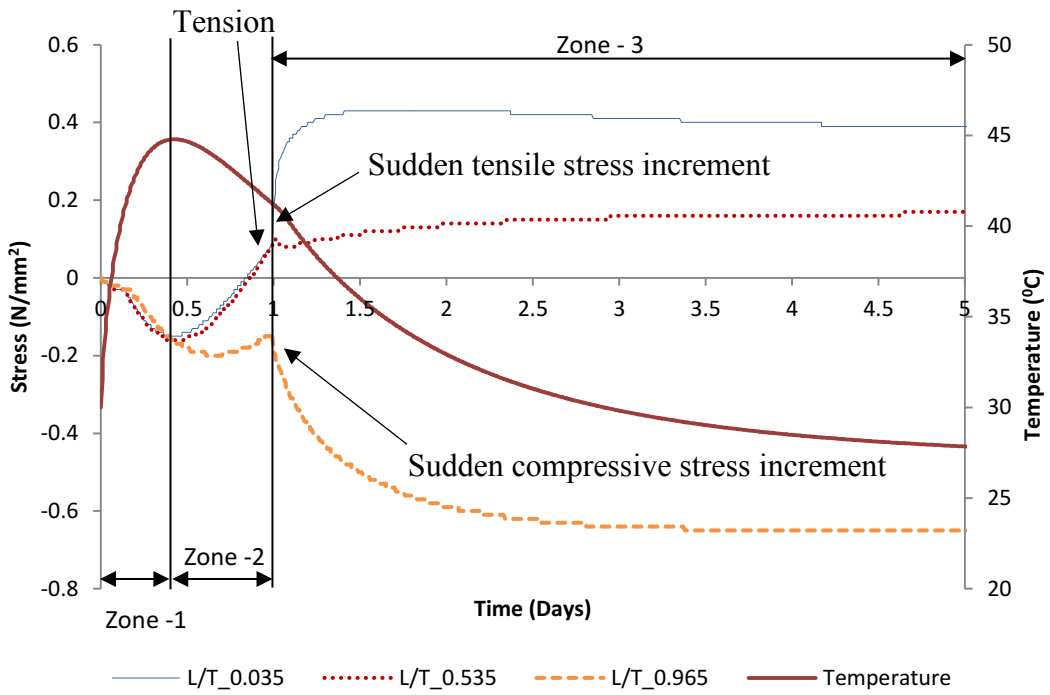

Figure 4.2 Temperature variation and stress variation at the crown – Location is shown as a ratio to the lining thickness from surface

4.2.1.1 Behaviour of isolated lining in imaginary conditions

As the starting point, to understand the mechanism in the three zones, another Idealized analysis was carried out by modeling only the second lining. Model is shown in Figure 4.3. This imaginary model was assumed to be in the adiabatic condition and analysis was conducted without gravity load for a temperature increment similar to hydration heat. The purpose was to understand the behaviour of a thick concrete arc, similar to the second lining, in a homogeneous temperature increment without external confinement but with a fixed bottom end.

Transverse stresses at the crown part are shown in Figure 4.3 (b). It was observed that the stresses in the outer elements (elements close to the surface) were in compression (L/T ratio 0.035) and the inner elements (L/T ratio 0.965) were in tension. The deformation at the crown was in the upward direction as shown in Figure 4.3 (c).

4.2.1.2 Mechanism of crown transverse stress generation of second lining in short term due to thermal movements and gravity

The stress generation mechanism is explained with the reference to the behaviour of isolated lining explained in the previous section

1. Behaviour in Zone 1

Stress variation in Zone 1 in the actual model is very different from the isolated lining behaviour. The actual model showed compressive stresses throughout the second lining thickness. This difference was caused by the restraint from the stiffer shotcrete layer and the surrounding rock which restrained the upward movement of the second lining. The restraints prevented the radial expansion of the second lining leading to the compressive stresses.

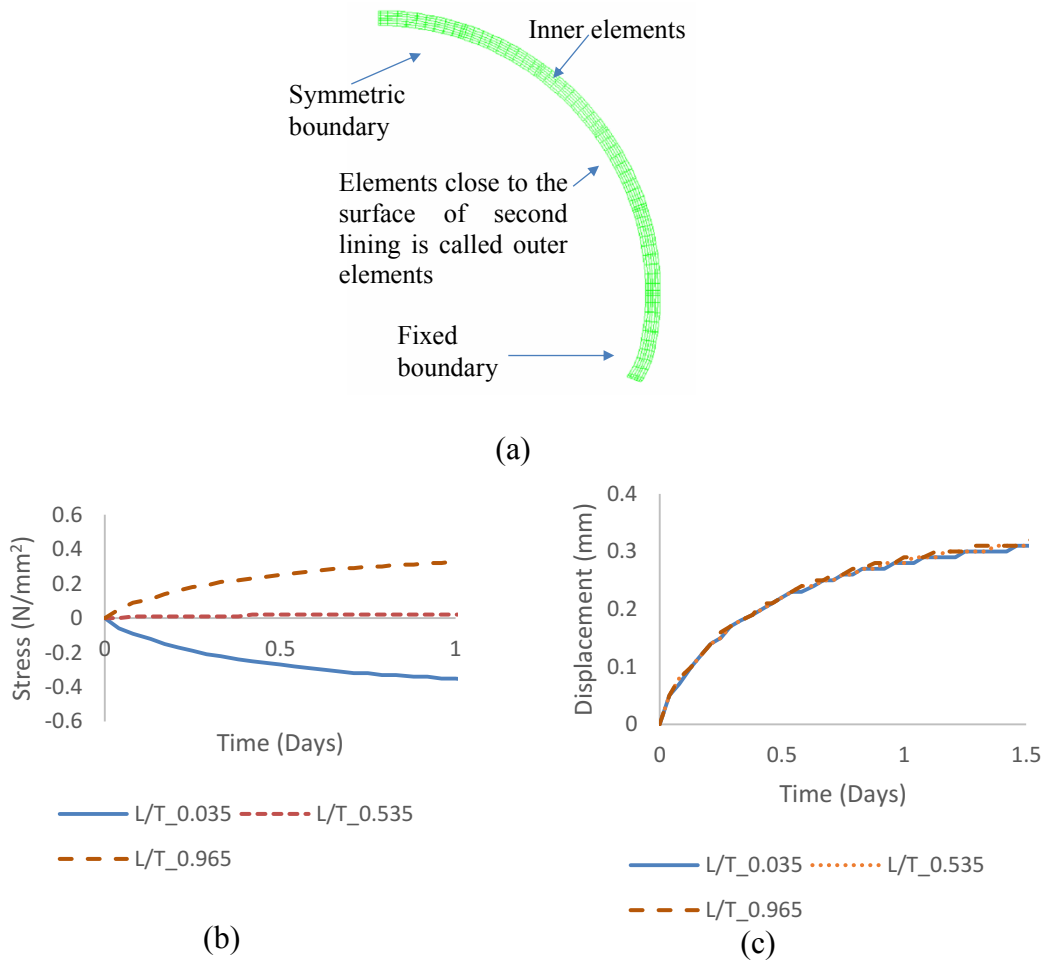

Figure 4.3 Imaginary, Isolated lining (a) FE model (b) Transverse stress at crown (c) Deformation at crown

2. Behaviour in Zone 2

With the decrease of temperature, the effective strain generated in Zone 1 was gradually reduced. Because of the strain reduction, the compressive stress was also reduced. In Figure 4.2, it can be noted that stress state in the outer element changed into tension while compressive

stress was kept in inner elements. The reason for this behaviour was thought to be a higher rate of temperature decrease of outer elements exposed to the environment. The temperature profile in the thickness direction is shown in Figure 4.4.

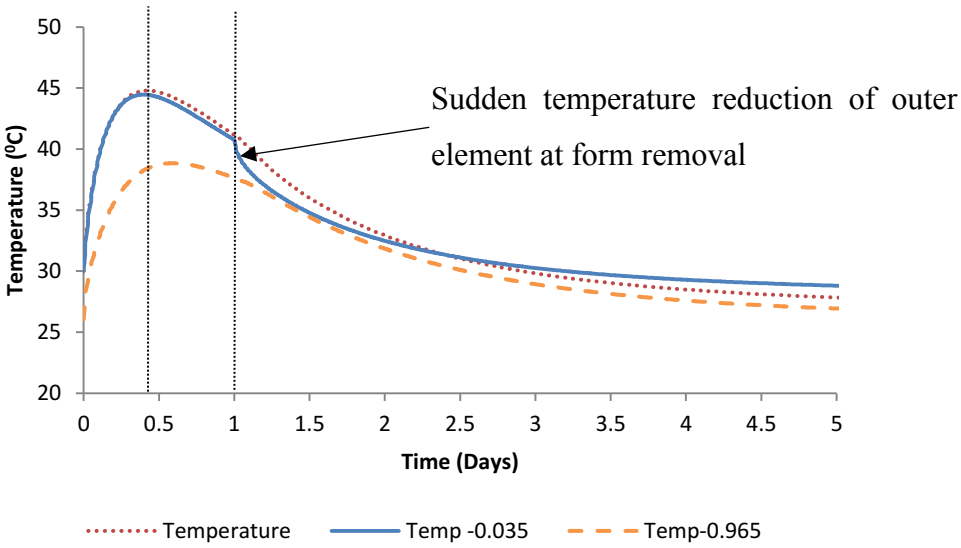

Figure 4.4 Temperature profile in thickness direction of the actual model at crown

1. Behaviour in Zone 3

Just after the separation second lining behaves as a beam close to the crown

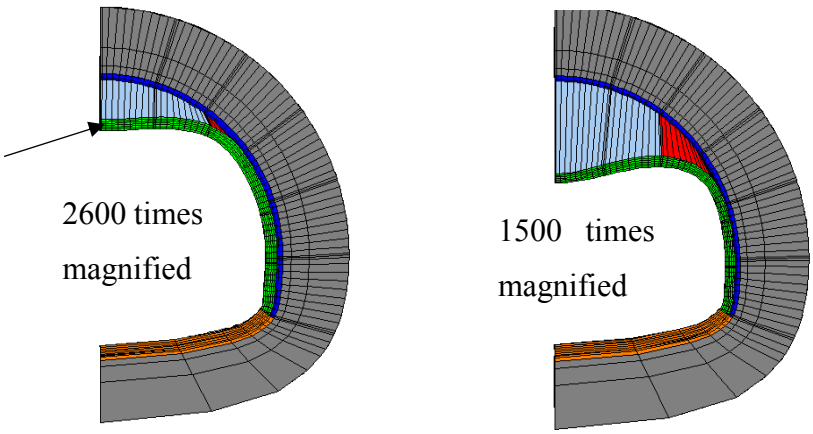

Figure 4.5 Deformation pattern of the second lining (a) Just after form removal 1.16 days (b) at 20 days

The stress behaviour in Zone 3 can be considered as the most important for practical applications as these stress variations occur after the form removal. Two main stress variation patterns can be observed up to 5 days in Zone 3. The first one is the sudden stress change just after adding gravity load (to simulate the form removal and the heat transfer coefficient is also

changed from 6 W/mK^{-1} to 14 W/mK^{-1} at the same time). It can be observed that at the inner gauss point compressive stress was increased, while at the outer gauss point, tensile stress was increased. This was thought to be caused by the combined effects due to beam behaviour of second lining close to the crown due to separation and the sudden temperature decrease caused by increasing the heat transfer coefficient on the surface. The deformation patterns at 1.16 days and 20 days are shown in Figure 4.5. The sudden temperature decrease in the surface can be seen in Figure 4.4.

The second behaviour pattern in Zone 3 is the gradual variation of stresses which follow the sudden stress variation. This gradual stress variation must have been caused by the gradual temperature decrease and can be explained considering reversed conditions of the isolated lining behaviour shown in Figure 4.3. In the separated lining with temperature decrease, outer elements might show tensile stress increment while inner elements show compressive stress increment as opposed to isolated lining with temperature increase.

4.2.1.3 Effect of the air void

In the actual calibration model explained in Chapter 3, an air void was assumed between first and second lining mainly considering the measured concrete temperature difference at the crown and close to the invert. The effect of this air void for stress conditions can be explained using the imaginary isolated lining shown in Figure 4.3. When stress generation pattern of the imaginary isolated lining was considered, the inner elements were in tension. Therefore, a small gap between the second lining and the first lining due to construction imperfections can generate tensile stresses during temperature rising period.

In the idealized simulation conditions, compressive stress generation due to confinement as explained in the behaviour of zone 1 is obvious. Therefore the initial tensile stress in actual measurements (Figure 3.33) might have occurred due to some imperfections of real structures. This observation supports the assumption of the existence of air void and the initial tensile strength generation with the air void can be seen in simulation results shown in Figure 3.33.

4.3 Stress behaviour of second lining governed by early age volume changes

After understanding the stress generation mechanism at the crown, a parametric study was carried out to understand the crown and invert stress variations with respect to a selected set of parameters which were thought to be important in early age stress behaviour. The objective of the study was to clarify the stress variations in two main locations, crown and close to invert, with respect to concrete properties which can be easily altered by the contractor (placing temperature) or at design stage (Autogenous shrinkage).

4.3.1 Comparison of analysis results

It was observed that the maximum value of the crown stress normally occurs at the surface of the lining. In the case of the longitudinal stress at location P, it varies in vertical direction and in the thickness direction. The maximum stress point was selected from the standard model and results were compared at this point. The longitudinal stress variation at the middle of the thickness in vertical and in the thickness direction at different times are shown in Figure 4.6. Gauss point with maximum stress was found as the 9th gauss point in the vertical direction from the invert and the fourth point from the surface.

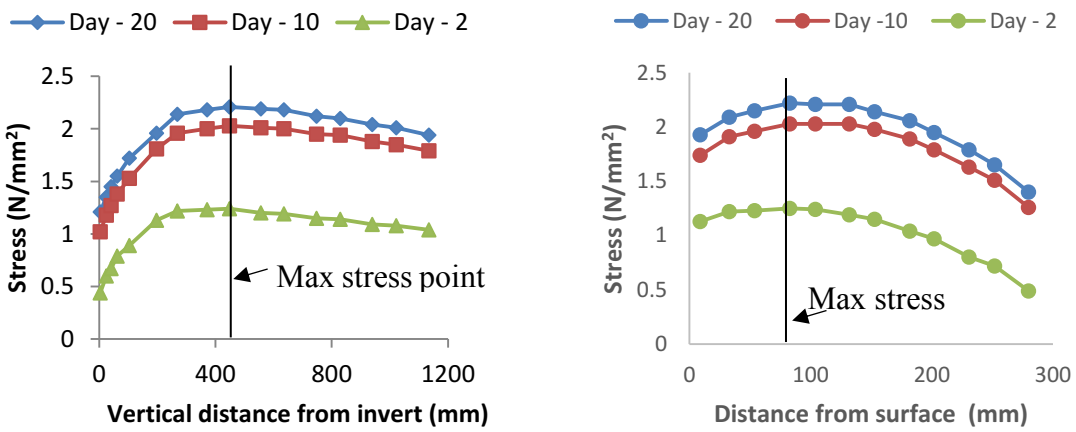

Figure 4.6 Longitudinal stress variation with distance (a) In vertical direction (b) Distance in thickness direction

4.3.2 Effect of Autogenous shrinkage on stress variations at the crown and close to the invert

The target of the study was to identify the effect of autogenous shrinkage on stress variation on two locations concerned. Therefore, autogenous shrinkage applied on base model was factored 0.5 and 1.5 to observe the stress variation patterns. Temperature dependent autogenous shrinkage calculated at the crown is shown in Figure 4.7.

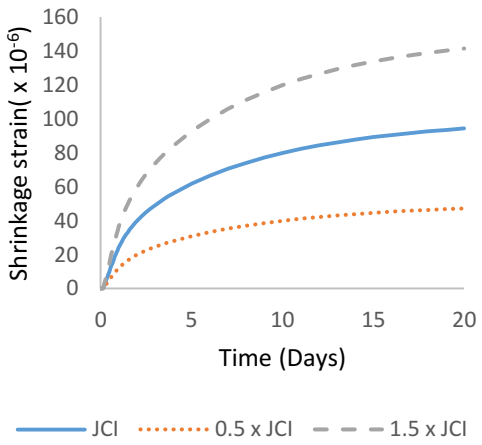

Figure 4.7 Calculated shrinkage strain at the crown according to JCI guideline

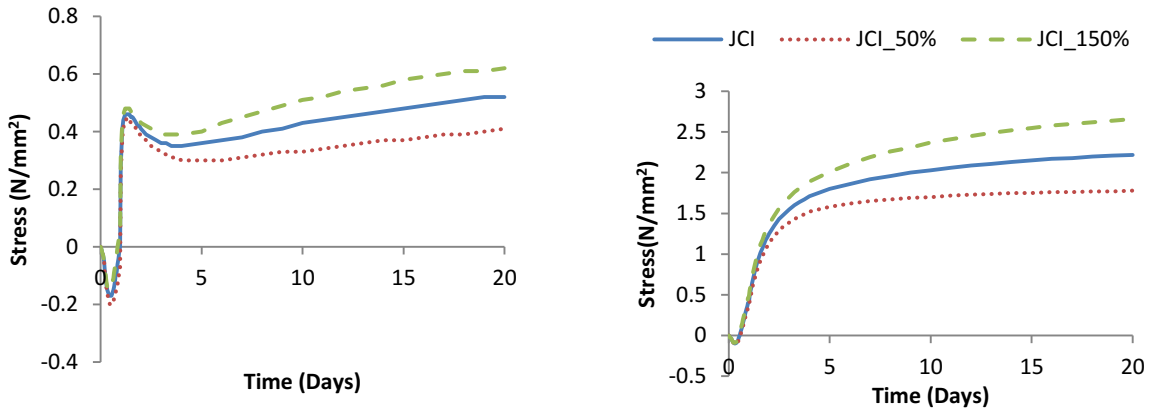

Figure 4.8 Stress variation with autogenous shrinkage (a) Crown transverse stress (b) Close to invert longitudinal stress

Variations of stresses are shown in Figure 4.8. It can be seen that the effect of autogenous shrinkage has a considerable effect on the stress close to the invert while the effect on transverse stress at the crown in minimal. The effect of stress increment close to invert can be expected because the external restraint from the invert will help to generate increased stresses.

In the case of crown transverse stress, some variation could be observed with changing autogenous shrinkage. To understand the importance of the level of variation of stresses, stress at selected points were sketched with respect to the tensile strength at that point as shown in Figure 4.9.

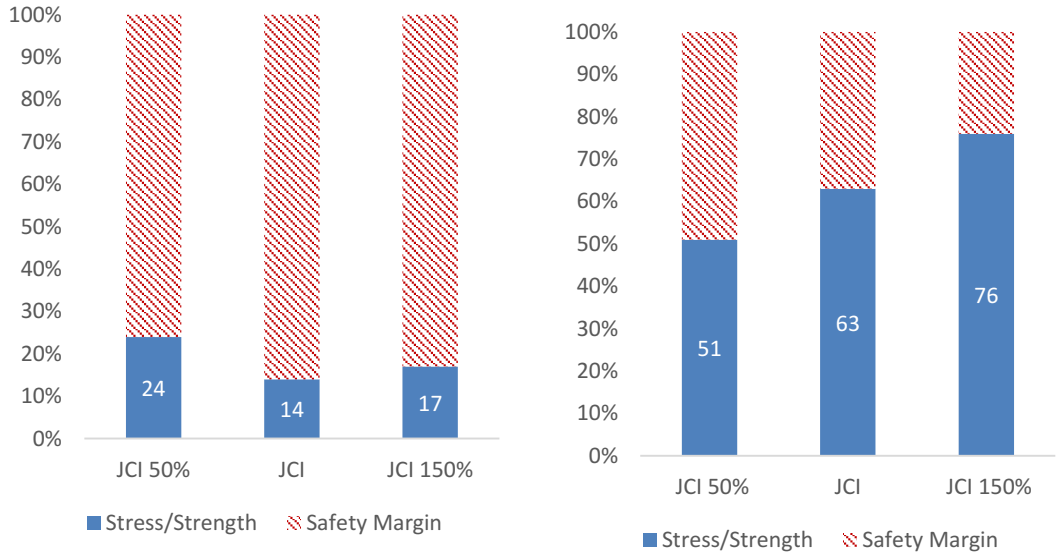

Figure 4.9 Effect of autogenous shrinkage, tensile stress/strength ratio (a) At crown (b) close to invert

When the crown tensile stress/tensile strength is compared as shown in Figure 4.9, it could be observed that the crown stress variation is almost negligible as all the stress values are smaller than ¼ of the tensile strength. Especially when autogenous shrinkage increased from 100% to 150% the cracking risk (Tensile stress/Tensile strength is referred as "Cracking risk") was only increased by 3%. When 50% of JCI calculated autogenous shrinkage was applied the maximum stress was observed at 1.3 days where in other two cases maximum stress was observed at 20 days. The Cracking risk is higher in 50% autogenous shrinkage case because tensile strength was not properly developed at this age.

In the case of longitudinal stress close to the invert, it could be seen that the cracking risk is changed up to 13% implying that autogenous shrinkage is an important factor to be considered to reduce cracking risk close to the invert.

4.3.3 Effect of the coefficient of thermal expansion of concrete on the crown and the invert stress

The coefficient of thermal expansion of concrete can be varied due to many factors such as the type of cement and aggregates, the age of concrete etc... As the early age stresses are governed by temperature variations due to thermal movements, the coefficient of thermal expansion of

concrete was expected to have a considerable effect on the stress variation in early age. The effect was studied based on the guidelines provided by JCI [8]. It was observed that the coefficient of thermal expansion can be varied between 4.5 $\mu/^0$C to 14.5 $\mu/^0$C based on the

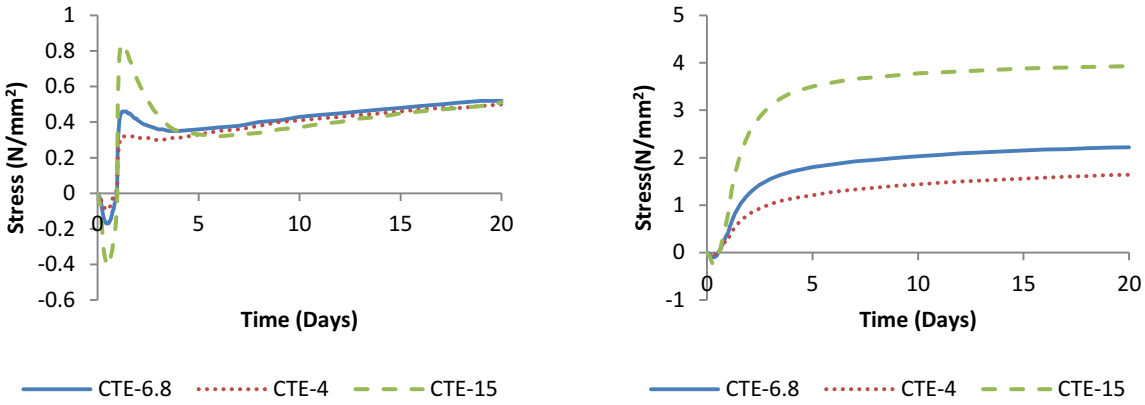

Figure 4.10 Stress variations with respect to coefficient of thermal expansion (a) transverse stress variation at crown (b) Longitudinal stress variation at invert

aggregate properties. For the parametric study 4 $\mu/^0$C and 15 $\mu/^0$C was used while the coefficient of thermal expansion of the base model was a measured value of 6.8 $\mu/^0$C.

Results of the parametric study are shown in Figure 4.10. When the stress behaviour of the crown is considered, it can be observed the effect of CTE on the final stress condition after 20 days is not considerably large. But a variation can be observed in the initial part before the form removal, the compressive stresses are increased with higher CTE due to the increased effective compressive strains even though the temperature increment is same for all three cases. Also, a major variation difference can be seen after the form removal. After the sudden stress variation followed by form removal the gradual stress reduction shows different gradients. This is also possible to explain according to the stress generation mechanism explained in section 4.2. According to the explanation, this gradual stress variation is governed by the temperature gradient of inner and outer elements. That implies, although the temperature gradients for all the four cases shown in Figure 4.10 are same, due to the difference of the value of CTE the thermal stress is varied ultimately leading to different stress patterns although the young's modulus is also identical in all four cases.

The stress behaviour at the invert shows a great sensitivity to the CTE. It can be observed the peak compressive stress during the temperature rising period and the final tensile stress has increased due to the increased thermal strain caused by increased CTE. This behaviour

complies with the expected stress generation mechanism at invert because when thermal strain is higher the effect of external restraint will generate higher stresses.

The importance of CTE to the cracking risk can be identified from Figure 4.11.

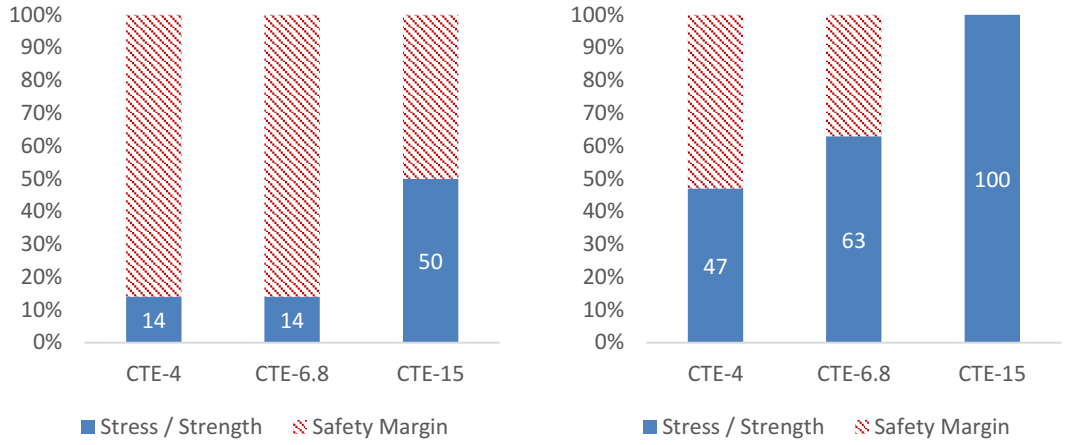

(a) (b)

Figure 4.11 Effect of CTE, tensile stress/strength ratio at maximum stress (a) at crown (b) at invert

It was observed that cracking risk has increased by 36% at the crown with minimum and maximum possible CTE values of concrete. Even though the stresses are not high enough to generate a crack only due to CTE, higher risk of cracking poses if the temperature increase get higher due to changes of cement type, initial temperature, environmental temperature increment etc. especially as drying shrinkage can increase the crown stress in a substantial amount as shown in Chapter 5, very high coefficient of thermal expansion can increase the risk of crown cracking in a substantial manner. The maximum crown cracking risk was observed at CTE-15. In this case also, the maximum risk was observed at 1.2 days from construction instead after 20 days.

In the case of the close to invert position, the variation of cracking risk is more than 50% and was large enough to cause a crack when CTE is maximum. So controlling the CTE of concrete by using low expansive aggregates or reducing temperature increase due to the heat of hydration is beneficial in case of reducing the cracking risk at both crown and close to invert positions. The maximum cracking risk was obtained at 1.4 days from casting in the case of close to invert case.

4.3.4 Effect of concreting temperature

Temperature variations of concrete can be occurred in several ways such as temperature increase due to hydration heat, environmental temperature variations, initial concreting temperature etc. The temperature of concrete can have a considerable effect on the behaviour of the concrete including the hydration process and strength gain. Especially as shown in previous section amount of temperature increment combined with high CTE of concrete can increase the tensile stress. The temperature of concrete at the time of placement is an important factor that can have a significant effect on the peak temperature of concrete gained due to hydration heat. Since this parameter can be controlled by the contractors, it is important to investigate the effect of concreting temperature on the stress variations at critical points.

In the case of the base model, the concreting temperature was used as 30^0C. Therefore, to observe the stress variation pattern with changing concreting temperatures two simulations were carried out with the concreting temperature of 20^0C and 40^0C. Here, it is important to mention that the highest concreting temperature is limited to about 35^0C to prevent thermal cracking by standards. But in practical scenario temperature of concrete is measured in the sites before pumping, and the pumping itself can increase the temperature of concrete from about 2-3^0C according to verbal conversations done with contractors. Therefore, for the sake of the investigation concreting temperature was set to an extreme 40^0C value. Stress variation results are shown in Figure 4.12.

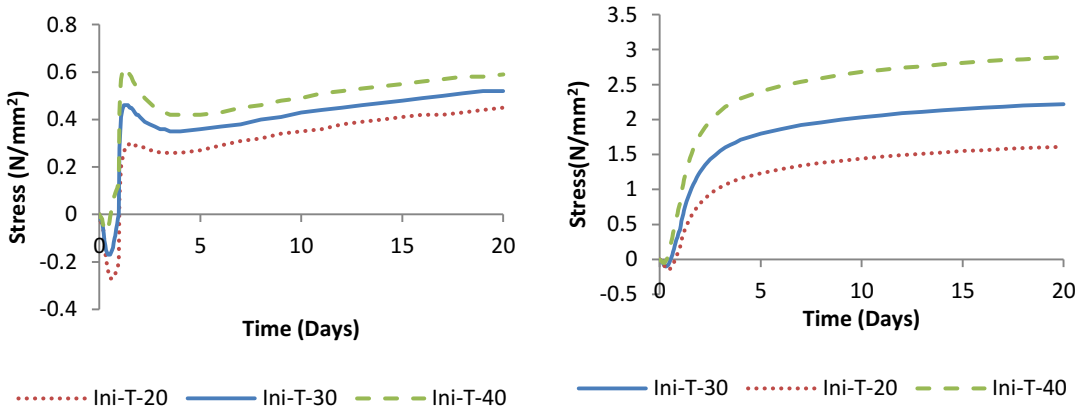

(a) (b)

Figure 4.12 stress variations with respect to initial concreting temperature (a) Transverse stress variation at crown (b) Longitudinal stress variation at invert

A significant variation of crown stress cannot be witnessed with respect to the concreting temperature at the crown except the slight stress variation after the form removal due to varied peak temperatures. But it can be observed that the invert stress is very sensitive to the

concreting temperature and by reducing initial concreting temperature early age thermal stress can be considerably controlled close to the invert.

Stress/ Strength ratio of concrete at the most critical stress is shown in Figure 4.13. It was observed that the low initial concrete temperature can significantly reduce the cracking risk close to invert. In the case of crown stress, even though a difference of cracking risk of 20% increment is observed in the case of 40^0C concreting, still the safety factor is considerably large enough to prevent cracking. But in this case, the critical Cracking risk was obtained at 1.25 days after casting.

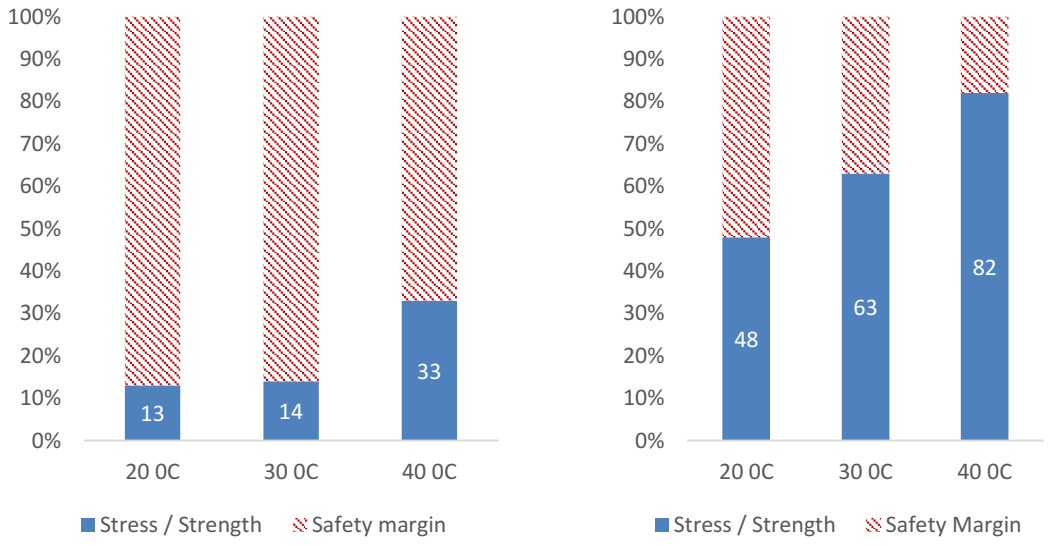

(a) (b)

Figure 4.13 Effect of concreting temperature, tensile stress/Strength ratio (a) At crown (b) At invert

4.3.5 Effect of time of formwork removal

By keeping the form for a long time, better quality concrete can be obtained by improved curing. But it is obvious that keeping form might impose external restraint for the volume changes of concrete due to hydration heat. Especially, with the assumption of separation of second lining from waterproofing layer, extended form retention can impose higher stresses.

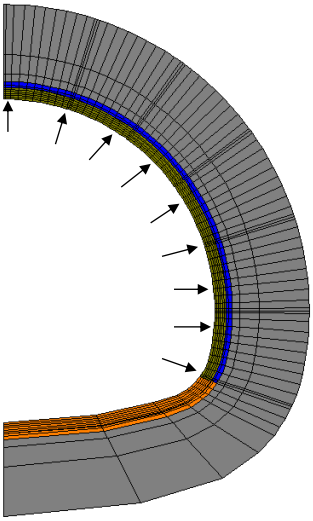

Figure 4.14 Idealization of the formwork

In the base model, form removal time was set to 24 hours. In the current analysis effect of form removal after 7 days was investigated to observe the change of stress patterns. But the important fact to notice is that in the calibrations carried out in Chapter 3 form removal was idealized as the equal to the application of the gravity load at the time of form removal. The restraint from the form was not modeled in that section. But, to investigate the external restraint from the form, the form was assumed to be equals to a set of nodal restraints which are perpendicular to the surface of the form as shown in Figure 4.14 . It was assumed that the form will not exert any significant friction in the longitudinal or in circumferential direction because the surface of metal form is smooth. This modeling was especially expected to provide an insight about

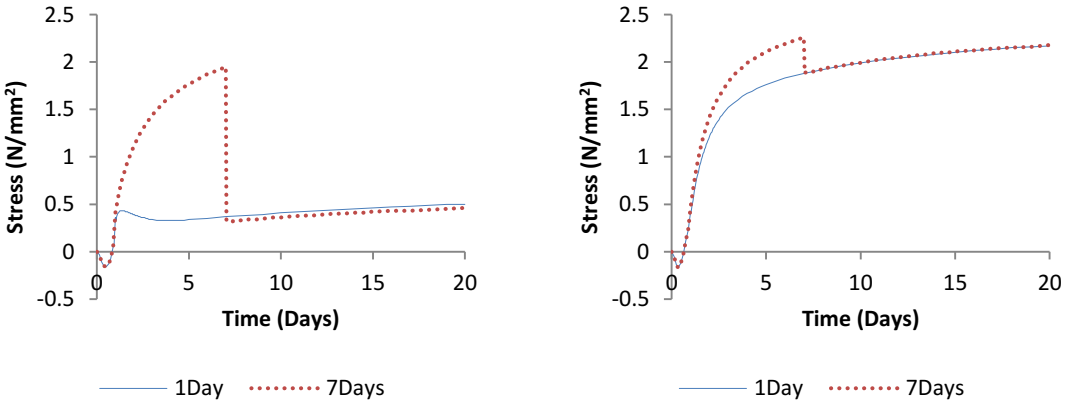

(a) (b)

Figure 4.15 Stress variations with respect to form removal time (a) transverse stress variation at crown (b) longitudinal stress variation close to invert

the possible stress increments during the temperature decreasing period after the peak

temperature due to hydration heat. The supports that used to represent the form were removed at the time of form removal.

The base model was again modeled with the external supports because of the possibility of changing the stress behavior due to the modeling of external restraint of the form system. Stress variations at the middle thickness of the lining are shown in Figure 4.15.

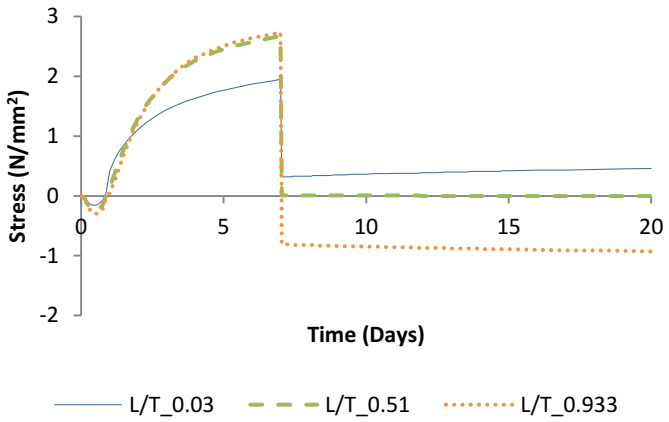

Figure 4.16 Crown stress variation in thickness direction

It was observed that the crown stress can be drastically increased if the form can provide a perfect external restraint. The effect on longitudinal stress close to invert is not significantly large. The stress distribution in the thickness direction at the crown is shown in Figure 4.16. It was found that the crown stress distribution can change if the form is capable of providing a significant level of external restraint in the normal direction. It depicted that, by keeping form in such a way that it causes a significant external restraint, a penetrating crown crack can be generated as whole crown thickness is in tensile stress.

Tensile stress to strength ratio is shown in Figure 4.17. It was noted that the cracking risk was increased over 50% in the case of crown and 14% increment close to invert. Therefore, to obtain high quality concrete by long form retention, proper care should be taken to reduce the restraining effect of concrete by the form.

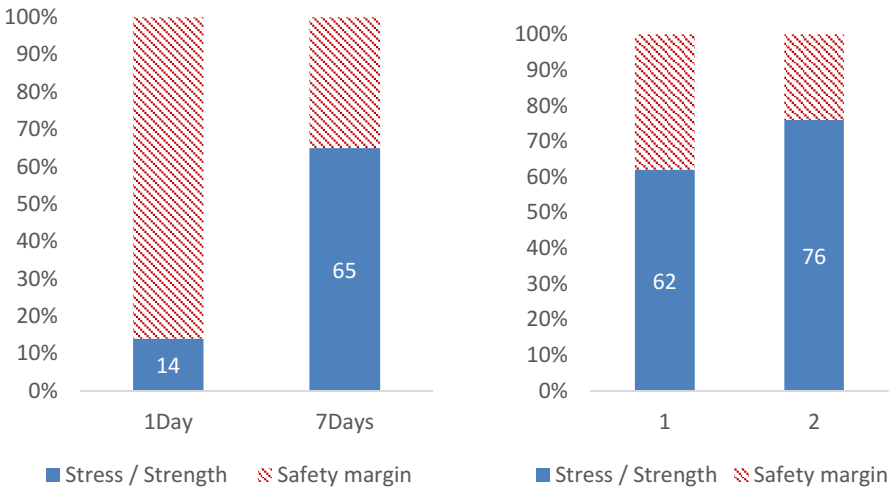

Figure 4.17 Effect of formwork removal, tensile stress/ tensile strength
(a) at crown (b) at invert

4.3.6 Crown and close to invert stress behaviour with respect to the existence of the air void between first and second linings at crown

It was noted from site measurements that temperature of concrete close to invert and crown is considerably different and could be taken into account by assuming an air gap between two linings considering practical construction process and site observations. This analysis was carried out assuming the air gap does not exist to investigate the stress behaviour. Stress variations are shown in Figure 4.18

From Figure 4.18 (a) and (b), it can be seen that the neither crown stress nor close to invert longitudinal stress shows a considerable dependency on the existence of air gap. It can be expected that the longitudinal stress close to invert might not depend on the existence of air gap because that does not modify temperature or restraint conditions close to invert. In the case of crown stress, even the temperature is higher with the air gap, the free to move nature of the lining at top part might have reduced the stress generation. It might not be reasonable to assume that this type of compensation can occur in every tunnel because the properties of the air gap and crown behaviour can vary with factors such as tunnel geometry, construction method, and mix proportion of concrete.

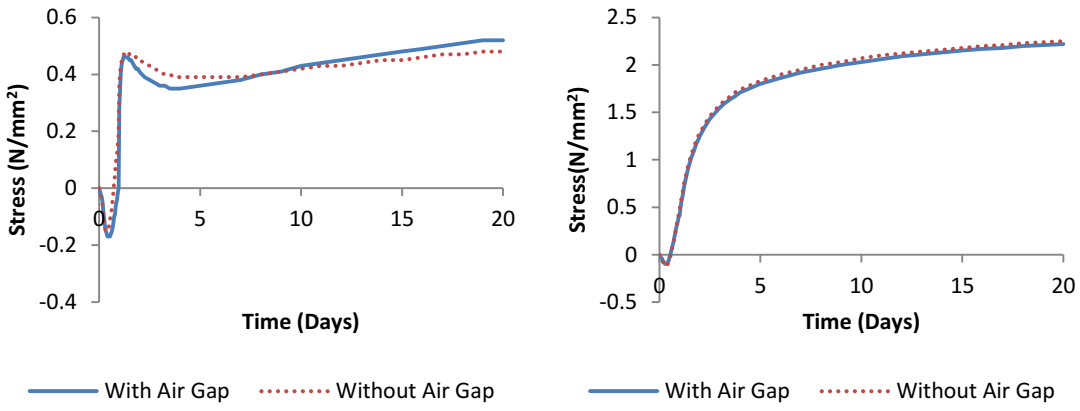

(a) (b)

Figure 4.18 Stress variations based on crown temperature (a) transverse stress variation at crown (b) longitudinal stress variation at location P

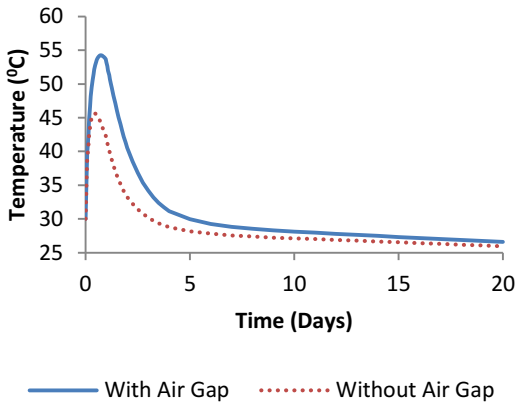

Figure 4.19 Temperature variation at crown middle thickness with and without air gap

4.3.7 Investigation the effect of expansive additive

Expansive additives are used to introduce an expansive strain in the initial stages of concrete hardening mainly to compensate the autogenous shrinkage in mass concreting. Many tunnel construction contractors believe that usage of expansive additive might be an effective solution for controlling both close to invert and crown stresses. An investigation of the effectiveness of expansive additives was carried out to find the level of stress control offered by the expansive additives. Expansive strain was calculated according to the JCI guideline [8] and the generated stresses are shown in Figure 4.20

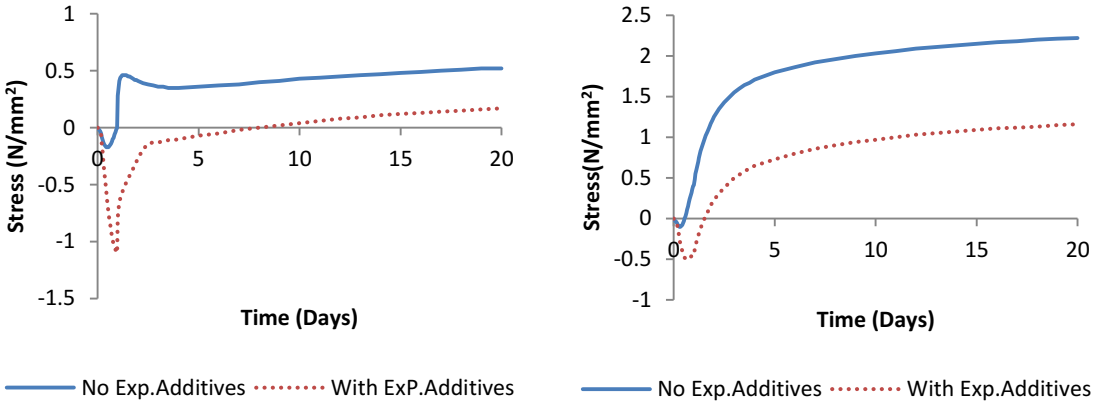

Figure 4.20 Effect of expansive additives on stress (a) Transverse stress variation at Crown (b) longitudinal stress variation at location P

From the stress variations graphs at two locations, it was seen that expansive additives can reduce the tensile stresses generated due to thermal effects. It was noted that in the case of crown stress the final reduction of stress due to expansive additives was 0.35 MPa at the crown surface and 1.06 MPa close to the invert. Stress and strength percentages are shown in Figure 4.21. When the ratios are considered it can be seen that cracking risk is not well pronounced in the case of the crown because the reduction of cracking risk is only 9%. But in the case of longitudinal stress close to invert, the cracking risk is reduced by 30% and can be much effective in reducing the longitudinal cracking risk

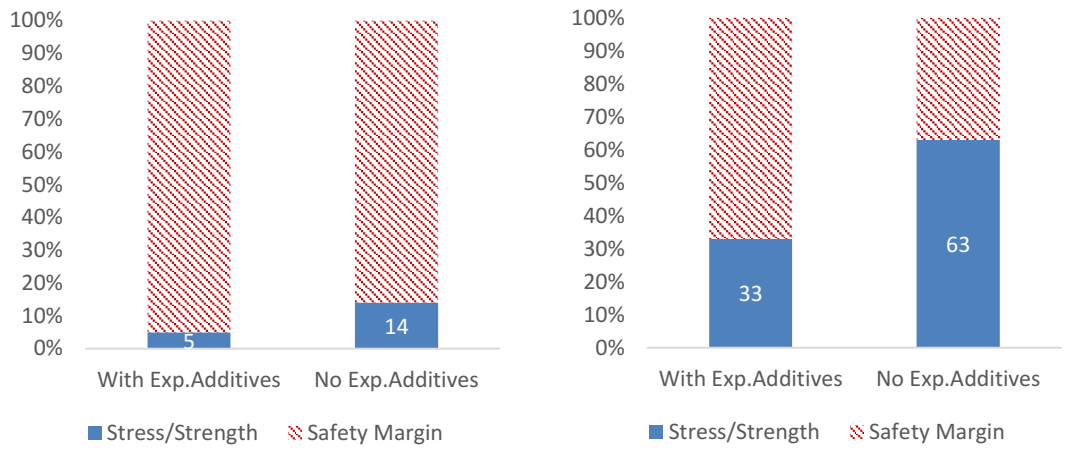

(a) (b)

Figure 4.21 Effect of expansive additives stress/strength ratio (a) at crown (b) close to invert

4.4 Summary

The objective of this section was to understand the stress variations of second lining governed by thermal stresses in a short period of time after the construction. In the first part, crown stress variation pattern was described with respect to the simulation results for a short period of time considering the effect of thermal stresses due to the heat of hydration. A parametric study was carried out to understand the crown and close to invert stress variations in the short term. It was observed from the analysis that any conditions which could increase the contraction of concrete could increase the stress close to invert. It was also observed the crown transverse stress only showed a high sensitivity to the conditions which could generate differential strain conditions in the thickness direction at the crown. Following facts could be observed from the study.

1. It could be observed that the crown stress behaviour at the middle of the lining is independent of the longitudinal direction and can be appropriately modeled with a 2D model.
2. According to the mechanism of crown stress, stresses before form removal was governed by temperature effects while the stresses after form removal were governed by both temperature and self-weight effects. The freedom of the second lining to move in vertical direction affected the behaviour at both before and after the form removal.
3. In the case of autogenous shrinkage, the cracking risk increment close to invert is more pronounced with higher autogenous shrinkage. In the case of crown cracking risk, the

stress variation was below 25% from strength when shrinkage strain was varied from 50% to 150% (about 90μ ultimate increment) pronouncing low sensitivity.

4. Very high coefficients of thermal expansion pose more risk of cracking at both close to invert and at the crown location.
5. The effect of initial concreting temperature is also higher in the case of close to invert stress and not so severe in the case of crown stress. The risk of close to invert vertical cracking might be able to be reduced by low temperature concreting.
6. Effect of form removal time has a high effect on crown stress. If the external restraint is fully effective (as the form is very stiff). It can lead to a penetrating crack at the crown with poor material properties. Hence, to obtain the advantage of long form retention to obtain good quality concrete, the form can be partially released to prevent activation of external restraint.
7. In the considered case, the existence of air void (which generate higher stresses at the crown) seemed to be not sensitive to the crown surface stress. This might be due to the stress reduction as the top part of the lining is free to move in the vertical direction with air void. But the behaviour might be different from case to case.
8. Usage of expansive additives might be effective in reducing the cracking risk close to invert but might not be so effective in the case of crown cracking because the decrease of stress seemed to be too small.
9. It was observed for some cases such as high CTE concrete the highest cracking risk at crown was observed just after the form removal instead of 20days.
10. Considering all the cases analyzed, it could be observed that the variation of crown stress is below 50% of strength except for long form retention. This depicts that the crown cracking might not be generated just due the effect of a single parameter just by thermal stresses. That implies, if cracking occurs in very early age at crown some combined effect should exist to generate high enough stress at the crown to cause cracking. Therefore, proper construction and ensured material quality might be the key to preventing very early cracking at the crown.

5 LONG-TERM STRESS BEHAVIOUR OF SECOND LINING GOVERNED BY DRYING SHRINKAGE

Withdrawal of water from the concrete surface by unsaturated dry air produces drying shrinkage in concrete [28]. It is an important phenomenon considering the long term durability of concrete and can have detrimental effects on concrete structures in extreme conditions. As mentioned before, drying shrinkage creates a moisture gradient from the surface to thickness direction as moisture movement is higher in the concrete surface. This gradient causes differential shrinkage which can result in internal restraint which can lead to cracking.

An analysis scheme was established in section 3.4 to analyses the stress generated due to drying shrinkage by estimating the drying shrinkage values with varying environmental conditions and feeding to the stress analyses software. Using the established simulation scheme a parametric study was carried out to investigate the effect of shrinkage property of concrete and tunnel section size on crown stress.

5.1 Calculating crown stress using calculated drying shrinkage strains

For initial investigations (which are described in this dissertation), the shrinkage strain was calculated assuming constant environmental conditions and stress analysis was carried by feeding the calculated strain values to Astea-Macs stress analysis software.

For the current study, environmental temperature was set as constant at 20^0C and environmental relative humidity was varied to 70% and 80%. Calculated drying shrinkage strain values from Link3D is shown in Figure 5.1. The stresses calculated after considering the calculated shrinkage strain values are shown in Figure 5.2(a). The thermal cracking index defined as the ratio of tensile strength of concrete to the generated tensile stress is shown in Figure 5.2(b). It could be seen the stresses are highly dependent on calculated shrinkage values and the crack index was higher when relative humidity is 80% representing a low cracking risk compared to the case with lower relative humidity value of 70%.

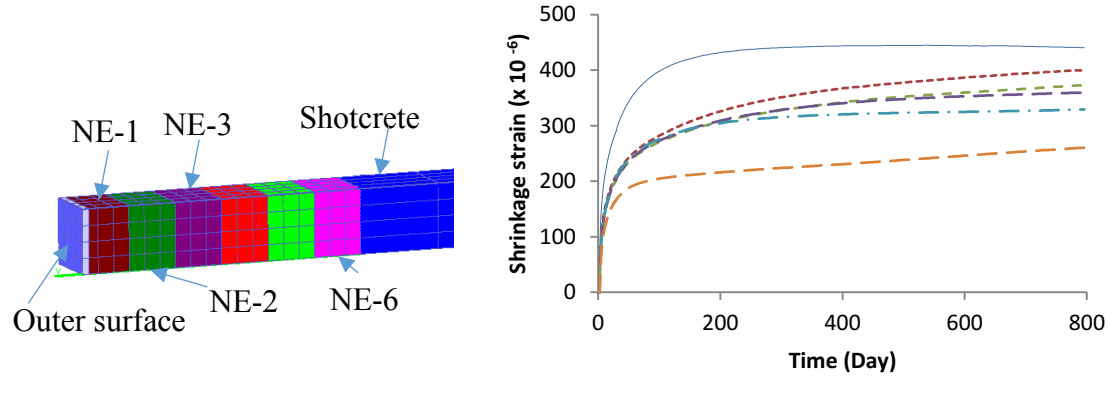

Figure 5.1 calculated shrinkage strains from Link3D after temperature adjustment relative humidity of 80%

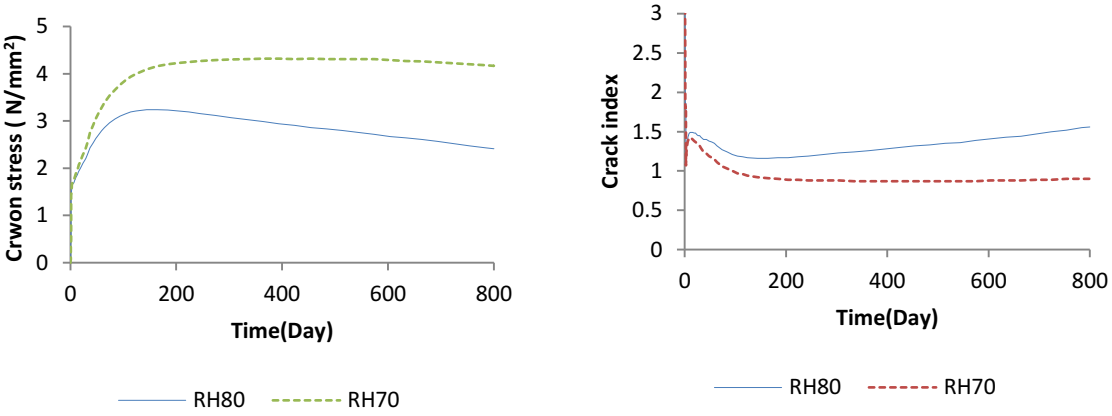

(a) (b)

Figure 5.2 calculated quantities by integrating with stress analysis tool (a) transverse stress at crown (b) Thermal cracking index at crown

5.2 Stress variation at the crown with changing tunnel section size

It was mentioned in Chapter 1 that type 1 crown cracking is not found as much frequently as the type 2 vertical cracking close to the invert. One of the locations that crown cracking is more prominent is the enlarged sized blocks with evacuation areas. Generally, the length of such blocks are shorter than normal sized tunnel blocks and the thickness of the lining can also be different from normal block.

The effect of tunnel section size was investigated using the established simulation methodology to investigate the cracking risk in enlarged tunnel section compared to normal size section. The Same process was followed as explained in section 5.1. Drying shrinkage was calculated

assuming the environmental conditions are constant. Block details with normal and enlarged tunnel sections are shown in Figure 5.3

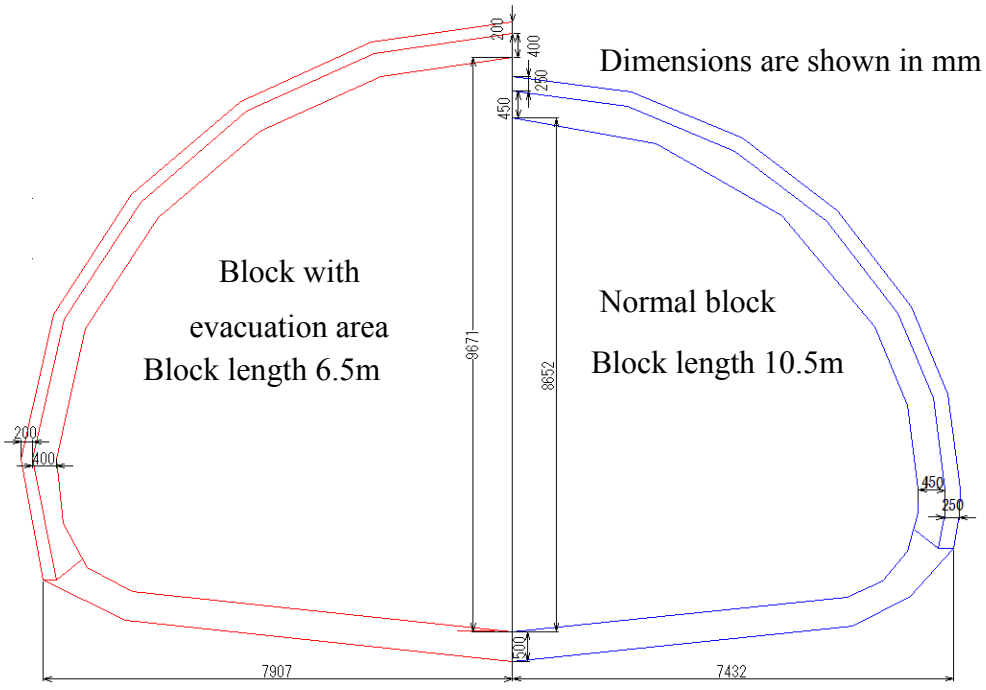

Figure 5.3 Normal and service sections in the Kodzuchi tunnel

A new model which can represent the thickness of the second lining in the large block was created to obtain the drying shrinkage from LINK3D. This LINK3D model is shown in Figure 5.4. Large size section model in Astea-Macs with reduced block length is shown in Figure 5.5

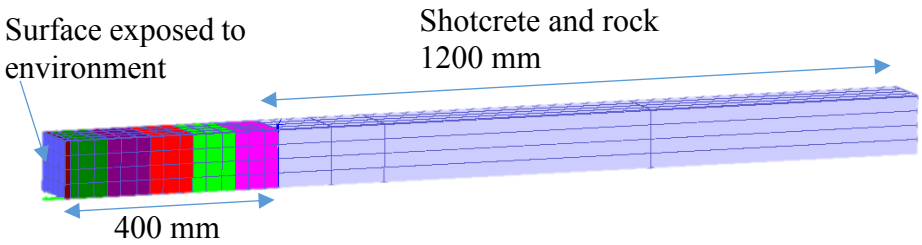

Figure 5.4 LINK3D model to calculate drying shrinkage values for large service sections.

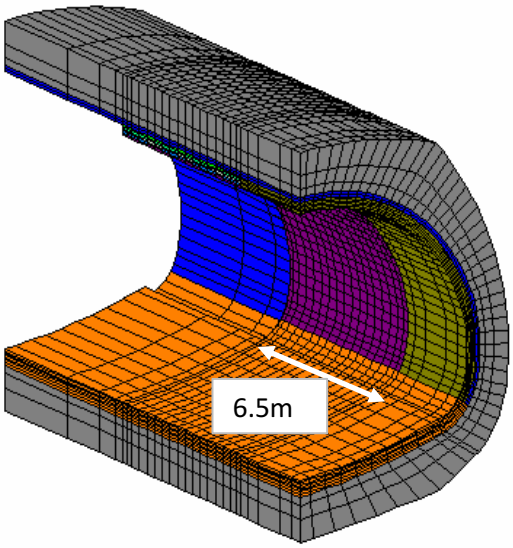

Figure 5.5 Astea-Macs model for stress analysis of large service section

The analysis was carried out in two sections considering two relative humidity values of 70% and 80%. Calculated shrinkage strain variations are shown in Figure 5.6. It can be noticed that calculated shrinkage values are almost same on the surface as expected and little different in the innermost element.

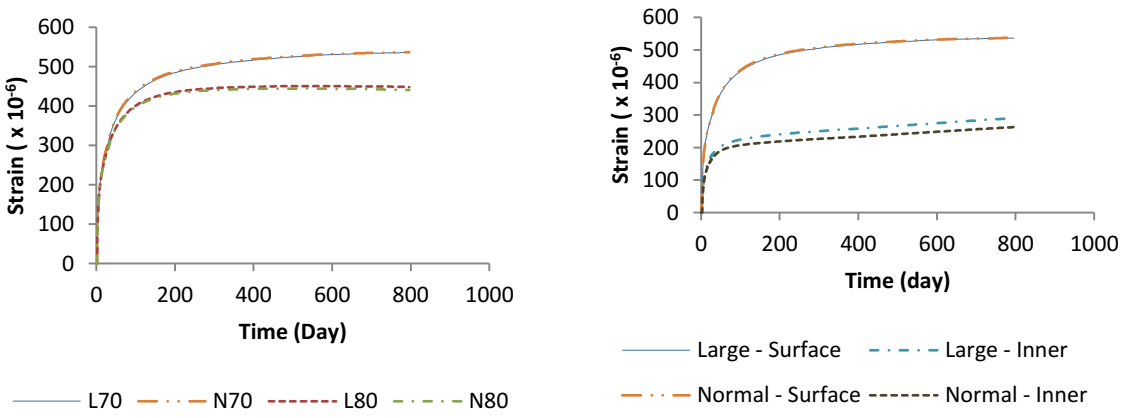

Figure 5.6 calculated strain variations for large and normal sections (a) strain variation at surface with varied relative humidity (b) strain variation comparison in thickness direction for 70% relative humidity

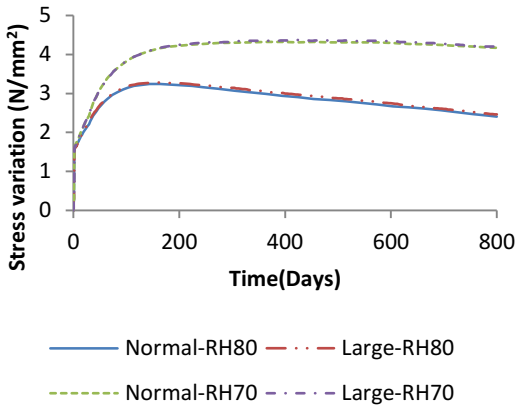

Figure 5.7 Stress variations at crown of large and small sections at different relative humidity values

Stresses were calculated with above calculated strain values and shown in Figure 5.7 in surface elements as these elements govern the visible cracking. It could be observed that the stress level was only increased with respect to the lower humidity value but stresses are not increased with respect to the increased section size. But it might not be appropriate to conclude that the section size does not increase cracking risk because this analysis was carried out only considering some of the driving forces, mainly drying shrinkage under constant relative humidity and temperature. There are other factors which might affect such as creep of concrete and even varying environmental conditions can change the stress behaviour.

5.3 Variation of stress at crown with varying concrete shrinkage

Effect of shrinkage property of concrete on crown stress was studied by using different concrete with different levels of shrinkage property. “Shrinkage property” here refers to the shrinkage strain of concrete calculated by standard JIS tests after 6 months. Figure 5.8 shows the range of concrete shrinkage values cast with varying aggregate properties used in all over Japan. It can be clearly seen the shrinkage values can fall within a very large range about 300-1350 microns. Based on these observations, it was thought to be important to understand the effect varying shrinkage property of concrete on crown stress.

The analysis was carried out considering three higher additional values of concrete shrinkage property values of 900, 1075, and 1200 where shrinkage property of calibrated concrete was 650 microns. Calculated shrinkage strain for surface elements are shown in Figure 5.10 and it could be seen the shrinkage strain of tunnel lining also increase when shrinkage property of concrete is increased.

Crown stresses obtained by changing the shrinkage property of concrete is shown in Figure 5.9. The obvious observation was the crown stress has increased with increasing shrinkage property of concrete due to the increase differential shrinkage occurred at the crown.

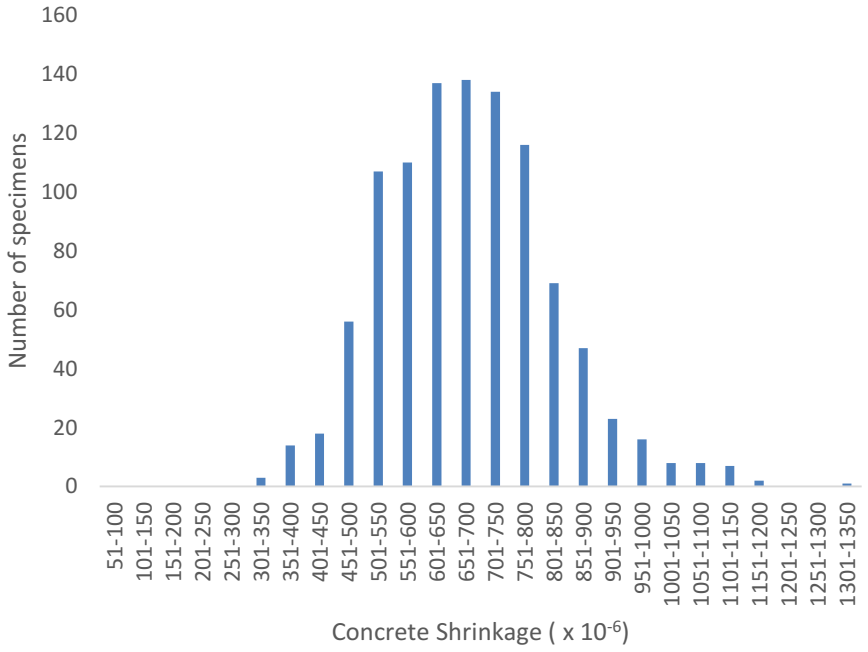

Figure 5.8 Variation of shrinkage of concrete

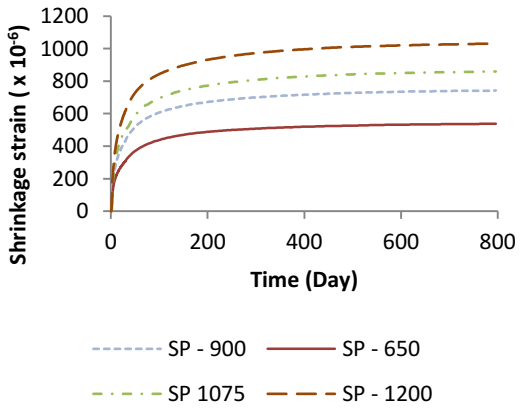

Figure 5.10 Calculated shrinkage for tunnel lining based on varying shrinkage property

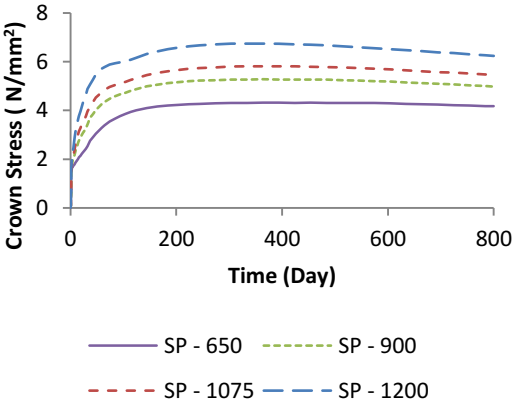

Figure 5.9 Crown stress variation based on varying shrinkage property

5.4 Summary

A simplified parametric study was carried out based on the simulation scheme established for long-term stress analysis in the second lining at the crown in section 3.4. Main parameters studied were the critical relative humidity level for cracking considering constant temperature and relative humidity of the air. Which was found to be a little higher than 70%. Then the effect of tunnel section size was investigated to see the risk of crown cracking engaged with changing section sizes. Finally, the effect of shrinkage property of concrete on stress condition at the crown of second lining concrete was studied based on statistical data published in Japanese standards. It was observed that the section size does not have a considerable effect on crown stress governed by drying shrinkage while shrinkage property of concrete highly influences the crown stress condition. However, it was observed that the drying shrinkage itself has a major influence of the crown stress because of differential shrinkage in the thickness direction.

The proposed simulation scheme should be further improved and verified before obtaining final conclusions regarding the long term stress behavior of the tunnel lining. Especially, the early age creep was modeled in current simulation by reducing the young's modulus of concrete according to JCI guideline [8]. This reduction can underestimate the stress generated due to drying shrinkage strains.

6 CONCLUSIONS

Findings from this research are summarized in this chapter with future tasks.

6.1 Conclusions regarding finite element modeling of second lining of NATM tunnels

1. In general, there can be many structural imperfections in NATM tunnels such as increased or decreased thickness of second lining, or existence of air void between first and second lining near the crown. These conditions might cause the simulation results to be different from actual site measurements and should be carefully assessed with proper engineering judgment, sufficient evidence and good experience to establish a reliable analysis model.
2. Main structural modeling assumption was made on modeling of joints. Joint models were proposed for the joint formed by waterproofing sheet and for the vertical construction joint with small normal tensile strength and shear strength and with high normal compressive strength. The behaviour of second lining concrete after form removal was appropriately simulated with the proposed joint models.
3. Major assumptions regarding thermal analysis were made with respect to the vertical distribution of air temperature and thermal properties of the composite waterproofing membrane. The vertical air temperature distribution was adopted from a past research and the thermal properties of composite waterproofing membrane were calculated assuming steady state heat transfer conditions with an air gap close to the crown. Temperature variation at the crown and close to the invert was simulated with acceptable accuracy with the assumptions.
4. From the simulation results, it could be observed that the vertical cracks close to the invert can be penetrating cracks and the longitudinal cracks at the crown can be non-penetrating cracks.
5. By comparing 2D and 3D versions of the finite element models, it can be stated that crown stress at the middle of the span can be molded reasonably well without considering factors in the longitudinal direction.

6.2 Conclusions regarding short term stress behaviour of second lining governed by thermal stress

1. Before the form removal, crown stress was governed by temperature variations and according to the possibility of movement due to the air void. After the form removal, stress behaviour was governed by self-weight, temperature decrease and the deformation capability of the second lining at the crown. Stress conditions might considerably depend on the cooling rate of the crown region.
2. Crown transverse stress was sensitive to the prolonged form retention which could cause external restraint for contraction of the second lining during temperature decreasing period. If it is necessary to obtain the advantages of longer form retention, proper care should be taken to make sure that the contraction of the second lining is not restrained.
3. Among the investigated material properties, the coefficient of thermal expansion and autogenous shrinkage had a considerable influence on the longitudinal stress near invert.
4. Low temperature concreting might be helpful in reducing the invert longitudinal stress but might not affect the crown transverse stress so much.
5. Expansive additive might be effective in controlling the stresses close to the invert. On the other hand, it might not be highly effective in controlling the stress at the crown because the expansive strain development occurred in about first 20-30 days of construction and the stress increment of the crown is mainly governed by long-term drying shrinkage. As future tasks, the other effects of expansive concrete beside the expansive strain such as the effect on tensile strength should be carefully determined to assess the actual effects of expansive concrete.
6. Considering all the cases analyzed, it could be observed that the tensile stress near the surface at crown was below 50% of tensile strength without considering drying shrinkage. This depicts that the crown cracking might not be generated by thermal stress and self-weight. Therefore, proper construction and ensured material quality might be the key for preventing early age cracking near the crown.

6.3 Conclusions regarding long term stress behaviour of second lining governed by drying shrinkage

1. A calculation method was proposed to investigate the effect of time dependent drying shrinkage on second lining stress by integrating two commercial finite element packages. Free drying shrinkage strain was calculated from LINK3D software by assigning shear stress free joints between elements to reduce the generation of internal stress. The calculated drying shrinkage strain was given as an input for the stress analysis software ASTEA-MACS.
2. When compared with the case of short term stress analysis, High level of stress generation at crown was observed with drying shrinkage. Therefore, it can be stated that drying shrinkage might be considered as a major driving force for the crown cracking. As the drying Shrinkage strain increases with shrinkage property of concrete, it might be possible to reduce crown stress by using concrete with low shrinkage property.
3. Large tunnel sections do not pose a higher risk of cracking at crown only due to drying shrinkage. The stress variation at crown was almost identical at the surface for considered tunnel sections in this study.
4. The calculation method should be properly verified before conducting detailed a parametric study. Especially, the effect of accounting for early age creep should be verified because the currently used method modifies the young's modulus of concrete. This can underestimate the stresses generated due to drying shrinkage according to the proposed simulation scheme.

6.4 Future tasks.

1. This study was carried out mainly with measurement data obtained from a past research. A detailed site measurement plan to obtain second lining behaviour is proposed based on the experience obtained from the current study and planned to be carried out in near future. The main objective is to properly verify the modeling assumptions with higher confidence. Temperature and stress/strain measurements were proposed at crown not and close to invert not only in middle thickness but also in the surface to obtain the stress-strain distribution in the thickness direction. Strain measurements close to invert is also proposed to determine the restraint effect of invert. Air temperature variation in

a vertical direction inside the tunnel is also proposed to verify the used air temperature model in this study.

2. One of the challenging areas in the concrete simulation is the estimation of drying shrinkage with varying environmental conditions. A simulation technique is proposed to take this effects into account for the stress analysis of second lining concrete by combining two simulation tools. However, in the current study long term drying shrinkage was only studied under idealized environmental conditions (constant temperature and constant relative humidity). The accuracy of the simulation should be improved by taking the realistic environmental conditions into account.
3. Even though the effect of expansive additives was studied under the short term behaviour of second lining, any nonlinear effects of expansive concrete were not simulated in the current study, it might be necessary to improve the simulation to grasp the exact behaviour of expansive concrete in second lining concrete.

REFERENCES

[1] "Technical Manual for Design and Construction of Road Tunnels - Civil Elements." U.S. Department of Transportation, Federal Highway Administration, Dec-2009.

[2] Y. Li, X. Jin, Z. Lv, J. Dong, and J. Guo, "Deformation and mechanical characteristics of tunnel lining in tunnel intersection between subway station tunnel and construction tunnel," *Tunn. Undergr. Space Technol.*, vol. 56, pp. 22–33, Jun. 2016.

[3] A. S. Khanooja, S. Chandra, G. C. Nayak, and B. Singh, "Analysis of a typical shaped tunnel lining by finite element method," *Comput. Struct.*, vol. 21, no. 5, pp. 1079–1084, Jan. 1985.

[4] D. L. N. de F. Amorim, S. P. B. Proença, and J. Flórez-López, "Simplified modeling of cracking in concrete: Application in tunnel linings," *Eng. Struct.*, vol. 70, pp. 23–35, Jul. 2014.

[5] N.-A. Do, D. Dias, P. Oreste, and I. Djeran-Maigre, "2D numerical investigation of segmental tunnel lining under seismic loading," *Soil Dyn. Earthq. Eng.*, vol. 72, pp. 66–76, May 2015.

[6] O. Arnau and C. Molins, "Theoretical and numerical analysis of the three-dimensional response of segmental tunnel linings subjected to localized loads," *Tunn. Undergr. Space Technol.*, vol. 49, pp. 384–399, Jun. 2015.

[7] A. Nakamura, M. Kunichika, H. Kameya, and H. Nakamura, "IDENTIFICATION OF THERMAL PROPERTIES IN THE INTIAL CRACK PREDICTION OF THE TUNNEL LINING CONCRETE AND ITS ANALYSIS," *Jpn. Soc. Civ. Eng. Pap. F1*, vol. Vol-70, no. No-3, p. I-1,I-16, 2014.

[8] The Japan Concrerte Institute, *The Guidelines for Control of Cracking of Mass Concrete 2008*. .

[9] 大野又稔 and 細田暁, "山口県の実構造物のデ ータベースの温度応力解析による分析," コンクリート工学年次論文集, vol. 34, no. 1, p. 1288,1239, 2012.

[10] Y. Shirane, M. Kagawa, A. Kikuchi, and T. Komatsu, "EVALUATION OF EFFECT FOR REDUCING CRACK OF LINING CONCRETE BY USING WATERPROOFING MEMBRANE WITH SMOOTH SURFACE(HIGH-EATAS) (in Japanese)," 前田技術研究所報, vol. VOL 53, 2012.

[11] Maeda Corporation, "High ETAS (Endurance Tunnel Arch Structure) method a new method for waterproofing mountain tunnels." .

[12] K. Nishioka, Y. Tezuka, G. Sakai, M. Suji, and K. Murakami, "EFFECT OF LINING CONCRETE CUREING BY A NEW TELESCOPIC FORMS," トンネル工学報告集, vol. 24, no. 2014–12, pp. 1–5.

[13] K. Nishioka and Y. Tezuka, "型枠存置時間 の 延長 による 覆工 コンクリート の 品質向上効果 = ツイン アーチ フォーム (TAF) 工法 の 展開 と 展望 =."

[14] "覆工技術 | 山岳トンネル技術 | 鹿島建設株式会社." [Online]. Available: http://www.kajima.co.jp/tech/c_mountain_tunnel/lining/index.html. [Accessed: 31-Jul-2016].

[15] "新着情報 - 西松建設株式会社." [Online]. Available: http://www.nishimatsu.co.jp/news/news.php?no=NjY=&icon=44GK55+l44KJ44Gb. [Accessed: 31-Jul-2016].

[16] "NETIS 新技術情報提供システム." [Online]. Available: http://www.netis.mlit.go.jp/NetisRev/Search/NtDetail1.asp?REG_NO=HK-120007. [Accessed: 31-Jul-2016].

[17] S. Kozo and I. Tadahiko, “マイ スター クリート 工法 の 開発 と 現場適用 (高品質な 山岳 トンネル 覆 エ コンクリート 打設工法).”
[18] A. Usman, “Evaluation of Covercrete Quality of RC structures using Surface Water Absorption Test.”
[19] H. Hidetoshi and M. Atsushi, “覆工マルチ工法と HDL 工法.”
[20] “前田覆工マルチ工法｜土木技術｜技術紹介｜前田建設工業株式会社.” [Online]. Available: https://www.maeda.co.jp/tech/all/td0072.html. [Accessed: 31-Jul-2016].
[21] “トンネル覆工におけるクラウン(天端)部充填管理の高度化技術を開発～多機能型型枠を中核技術とした「ＨＤＬ工法」～（2016/4/27）｜前田建設のオススメ｜前田建設のオススメ.” [Online]. Available: https://www.maeda.co.jp/select/2016/04/27/1585.html. [Accessed: 31-Jul-2016].
[22] R. M. Singh and A. Bouazza, “Thermal conductivity of geosynthetics,” *Geotext. Geomembr.*, vol. 39, pp. 1–8, Aug. 2013.
[23] D. Kopitar, Z. Skenderi, and B. Mijovic, “Study on the Influence of Calendaring Process on Thermal Resistance of Polypropylene Nonwoven Fabric Structure,” *J. Fiber Bioeng. Inform.*, vol. 7, no. 1, pp. 1–11, 2014.
[24] S. Sakthivel and T. Ramachandran, “Thermal conductivity of non-woven materials using reclaimed fibres,” *Int. J. Eng. Res. Appl. IJERA*, vol. 2, no. 3, p. 2986, 2012.
[25] ACI Committee 207, “Mass Concrete,” ACI Committee, 1997.
[26] J. L. Cope, R. W. Cannon, E. A. Abdun-Nur, L. H. Diaz, R. F. Oury, F. A. Anderson, T. P. Dolen, J. M. Raphael, H. L. Boggs, K. D. Hansen, and others, “Effect of restraint, volume change, and reinforcement on cracking of mass concrete,” *ACI Man. Concr. Pract.*, 2002.
[27] Y. Sun, M. McRae, and J. Van Greunen, “Load Sharing in Two-pass Lining Systems for NATM Tunnels.”
[28] A. M. Neville, *Properties of concrete*, 4th and final ed., Reprint. Harlow, Essex: Longman, 1997.
[29] T. Usui, T. Otomo, and et. al, “Effect of Application of Expansive Concrete on Reducing Thermal Stress of Secondary Lining of Tunnels,” *Taisei Corp Tech. Rep.*, vol. 2, 2009.
[30] “ASTEA MACS｜ASTEA MACS｜製品案内｜計算力学研究センター RCCM.” [Online]. Available: http://www.rccm.co.jp/product/concrete/astea-macs/. [Accessed: 31-Jul-2016].
[31] Research Center of Computational Mechanics. Inc., “ASTEA MACS for Windows Ver. 8 使用法補足.” 株式会社 計算力学研究センター, Mar-2015.
[32] D. L. Logan, *A first course in the finite element method*, 5th ed. Stamford, CT: Cengage Learning, 2012.
[33] Japan Society of Civil Engineers (JSCE), “STANDARD SPECIFICATIONS FOR CONCRETE STRUCTURES -2007 ‘Design.’” subcommitee on English Version of Standard Specifications for Concrete Structures -2007, 2010.
[34] R. Sato, T. Shimomura, I. Maruyama, and K. Nakarai, “Durability Mechanics of Concrete and Concrete Structures Re-Definition and a New Approach,” in *Committee Reports of JCI, 8th International Conference on Creep, Shrinkage and Durability of Concrete and Concrete Structures (CONCREEP8), Ise-Shima, Japan*, 2008, vol. 1.
[35] R. Springenschmid, *Prevention of Thermal Cracking in Concrete at Early Ages*. CRC Press, 1998.
[36] M. Al-Gburi, J. E. Jonasson, M. Nilsson, H. Hedlund, and A. Hösthagen, “Simplified methods for crack risk analyses of early age concrete,” *Part*, vol. 1, pp. 17–38.

[37] “Finite difference method,” *Wikipedia, the free encyclopedia*. 10-Jul-2016.
[38] “Conjugate gradient method,” *Wikipedia, the free encyclopedia*. 19-May-2016.
[39] K.-J. Bathe and K.-J. Bathe, *Finite element procedures*. Englewood Cliffs, N.J: Prentice Hall, 1996.
[40] K. Maekawa, T. Ishida, and T. Kishi, *Multi-Scale Modeling of Structural Concrete*. .
[41] K. Maekawa, H. Okamura, and Pimanmas, *Non-Linear Mechanics of Reinforced Concrete*. .
[42] K. Maekawa, T. Ishida, and T. Kishi, “Multi-scale modeling of concrete performance,” *J. Adv. Concr. Technol.*, vol. 1, no. 2, pp. 91–126, 2003.
[43] H. Okamura and K. Maekawa, *Nonlinear Analysis and Constitutive Models of reinforced concrete*. .
[44] T. Yoneda, T. Ishida, K. Maekawa, E. Gebreyouhannes, and T. Mishima, “Simulation of early-age cracking due to drying shrinkage based on a multi-scale constitutive model,” *Proc. Am. Soc. Civ. Eng. Poromechanics V*, pp. 579–588, 2013.
[45] “Ethylene-vinyl acetate,” *Wikipedia, the free encyclopedia*. 24-May-2016.
[46] “3. 防水排水(山岳資材検索リスト).” [Online]. Available: http://www.japan-tunnel.org/ysizai300. [Accessed: 23-Jul-2016].
[47] R. W. Lewis, P. Nithiarasu, and K. N. Seetharamu, *Fundamentals of the Finite Element Method for Heat and Fluid Flow*. Wiley Online Library, 2004.
[48] T. Ito, A. Hosoda, K. Hayashi, T. Nishio, and D. Yamaki, “PDCA FOR IMPROVING QUALITY OF CONCRETE LINING IN MOUNTAIN TUNNEL AND EVALUATION OF COVERCRETE QUALITY.”
[49] S. Yagi, C. Aquino, M. Inoue, and T. Okamoto, “Volume change of limestone and its effects on drying shrinkage of concrete,” in *Advanced Materials Research*, 2011, vol. 168, pp. 738–741.
[50] T. Kanda, H. Momose, and K. Imamoto, “Shrinkage Cracking Resistance of Blast Furnace Slag Blended Cement Concrete - Influencing Factors and Enhancing Measures,” *J. Adv. Concr. Technol.*, vol. Vol. 13, no. January 2015, pp. 1–14.

APPENDIX- 1

Algorithm to create AsteaMacs finite element mesh by exporting from LINK3D

Process for exporting the mesh from LINK3D to Astea-Macs. Created using Microsoft Excel Visual Basic for Application (Excel VBA)

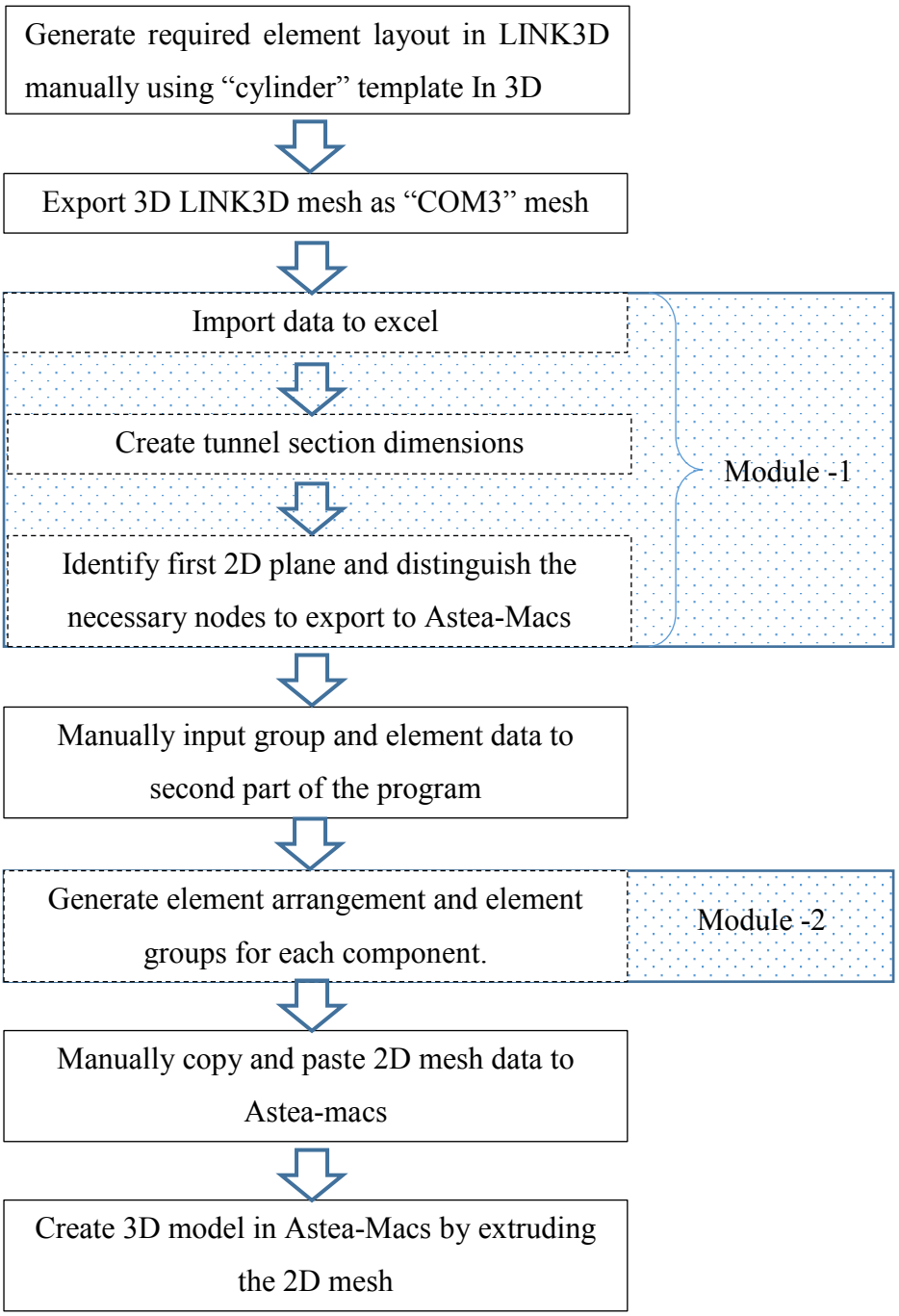

Module-1 Import nodes from LINK3D and create the tunnel cross section profile

```
Dim myfile As String
Option Explicit

Sub IMPORT_NODES()

Dim cellValue As String, i As Integer, j As Integer
Dim celltext As String
Dim textlength As Integer
Dim nspace As Integer
Dim row n As Integer
Dim fileline As String
Dim sppos As String
Dim starr() As String
Dim delimchars As String
Dim msgrep As Variant
Dim intChoice As Integer
delimchars = " "

Close #1
Close #2

Range("a1").Select
ActiveCell.CurrentRegion.Cells.Clear

'only allow the user to select one file
Application.FileDialog(msoFileDialogOpen).AllowMultiSelect = False
'make the file dialog visible to the user
intChoice = Application.FileDialog(msoFileDialogOpen).Show
'determine what choice the user made
If intChoice <> 0 Then
'get the file path selected by the user
    myfile = Application.FileDialog( _
    msoFileDialogOpen).SelectedItems(1)
Else
MsgBox "No files choosen exitng"
Exit Sub
End If

'myFile = ActiveWorkbook.Path & "\tmp-HYGR.dat"
Open myfile For Input As #1

Do Until EOF(1)
    Line Input #1, fileline
    If fileline = "NODE" Then
        Exit Do
    End If
Loop

Do Until EOF(1)
    Line Input #1, fileline
    If fileline = "ELEM" Then
        Exit Do
    Else
        ActiveCell.Value = fileline
        ActiveCell.Offset(1, 0).Select
    End If
Loop

Range("a1").Select
Application.DisplayAlerts = False
Range("a:a").TextToColumns Space:=True
Application.DisplayAlerts = True

Close #1

msgrep = MsgBox("Run the profile calculation?", vbYesNo, "Run the Tunnel Profile calculation?")
If msgrep = vbYes Then
    Call calculatecoordinate
Else
End If
End Sub

Sub calculatecoordinate()

Dim lastcol As Long
Dim lastrow As Long
Dim xcord As Double
Dim ycord As Double
```

```
Dim grad As Double
Dim angle As Double
Dim angle_2 As Double
Dim xvalue As Double
Dim yvalue As Double
Dim msgrep As Variant
Dim i As Integer
Dim radious As Double


Close #1
Close #2

lastcol = ActiveSheet.UsedRange.SpecialCells(xlCellTypeLastCell).Column
lastrow = ActiveSheet.UsedRange.SpecialCells(xlCellTypeLastCell).row

'inside loop-----------------------------------------------------------------------------------------------
---
For i = 1 To lastrow

'Cells(i, 1).Select
xcord = UsedRange.Cells(i, 3).Value
ycord = UsedRange.Cells(i, 5).Value

'To prevent division by zero-------------------------------------------------
If xcord = 0 Then
xcord = 0.00001
End If

If ycord = 0 Then
ycord = 0.00001
End If
'----------------------------------------------------------------------------
grad = ycord / xcord
angle = Round(Atn(grad) * 180 / (Application.WorksheetFunction.Pi), 6#)

 radious = Round(Sqr(xcord * xcord + ycord * ycord), 6)

If (angle > -12) Or angle = -12 Then
    xvalue = xcord
    yvalue = ycord
Else   'If angle > 6.6753 Then

    Dim scbx As Double
    Dim scby As Double
    Dim scbr As Double
    Dim xcord_2 As Double
    Dim ycord_2 As Double

    scbx = 391.4 '472.6
    scby = -82.3 '-96
    scbr = 150 '67.8
    ' transfer cordinates
    xcord_2 = xcord - scbx
    ycord_2 = ycord - scby

    'calculate angle

    angle_2 = Round(Atn(ycord_2 / xcord_2) * 180 / (Application.WorksheetFunction.Pi), 6#)

        If angle_2 > -73 And angle_2 < -12 Then
            xvalue = calx30(radious, xcord_2, ycord_2)
            yvalue = xvalue * ycord_2 / xcord_2
            xvalue = xvalue + scbx
            yvalue = yvalue + scby
        Else
            scbx = 0
            scby = 1204.4
            scbr = 1495
            xcord_2 = xcord - scbx
            ycord_2 = ycord - scby
            xvalue = calxzone3(radious, xcord_2, ycord_2)
            yvalue = xvalue * ycord_2 / xcord_2
            xvalue = xvalue + scbx
            yvalue = yvalue + scby
        End If
End If

   UsedRange.Cells(i, 3).Value = Round(xvalue, 3)
   UsedRange.Cells(i, 5).Value = Round(yvalue, 3)

Next i

Range("A1", Cells(lastrow, lastcol)).Select
'end of loop-----------------------------------------------------------------
```

```
msgrep = MsgBox("Export COM3D Data?", vbYesNo, "Export COM3D Data?")
If msgrep = vbYes Then
Call Com3D_Node_Export

Else
End If
End Sub

Function calx30(radious As Double, xcord_2 As Double, ycord_2 As Double) As Double

Dim a As Double
Dim b As Double
Dim r As Double
Dim p As Double
Dim rfixed As Double

rfixed = 550
a = 0
b = 0
r = 150
p = ycord_2 / xcord_2

r = r + radious - rfixed

calx30 = ((a + b * p) + Sqr((a + b * p) ^ 2 - (1 + p * p) * (a * a + b * b - r * r))) / (1 + p * p)

End Function

Function calxzone3(radious, xcord_2, ycord_2) As Double
Dim a As Double
Dim b As Double
Dim r As Double
Dim p As Double
Dim rfixed As Double

rfixed = 550
a = 0
b = 0
r = 1495

p = ycord_2 / xcord_2

r = r + radious - rfixed

calxzone3 = ((a + b * p) + Sqr((a + b * p) ^ 2 - (1 + p * p) * (a * a + b * b - r * r))) / (1 + p * p)

End Function
```

Module -2 – Writing element and group data in Astea-Macs format

```
Option Explicit

Sub findfirstface()

Dim i As Integer
Sheet1.Activate
Cells(1, 1).Activate

For i = 1 To Range("c1", Range("c1").End(xlDown)).Rows.Count

    If ActiveCell.Offset(0, 3).Value = 0 Then
        ActiveCell.Offset(1, 0).Activate
        Else
        ActiveCell.Rows.EntireRow.Delete
    End If
Next i
End Sub

Sub nodegenandwriteelement()
Dim i As Integer
Dim j As Integer
Dim noderow As Integer
Dim nodenumber As Integer
Dim elementnumber As Integer
Dim elerowindex As Integer
Dim elepositioninrow As Integer
Dim numberofelements As Integer

Dim grouprange As Range

numberofelements = Range("B18").Value
```

```
Worksheets("Sheet6").Activate
Range("f2", Range("m2").End(xlDown)).ClearContents
Range(Range("r1").End(xlDown), Range("r1").End(xlToRight)).ClearContents

nodenumber = Range("b2").Value

noderow = 1

Range("R1").Select

For j = 1 To Range("b4").Value
    For i = Range("b2").Value To Range("B3").Value
        ActiveCell.Value = nodenumber
        ActiveCell.Offset(1, 0).Select
        nodenumber = nodenumber + 1
    Next i
    ActiveCell.Offset(-1, 0).End(xlUp).Select
    ActiveCell.Offset(0, 1).Select
Next j

'write the small circle

Range("R1").End(xlDown).Offset(1, 0).Select
nodenumber = (nodenumber - 1) * 2 + 1

For j = 1 To Range("b9").Value
    For i = 1 To Range("B8").Value
        ActiveCell.Value = nodenumber
        ActiveCell.Offset(1, 0).Select
        nodenumber = nodenumber + 1
    Next i
    ActiveCell.Offset(-1 * Range("b8").Value, 1).Select
Next j

' write element

elementnumber = 1
Range("R1").Select

For j = 1 To Range("b4").Value - 1
    For i = Range("b2").Value To Range("r1", Range("r1").End(xlDown)).Rows.Count - 1 'Range("B3").Value - 1
        Cells(elementnumber + 1, 6).Value = elementnumber
        Cells(elementnumber + 1, 10).Value = ActiveCell.Value
        Cells(elementnumber + 1, 11).Value = ActiveCell.Offset(1, 0).Value
        Cells(elementnumber + 1, 12).Value = ActiveCell.Offset(1, 1).Value
        Cells(elementnumber + 1, 13).Value = ActiveCell.Offset(0, 1).Value

        'seting the groups

        elerowindex = (elementnumber - (elementnumber Mod numberofelements)) / numberofelements + 1
        elepositioninrow = elementnumber Mod numberofelements

        If elepositioninrow = 0 Then
          elepositioninrow = Range("b18").Value
        End If

        Set grouprange = Range("b12", "d16")

            If elerowindex <= grouprange.Cells(1, 3) = True And elepositioninrow <= grouprange.Cells(1, 2)
= True Then
            Cells(elementnumber + 1, 9).Value = grouprange.Cells(1, 1)
            ElseIf elerowindex <= grouprange.Cells(2, 3) = True And elepositioninrow <= grouprange.Cells(2,
2) = True Then
            Cells(elementnumber + 1, 9).Value = grouprange.Cells(2, 1)
            ElseIf elerowindex <= grouprange.Cells(3, 3) = True And elepositioninrow <= grouprange.Cells(3,
2) = True Then
            Cells(elementnumber + 1, 9).Value = grouprange.Cells(3, 1)
            ElseIf elerowindex <= grouprange.Cells(5, 3) = True And elepositioninrow <= grouprange.Cells(5,
2) = True Then
            Cells(elementnumber + 1, 9).Value = grouprange.Cells(5, 1)
            Else
            Cells(elementnumber + 1, 9).Value = grouprange.Cells(4, 1)
        End If

        'Element Type
        Cells(elementnumber + 1, 7).Value = 12
        'Liftnumber 1
        Cells(elementnumber + 1, 8).Value = 1

        ActiveCell.Offset(1, 0).Select
        elementnumber = elementnumber + 1
    Next i
ActiveCell.Offset(-1, 0).End(xlUp).Select
ActiveCell.Offset(0, 1).Select
```

```
Next j
Range("R1").End(xlDown).Cells.Interior.Color = vbYellow
Range("A1").Select
End Sub
```